공학박사학위논문

계단등반을 위한 하이브리드 링크 구조를 갖는 실내용 이동플랫폼 개발

Hybrid Linkage-based Stair-climbing Mobile Platform for Indoor Applications

2016년 2월

서울대학교 대학원

기계항공공학부

홍 희 승

계단등반을 위한 하이브리드 링크 구조를 갖는 실내용 이동플랫폼 개발

Hybrid linkage-based stair-climbing mobile platform for indoor applications

지도교수 김 종 원

이 논문을 공학박사 학위논문으로 제출함

2015 년 12 월

서울대학교 대학원

기계항공공학부

홍 희 승

홍희승의 공학박사 학위논문을 인준함

2015 년 12 월

위 원 장 : 박 희재

부위원장 : 김 종원

위 원 : 안 성훈

위 원 : 조 규진

위 원 : 김 학수

Abstract

In this thesis, a mobile platform which uses a new hybrid link mechanism is developed, including its control method to maximize stair climbing performance.

As the first step to obtain stair climbing ability to the mobile platform, a new hybrid link mechanism is developed. A new hybrid link mechanism is selected from candidates created by using an engineering design methodology, which has a combined passive rotation joint and active prismatic joint so that can move its center of mass freely to climb stairs easily.

To ensure high mobile stability, efficiency and adaptability while climbing stairs, kinematic design parameters optimization is applied. Minimizing backward movement and maximizing straightness of the center of the body trajectory are selected as objective functions. Also various conditions and constraints are defined to obtain optimized link sizes and wheel radius through GA procedure.

The actual mobile platform is designed and manufactured while considering both optimized design parameters and interferences between the stairs and the mobile platform. The constructed mobile platform has a size of 650 mm (W) X 600 mm (L) X 460 mm (H), the weight of 35kg and its max speed is 2 m/s. It is controlled by 'CompactRIO' as the main controller which located at the mobile platform body and it communicates with the platform remotely by a 'LABVIEW' program from laptop terminal.

To adapt any stairs with unknown dimensions, strategy creation process is suggested.

Position recognition process also created to drive wheels and active slide joints effectively during stair climbing. Before the stair climbing process, stair dimensions are obtained by 2-D laser scanner and processed with dimension acquisition algorithm. As a result, a unique look up table is created. When the mobile platform starts to climbing stairs, it compares actual link angles with table to recognize its position and posture. So that platform can derive appropriate slide joint position to maintain its stability, as well as wheel contact angles to control speed of wheel based on the wheel Jacobians.

Also, MPC(Model Predictive Control) is implied to minimize the posture imbalance (which can be caused by external conditions) to maintain the stability and posture accuracy of the mobile platform on the staircases. Speed of each wheel is adjusted by MPC implementation, and superiority of this method is proven from experiments comparison with both none-controlled and PI controlled cases. As the last phase of the experiment, stair climbing in the real circumstance is performed and the result proved the effectiveness of the mechanism and its control architecture.

Keywords: Hybrid-link mechanism, Mobile platform, Stair climbing, Kinematic analysis, Kinematic optimization, Model Predictive Control

Student Number: 2010-30970

Contents

List of Figures

Chapter 1

Introduction

1.1 Motivation

Mobility is the most important function for most robots. Recently, various robots are introduced and applied in a wide range of tasks, such as industrial, military and security applications[1, 2, 3, 4, 5], planetary exploration[6, 7, 8, 9], rescue and hazardous environmental works[10, 11], and indoor applications such as home, office and medical services [12, 13]. To accomplish desired task perfectly, sufficient mobility for task circumstances is essential. Therefore, it is reasonable to consider high mobility as the most important factor among others when evaluating the performance of the mobile robots [14].

Based on their locomotive mechanism variations, mobile robots can be categorized into following categories: Track-type, leg-type, and wheel-type mobile robots. The track-type mobile robots offer high mobility and stability based on their inherited traditional caterpillar-based mechanism, but excessive track friction loss during movements cause poor energy efficiency [15]. Fig. 1.1 and Fig. 1.2 are examples of track-type stair-climbing robots. The Packbot and the ROBHAZ are military/hazardous environment purpose robots.

Figure 1.1: Packbot - track type mechanism

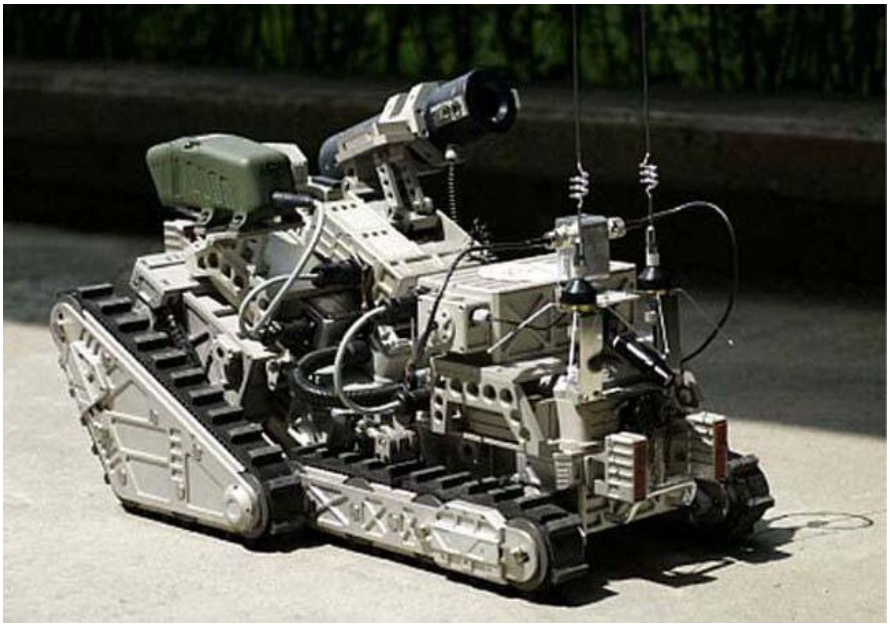

Figure 1.2: Robhaz-DT3 - track type mechanism

The leg-type mechanisms are also take part in a significant portion of the mobile platform mechanism variations. Fig. 1.3 shows ASIMO, a well-known humanoid developed by HONDA, which has two-legs for its locomotion. Although the leg-type mechanism can grant relatively superior adaptability to mobile robots for most circumstances, its highly complicated mechanism also requires complex control algorithm, which can brings slow movement speed as well as poor energy efficiency [16, 17]. Besides, Rhex depicted in Fig 1.4 has six simple legs, which rotate like wheels. So that Rhex can move on rough terrain with a relatively high speed. But due to its simple mechanism, bigger shock and strong vibration from the ground are inevitable.

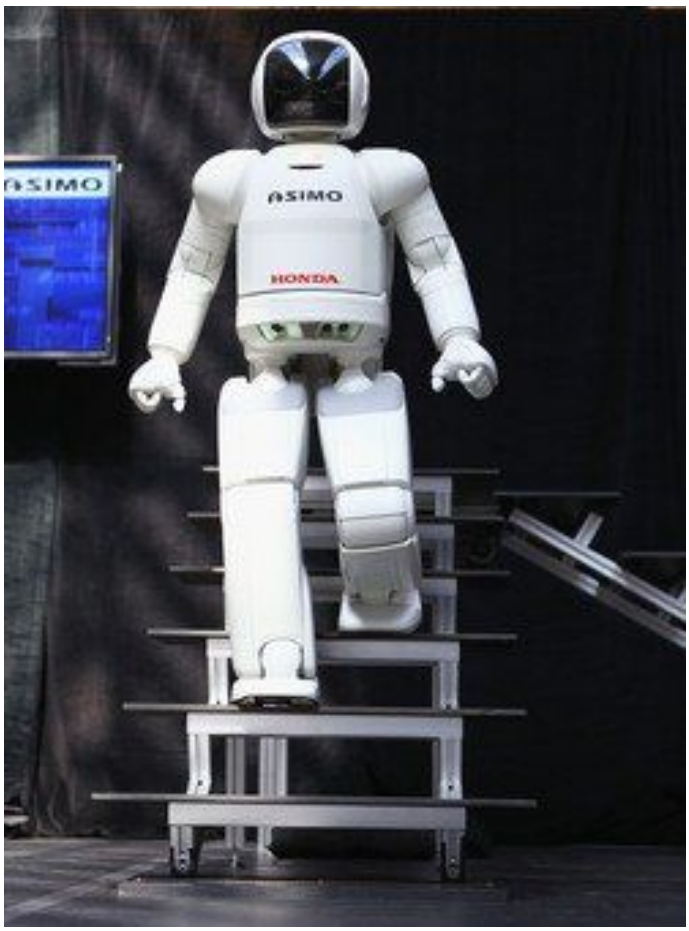

Figure 1.3: ASIMO - legged mechanism

Figure 1.4: Rhex - wheel-leg mechanism

The wheel-type mechanisms grant relatively high efficiency when compared with the other mechanism, but their environmental adaptability is not sufficient. Moreover, their mobility can be highly affected from the type and size of encountered obstacle [17,18]. To enhance its adaptability especially for the stair structures, modified wheel-type locomotive mechanisms were introduced. Fig. 1.5 to 1.7 depicts stair-climbing wheel-type mobile robots. As shown in Fig. 1.5(MSROX using star-wheel system), it has total 12 small wheels. Helios-V from Fig. 1.6 has six-wheels which connected by links. Also, a well-known electric wheelchair IBOT 4000 is presented in Fig. 1.7, which can adjust its height and climb staircases by using four-wheel mechanism and balance control algorithm.

Besides, combined-type mechanisms based on mobile robots have been introduced as a new solution which combines two or more locomotive systems together [14, 19, 20]. However, these mechanisms are more complicated than ordinary wheel-type mechanisms, so creating proper locomotion control algorithm is an important issue [18]. On the other hand, passive linkage attached wheel-type mobile robots are suggested based on the

verified performance data in real circumstances, for instances, Mars Exploration Rovers (MERs) such as Sojourner, Rocky7, Spirit and Opportunity [6, 7, 8], ORF-L [9], CEDRA [10], SHRIMP [15], etc.

Fig. 1.8 shows the rocker-bogie robot with stair climbing ability, introduced in the previous research [21]. The rocker-bogie robot has a famous rocker-bogie mechanism, which consists of two structural elements such as “rocker” and ”bogie”. A schematic diagram of a six-wheeled rocker-bogie mechanism and the real photograph of Spirit adopting this mechanism are shown in Fig. 1.9(a) and 1.9(b). This mechanism allows a mobile robot to maintain its balance at the average pitch angle of both rockers so that the possibility of tip-over can be reduced [22, 23]. But due to its inheritance limits from the passive linkage mechanism, it has insufficient adaptability to obstacles. To enhance both adaptability and stability during passing obstacles such as stairs, combining passive and active linkage mechanism can be proposed as a solution, so that both simplicity and adaptability can be achieved.

Figure 1.5: MSRox - Star-wheel mechanism

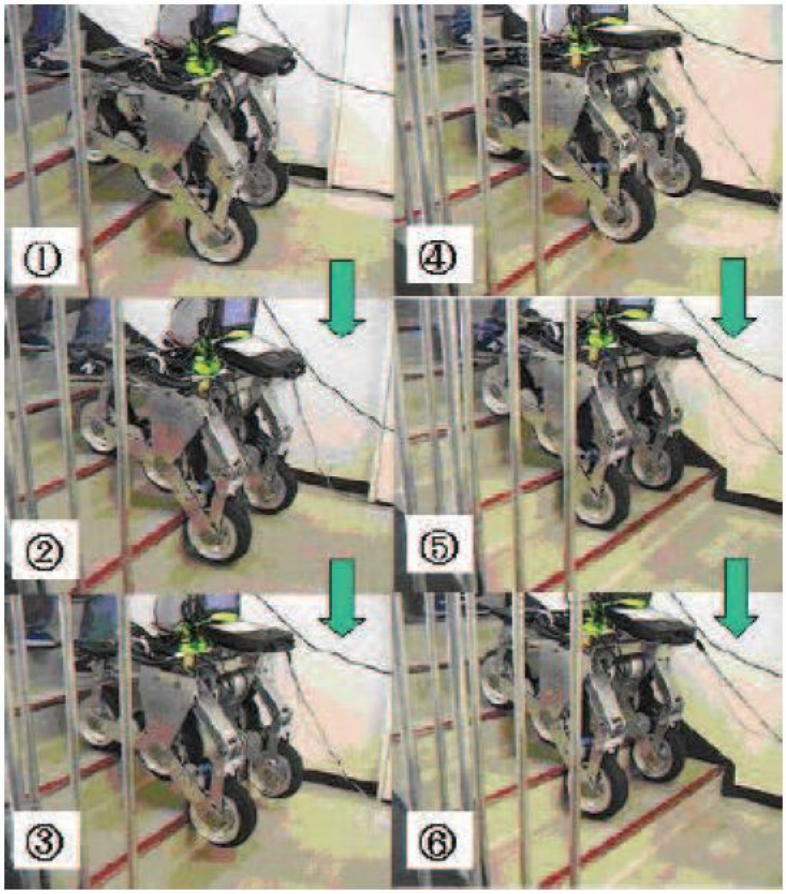

Figure 1.6: Hellios V- wheel type mechanism

Figure 1.7: IBOT 4000 - Wheel type mechanism

Figure 1.8: Rocker-bogie robot [21]

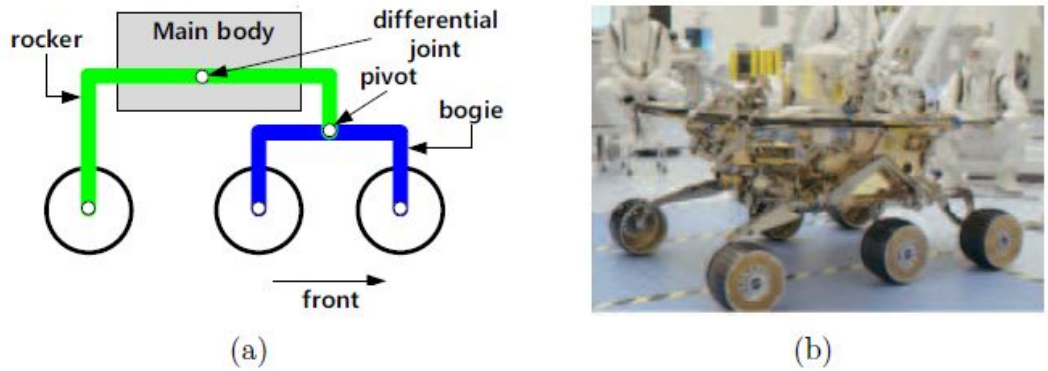

Figure 1.9: (a) Schematic diagram of a rocker-bogie (b) NASA MER: Sprit

1.2 Previous research

1.2.1 Wheel velocity control

In many cases, wheel speed of the mobile robots commonly fixed during moving on surfaces, while ignoring postures of robot and environmental changes. This fixed wheel speed application may cause significant wheel slip easily. Also it can even lead to critical driving failures. To minimize wheel slip failure, detailed wheel velocity control based on the posture and circumstance recognition process is required. This recognition process can be replaced into an estimation method based on other reasonable information, so that can enable the process with a less complicated way.

The status estimation method is depicted in Fig. 1.10, as mentioned above [24]. Each wheel has its own wheel contact angle $\gamma 1$ and $\gamma 2$, also means of movement direction. The contact angles can be derived from geometric constraints, from every velocity of wheel center are calculated by wheel rotation speed. But 'no wheel slip' assumption causes inaccuracy of the estimation results.

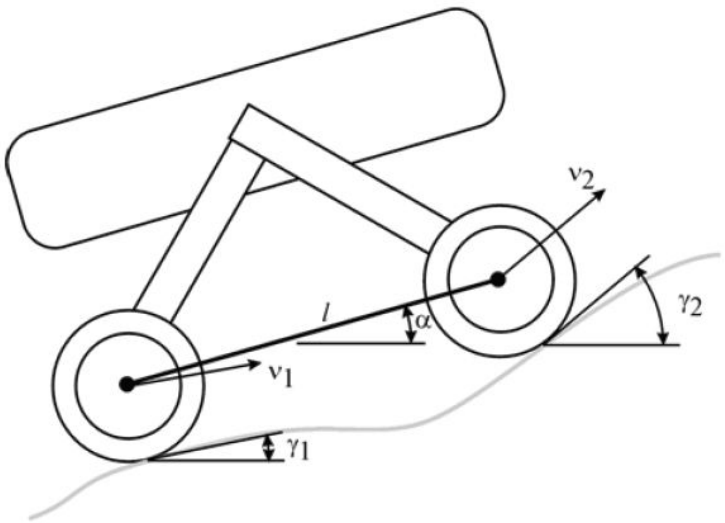

Figure 1.10: Contact angle estimation of RTC (Rough Terrain Control)

In the previous research [21], the rocker-bogie robot used preliminarily produced look-up tables to control wheels, so that the wheel contact angles from tables can be used to calculate wheel speed by using wheel Jacobians. This method limits the adaptability for unknown stair structures of the rocker-bogie robot. By adding a stair-recognition method, a mobile platform can enhance its adaptability for the unknown stair structures.

1.2.2 Posture and Movement control

As described beforehand, slip minimizing method based on primal wheel speed control is the backbone of mobility and stability of the mobile platform. But stacked posture error and imbalance during its movement in the real circumstances cannot be evaded easily, so that proper movement and postures are hard to maintain. For example, when the mobile platform is in stair climbing process, it has a significant left-right imbalance caused by contact surface conditions, this will cause global posture error and the mobile platform can't identify exact posture and location accurately. Therefore, if wrong actuator directions are given it will cause climbing failure finally.

To prevent this, additional posture and movement control is essential to indoor stair climbing mobile platform. Related researches about maintaining mobile platform trajectory control methods are introduced.

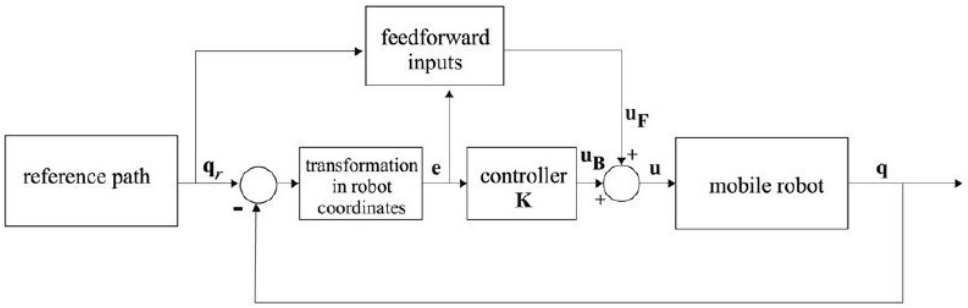

Figure 1.11: Mobile- robot control schematic

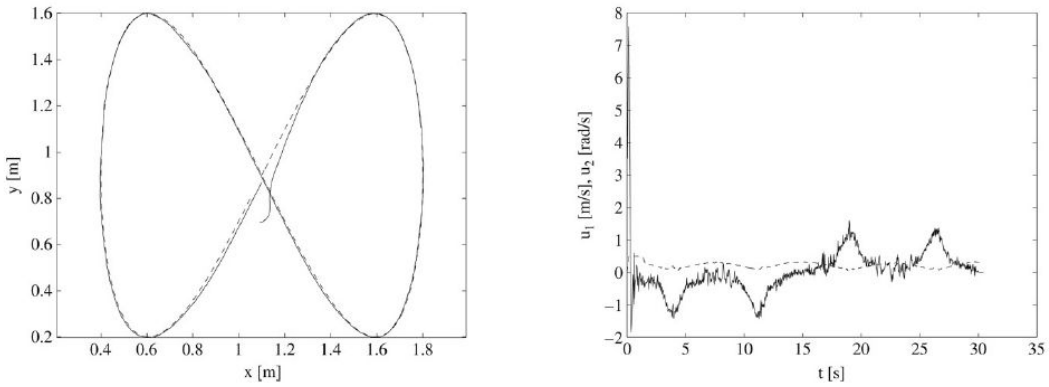

Figure 1.12: MPC implementation experiment result

Fig 1.11, 12 shows the control schematic and its implementing experiment result for the mobile Robot with MPC (Model Predictive Control) method, based on linearized tracking-error dynamics to predict future system behavior [25]. This research proved that the MPC method can be implemented to the mobile platform posture and movement control. Also, Detailed MPC implementation examples for mobile platforms are introduced. Linear and nonlinear MPC cases are compared [26], while the other research explained how faster optimal control can be obtained by explicit MPC method [27].

As explained above, it is highly effective to use MPC-based trajectory following control method for mobile platforms, but theses researches are focused to 2-D flat surface movement. In this thesis, MPC is implemented to 3-D condition: stair climbing mobile platform movement and posture control. Also, its effectiveness is verified through a real condition test as well as comparing with an ordinary PI-based control method.

Chapter 2

Hybrid-link mechanism

2.1 Hybrid-link mechanism concept

The hybrid mechanism which applied in this research is the mechanism based on the combination of the passive joint and active joint. The passive link mechanisms have advantages, such as relatively simple mechanism and easier controls compared to the other mechanisms. But its lack of ability to adapt critical posture or position while ascending or descending stairs, which can cause failure situations. On the other hand, The active link mechanisms can change their structure by using actuators so that they can achieve better field adaptability, but their complicate mechanism bring heavier structures, which requires more complex control system to maximize the performance of the mechanism.

Because of the reasons described above, the new hybrid link mechanism can be introduced as an alternative solution. The process of the development of hybrid mechanism including candidate production, selection, and review is introduced in this chapter.

2.2 Mechanism idea development process

2.2.1 Design candidate creation

To invent a new hybrid link mechanism for the mobile platform design, a detailed requirement list is suggested based on the various resources, such as the experience obtained during the previous researches, other related researches about mobile platforms and the indoor environment codes established by the government of Republic of Korea and United States of America. Table 2.1 shows a major requirement list for a stair-climbing indoor mobile platform. This list is employed as a guideline and evaluation indicator of the mobile platform to be developed throughout this research.

Table 2.1: Major requirements list for stair-climbing indoor mobile platform [28-30]

List	Requirements
Geometrical shape	Width x Depth x Height < 600 mm x 600 mm x 450 mm
Force	Body weight: 20 kg Payload: 10 kg
Circumstance condition	- Step depth > 254 mm, Step height <196 mm, Step width > 914 mm (From International Residential Code) - Install landing (depth > 1200 mm) if the height of steps more than 2m (Housing construction standards regulations #16) - 600mm < (Step depth) + 2 × (Step height) < 660 (ISO 14122-3:2001)
Motion	On a plane surface : Faster than 0.8m/s (2/3 of walking speed) Stair climbing speed: 0.2 m/s

In this section, a systematic design process is carried out using the engineering design methodology [31] to develop a new mobile platform adopting a hybrid link mechanism. Design problem is defined on the basis of the requirement list consisting of five functions essential to a stair-climbing mobile platform. Table2.2 shows the extracted working principle for the five functions of the mobile platform and several working principles are selected for each function. Basically, a mechanism to control body angle is required to

stabilize its main body combined with payloads. A suitable suspension and actuation mechanisms for front and rear wheels are also required to guarantee mobile stability and adaptability while climbing stairs. Design candidates for a new mechanism are obtained by tactfully combining these working principles.

Table 2.2: Extracted working principle list

	1	2	3	4	5	6	7
Body Angle Control	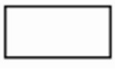 Fixed	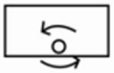 Rotating	 Linear				
Front Suspension Mechanism	 Fixed	 Rocker	 Bogie	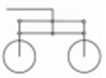 Parallel	 Fork	 Up/Down	 Lifter
Rear Suspension Mechanism	 Fixed	 Rocker	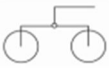 Bogie	 Parallel	 Fork	 Up/Down	 Lifter
Front Actuation	None	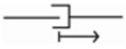 Linear	 Rotation	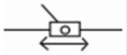 Slide			
Rear Actuation	None	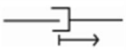 Linear	 Rotation	 Slide			

2.2.2 Candidate review & comparison

Based on the working principle list shown on Table 2, the candidates for the hybrid link mechanism of the mobile platform are created from the combination of working principles of Table 2. To maintain efficiency during the comparison and selection process, realistic candidates are selected from those primitive candidates. Fig. 2.1 shows the four selected candidates from the primitive candidates. The standards of the review and comparison of the candidates are from the predicted available critical cases: A. Rear wheel climbing the vertical wall of the stair, B. Front wheel climbing the vertical wall of the stair, C. Stability maintaining ability during the stair climbing. For every mechanism candidate, its

evaluation point is focused to how can handle these cases by using their unique mechanism. The concepts and evaluation results of the major critical cases handling ability of the design candidates are explained below:

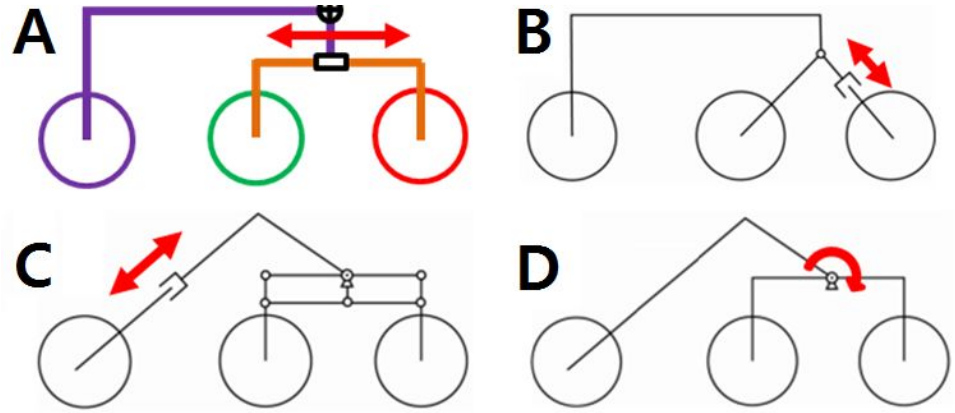

Figure 2.1: Four design candidates for the hybrid link mechanism mobile platform

Candidate A

A slide-rotation joint mixed mechanism: Passive rotation joint and active prismatic joint are combined into one hybrid joint in this candidate. Relatively larger, more efficient movement of the center of mass than the other candidates can be achieved by adopting this simple mechanism while climbing staircases. As the drawback of this mechanism, the slide mechanism requires relatively longer shape, so it can cause the interference problem between the mobile platform and the stair structures.

Candidate B

A variable front link mechanism: the front area of the bogie link of this mechanism can stretch by using active actuation mechanism while the other part are similar to an ordinary rocker-bogie mechanism. Its relatively simple mechanism can be a strong point of this mechanism candidate, but its stretch length is restricted by its mechanism characteristic to adapt to the stair structure conditions. Also, stretching its front link can heightens its center of mass, as well as cause unstable condition to the mobile platform.

Candidate C

A variable rear link mechanism: in contrast to candidate B, its rear link is stretched, while the front link mechanism has a four-bar linkage system. This front mechanism reduces backward movement situation of the front wheel when the front wheel starts climbing the stair wall. But the excessive biased posture can be caused by the combination of the complicated front link mechanism and rear link angle.

Candidate D

An active rotation joint mechanism: Based on the simple rocker-bogie mechanism, its passive rotation joint is replaced into an active rotation joint, so that artificially instantaneous support can be obtained to enhance stair climbing ability. But this actuation movement can push away the mobile platform from the stair wall due to its reaction forces. Also, highly accurate actuator control and center of mass calculation during the design and manufacture process are highly essential to evade the stair climbing process failures, such as wheel stuck situations and fall-down of them mobile platform.

The summary of the evaluation result for each mechanism candidates are summarized in Table 2.3. Candidate A has the highest critical case handling ability evaluation, because the other candidates – B, C and D can't utilize their center of mass effectively to maintaining their stability procedure. In the case of candidate C, it is the strongest the alternative candidates, but it lacks the fall-down prevention ability during the stair climbing procedure. For the reason explained above, candidate A is selected as the final design candidate of the new hybrid link mechanism for the stair climbing mobile platform. The detail of the final design candidate for the mobile robot is described in the section 2.2.3.

Table 2.3: The evaluation result for each mechanism candidates

Critical Situation	Candidate A	Candidate B	Candidate C	Candidate D
Rear wheel wall climbing	Slide joint moves front (C.G forward)	Not available	Can't handle this situation	Actuate joint to lift rear wheel
Front wheel wall climbing	Slide joint moves backward (C.G backward)	Slight effect	Control slide length to keep rear wheel on horizontal plane	Actuate joint to lift front wheel
Fall-down Prevention	Slide joint moves front (minimize rear load)	Not available	Stretch rear link length	Can't support rear wheel to stick to the stair surface
Summary	Can manage all situations by moving its C.G. using its joint	Stretching mechanism is not effective	Can't support rear wheel climbing process	Control support limited to the front and center wheels.

2.2.3 Final candidate selection

In the previous section, the final hybrid link mechanism candidate for the stair climbing mobile platform is selected. This hybrid link mechanism has a mixed joint of an active prismatic joint and passive rotational joint. As shown in Fig. 2.2, *Link 1*, is the front bogie link which attached with two wheels, while *Link 2*, the rear link has one wheel at the end point of the link. Also body is attached to *Link 2*.

The joint part which connects these *Link 1* and *Link 2* is the core of the hybrid link mechanism. As explained previously, this hybrid joint is a combination of passive rotational joint and active prismatic joint. Like a rocker-bogie mechanism, passive rotational joint functions as a suspension of the mobile platform, to maintain contact between wheels and stairs. On the other hand, active prismatic joint moves passive rotation joint to a desired location. By using this combination of joints, active load distribution to

maintain the stability of the mobile platform during ascending and descending staircases is available, so that can minimizes failure situation and widen the adaptability to more various stair dimensions. To maintain the horizontal posture of the body part attached to the *Link 1*, an independent angle adjust mechanism is applied with actuator.

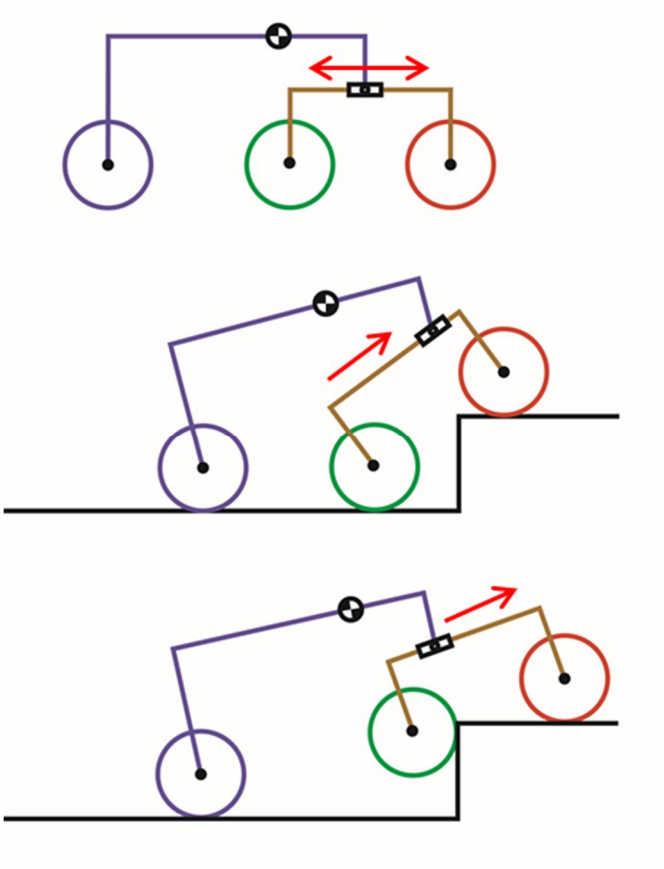

Figure 2.2: The kinematic shape of the new hybrid link mechanism

During this chapter, design candidates for the new hybrid-link mechanism are created, and the slide-rotation joint mixed mechanism is chosen as the final mechanism candidate. Based on the kinematic hybrid-link mechanism concept, optimization of the kinematic design variables, such as wheel radii and link length parameters is processed in chapter 3.

Chapter 3

Design parameter optimization

To maximize the performance potential of the suggested mechanism in chapter 2, the design parameter optimization of the mobile platform is performed. The optimization is focused on the both stability and energy performance of the mobile platform. Based on the optimization result of the design parameters, the mobile platform prototype is manufactured and further performance improvement will be performed when implementing climbing strategy to the mobile platform.

3.1 Kinematic constraints

Before proceeded with the optimization process, it is important to derive constraints on the mobile platform which can prevent unwanted interference between the mobile platform components or the mobile platform and ground circumstances. As shown in Fig. 3.1, a 2-D simplified model of the hybrid link mechanism is created for the simplicity process of the optimization procedure. [15, 32,33] As shown in Fig, 3.1, the center of mass is assumed to be placed on the upper position of the slide joint, which connecting *Link 1* and *Link 2* and then, four link lengths (l_1, l_2, l_3, and l_4) and wheel radius for three wheels (R) are selected as

design parameters. Also, each wheel has same radius, but the wheel radii of each wheels are expressed as R_i (i=1,2,3) to clarify constraint explanation.

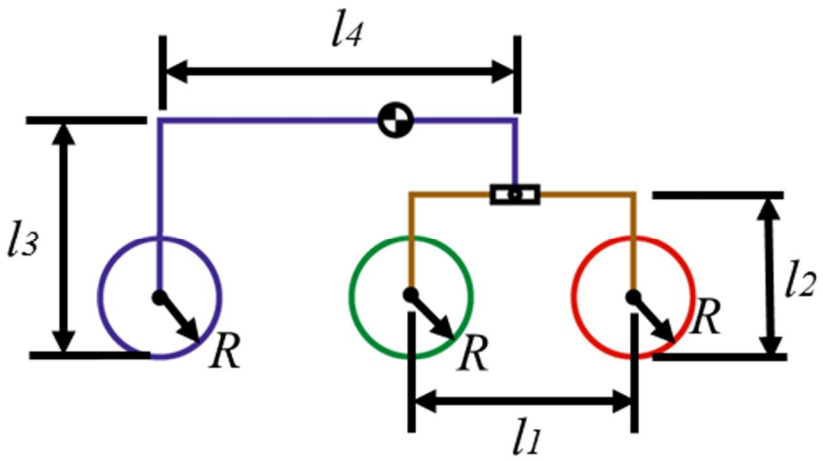

Figure 3.1: Schematic diagram of 2-D model for the rocker-bogie mechanism

In real applications cases, the mobile platform can encounter various stairs. To reflect this, three types of stair dimensions are considered to derive the kinematic constraints of the hybrid link mechanism. The detailed dimensions of imaginary three types of stairs are shown in Fig. 3.2.

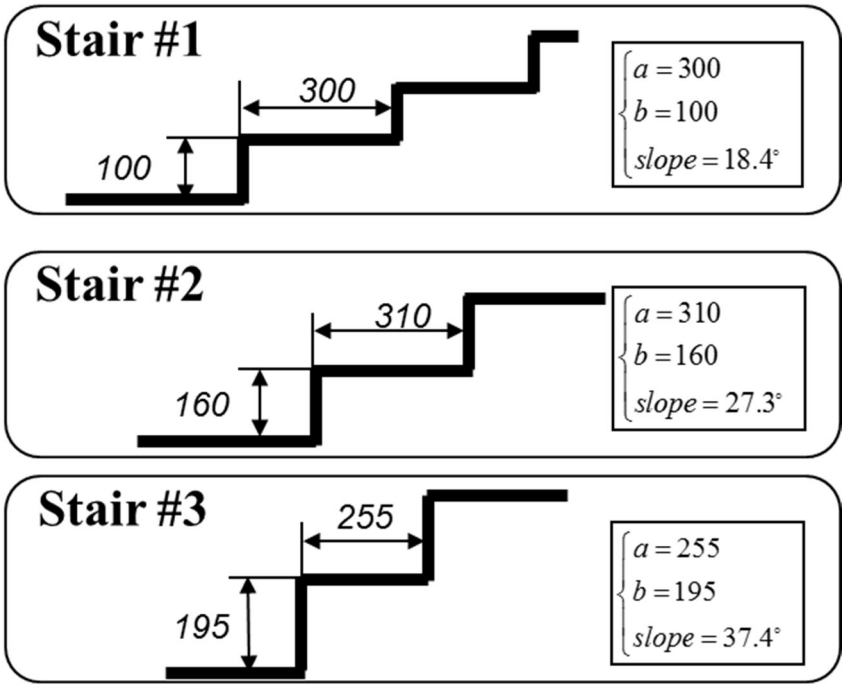

Figure 3.2: Three type of stair dimensions for optimization process

First, the radius ranges are determined from the stair size range. The kinematic constraint about the maximum wheel size is explained in the Fig. 3.3. While the wheel is on the tread of a stair, a wheel center must be on the tread to maintain its posture stable. Based on the dimension of the stair #3 in Fig 3.2(the stiffest case of the stair dimensions) the maximum wheel radius is 264mm. Also, the minimum size of wheel radius is determined to be 50mm, considering the smallest commercially obtainable wheel's size and effectiveness of the minimum sized wheel, related with its actuator specifications. Therefore, the constraint of the wheel radius R can be expressed by

$$50mm < R_i < 264mm \quad \text{(i=1,2,3)} \tag{3.1}$$

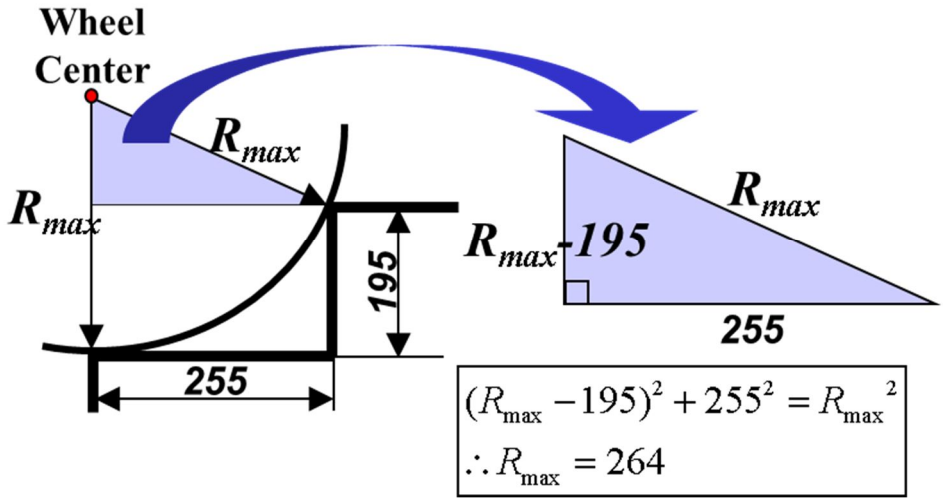

Figure 3.3: Wheel radius range derivation

Next, relation between the link 1 (including the front and middle wheel, W1, and W2) and stair shapes is implemented into the constraints list. When the front wheel finished climbing a step and on the plane surface of a stair, the position of the middle wheel is determined from the configuration of *Link 1*. In this situation, two conditions must be satisfied to maintain stability: a. Link 1 must keep distance from the stair surfaces, b. When the front wheel is on the plane surface, the middle wheel must contact the vertical wall or plane surface of the stair structures. Condition 'a' works as the interference avoidance constraint, while condition 'b' applied to give reality to the optimization results of real design process. Fig. 3.4 explains the posture of *Link 1*, as well as Eqn. (3.2) shown below are the minimum length constraints of l_1 and l_2.

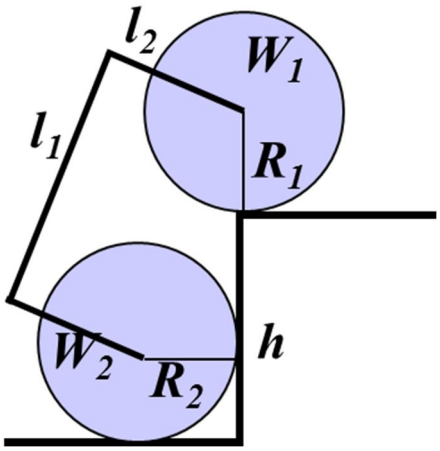

Figure 3.4: *Link 1* and its bogie wheels posture when the first wheel finished climbing a step

$$l_1 > \sqrt{\left(R_1 + R_2\right)^2 + \left(h - R_2 + R_1\right)^2}$$
$$l_2 > 1.5 \times \frac{h - R_2 + R_1}{l_1} \cdot \left(\sqrt{l_1^{\,2} - \left(h - R_2 + R_1\right)^2} \cdot \left(\frac{h - R_2}{h - R_2 + R_1} - R_2 \right) \right) \tag{3.2}$$

When considering the design of the real mobile platform phase, the body, which assumed as the center of the mass is placed above the wheels to prevent the interferences between the mobile platform body and stair structures. To implement this to the kinematic constraints, the height of *Link 2*(l_3) must be same or bigger than the height of *Link 1*(l_2). Fig. 3.5 and Eqn. (3.3) explains this constraint, including the design margin, 10% to the kinematic design.

$$l_3 > 1.1 \times l_2 \tag{3.3}$$

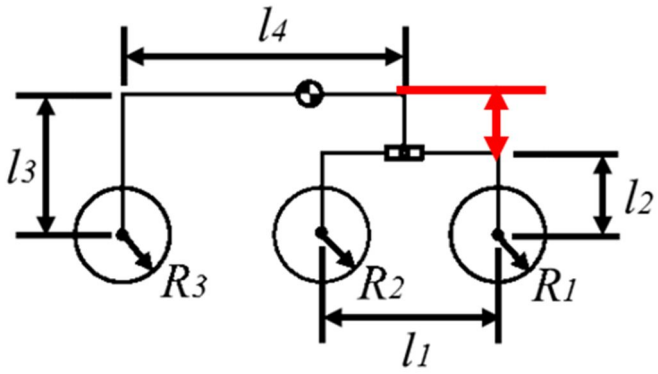

Figure 3.5: Joint height limitation

To avoid complicated control situations and maintain stable posture during the stair climbing process, the rear wheel (W_3) must be placed backward of the middle wheel (W_2) since if W_3 is positioned behind of W_2, they will maintain the order while climbing stairs. To express this as a constraint, the horizontal length of *Link 2* (l_4) must be longer than the horizontal length of *Link 1*(l_1). As shown in Eqn. (3.4).

$$l_4 > l_1 \tag{3.4}$$

As the last phase of the kinematic constraint definition process, maximum link dimension constraint are obtained from the maximum size limitation of the mobile platform. Fig. 3.6 shows the length definition of the mobile platform. When the size of mobile platform is minimized by moving its slide joint to its maximum forward position, its length is calculated by measuring distance between front and rear wheels, and the horizontal length of *Link 2* (l_4). Based on this idea, the last constraint is defined as Eqn. (3.5).

$$l_4 + R_1 + R_3 < D \tag{3.5}$$

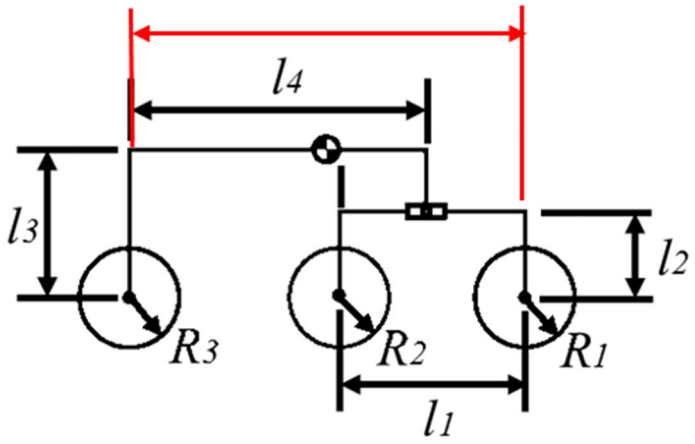

Figure 3.6: Maximum size limitation

3.2 Optimization procedure

3.2.1 Objective function

In this section, the optimization is carried out under the kinematic constraints in equations (3.1) to (3.5). The objective of the optimization is to achieve the combination of two aims: making the trajectory of the Center of Mass (CM) close to a straight line and minimize its backward movement during the stair climbing process.

In considering the former aim, instant required torque and energy consumption are proportional to stiffness of the trajectory at that time. [21, 34, 35] Based on this, the minimization of the CM trajectory slope deviation will grant less fluctuation and more stable movement, as well as minimizing maximum instant torque requirement and power consumption of the mobile platform. In this way more effective design can be selected. The relation example between the mechanisms and their CM trajectory is depicted in Fig. 3.7.

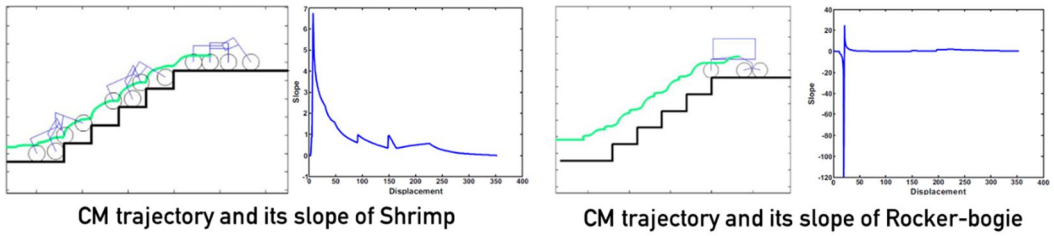

Figure 3.7: Example of the objective function element #1: Minimizing the deviation of the slope of the CM trajectory, the relation example between the mechanisms and their CM trajectory [35]

On the other hand, the backward movement occurrence of the Center of Mass during the movement on a staircases caused by the kinematic shape of the mobile platform is one of the major reason which weakens of the stair climbing ability. When the Center of Mass moving the opposite direction of the desired direction, contact conditions of specific wheels are slightly changed (such as move instantly in reverse directions, etc.) which bring critical failure cases. This can be partially controlled by some control technics such as speed control by wheel Jacobian matrices, but the minimization in the kinematic design phase will ease the whole process related in this situations. Fig. 3.8 shows the backward movement occurrence in the previous research [21].

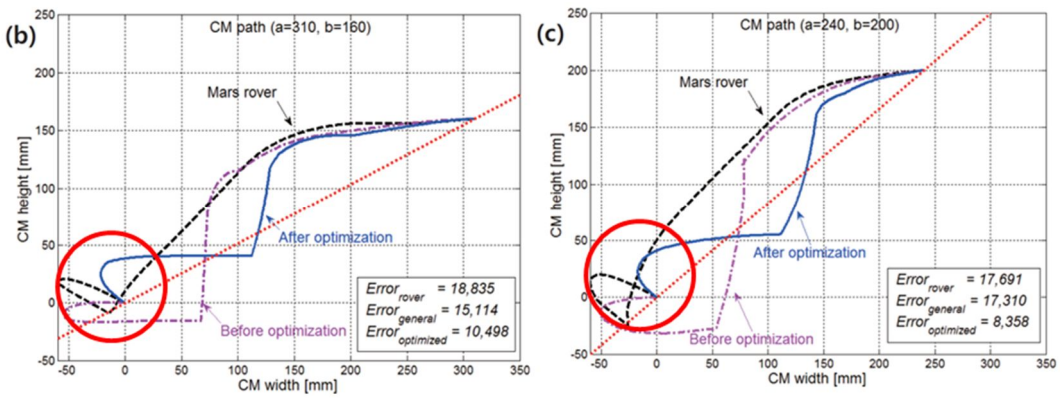

Figure 3.8: Example of the objective function element #2: Minimizing the backward movement, shows the backward movement occurrence in the previous research [21]

3.2.2 Optimization process using GA algorithm

In the previous research, kinematic design link variables of the robot are optimized by the Taguchi method [36-39]. In this research, Signal/Noise ratio concept from the Taguchi method is applied to the objective function, as the smaller-the-best targets of both objective function elements. Three stair structure dimensions suggested before are also applied to the objective function as the noise factors. Four link variables (l_1, l_2, l_3 and l_4) and one wheel radius variable to three wheels (R) are selected as the control factor.

After the problem definition procedure, Genetic Algorithm is implemented to obtain the optimized design variables, by using the optimization algorithm supported by MATLAB. The optimization result from the GA(Genetic Algorithm) process is shown in the next section.

3.2.3 Optimization result and discussion

As mentioned previously, GA algorithm is applied to the optimization procedure. Fig 9 depicts its process and the result. Through the generation progress, The Best, Worst and mean scores (same as the objective function value) are being improved, and the best optimization kinematic design variable is obtained in the fifth generation. The detailed optimization result is shown in Fig.3.10 to Fig. 3.11. Fig. 3.10 and they show the optimized values and the kinematic shape which the optimized design variables are applied. Fig.3.11 explains the detailed comparison between the pre-optimization and the optimized result. Firstly, the red dotted line means the slope of each stairs. The Blue line is the optimized result, while the purple dotted line is the result from the pre-optimization data. The black dotted line came from the result of the mobile robot created previously. As shown in the fig. Y, distinctive improvements are verified through the all stair dimensions.

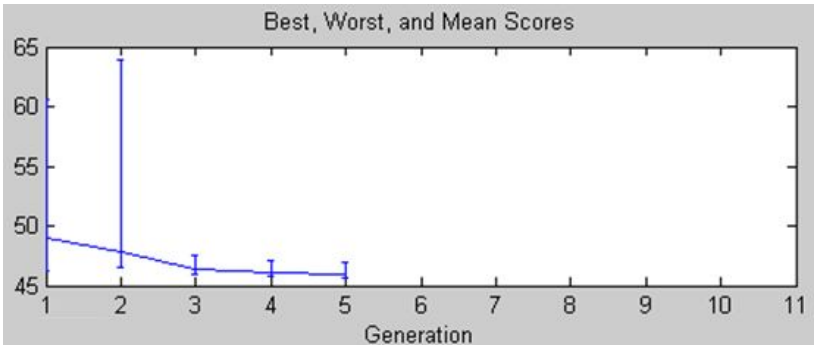

Figure 3.9: Optimization progress using the Genetic Algorithm

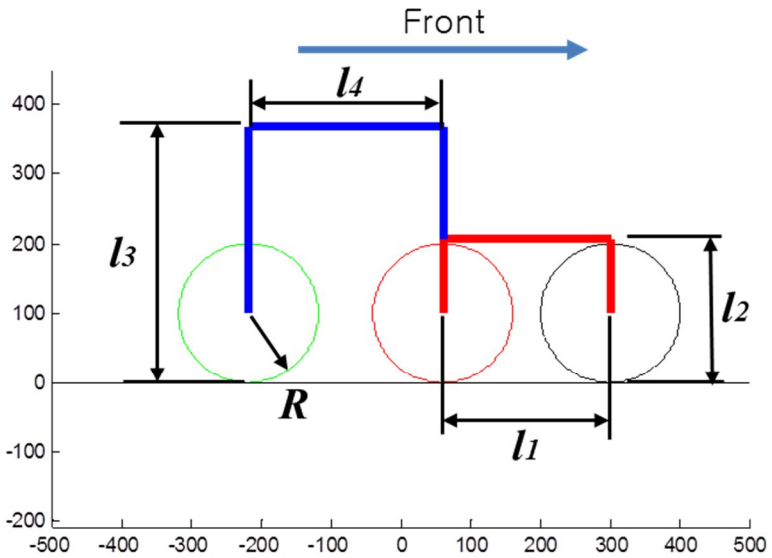

R	l_1	l_2	l_3	l_4
90	240	205	370	280

Figure 3.10: The optimized values and the kinematic shape

300/100	Pre-set	Optimized	Rocker Bogie
Backward	3.936 (-52.3%)	8.244	51.619 (+526%)
Slope Deviation	147.953 (+68.4%)	87.835	87.118 (-0.8%)
y_1	155.825 (+49.4%)	104.322	190.356 (+82.5%)

310/160	Pre-set	Optimized	Rocker Bogie
Backward	50.604 (+180%)	18.091	60.902 (+237%)
Slope Deviation	105.466 (+22.9%)	85.827	170.382 (+98.6%)
y_2	206.674 (+69.4%)	122.009	277.044 (+127%)

255/195	Pre-set	Optimized	Rocker Bogie
Backward	36.988 (+260%)	10.262	55.606 (+442%)
Slope Deviation	148.904 (-15.9%)	176.996	226.105 (+27.7%)
y_3	222.880 (+12.8%)	197.520	337.317 (+70.8%)

Figure 3.11: Comparison between the pre-optimization and the optimized result.

Chapter 4

Kinematic analysis

In the previous section, kinematic design variables are optimized via MATLAB in order to make the mobile platform's CM trajectory close to a straight line and minimize its backward movement during stair climbing sequence. In this section, the kinematic analysis is performed to obtain the most suitable movement direction strategy to maximize efficiency of climbing and descending ability of the mobile platform.

4.1 Description of the kinematics model

The kinematics model of the mobile platform is shown in Fig. 4.1. In 3-D condition, it has six wheels, but the model is expressed in 2-D has only three wheels. The mobile platform is bilaterally symmetric, so the palmar kinematics model can be suitable for conducting the kinematics analysis for the mobile platform. The model has five link parameters: four link lengths (l_1, l_2, l_3 and l_4) and one wheel radius (R), which means all wheel radii are same.

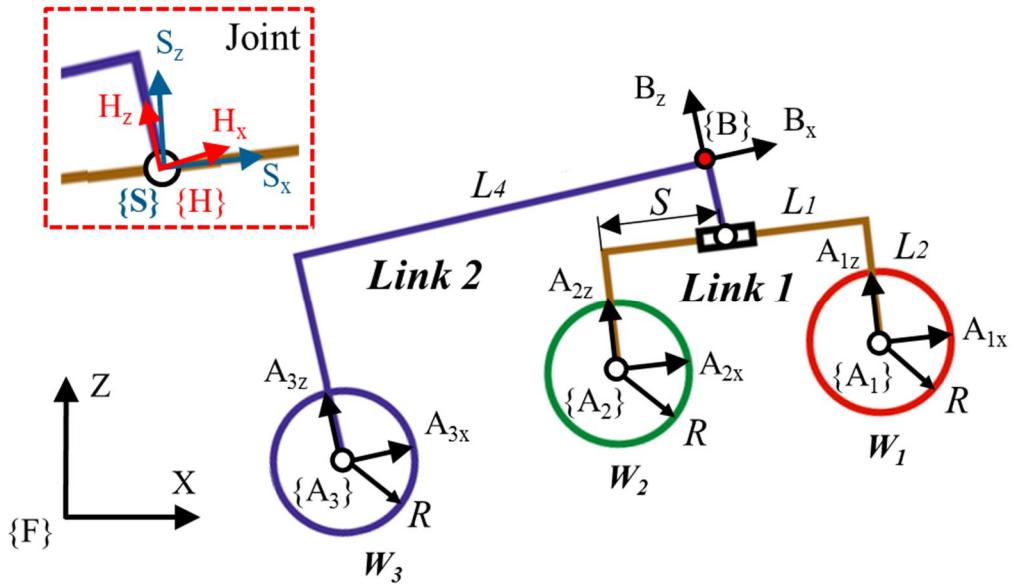

Figure 4.1: Kinematics model of the mobile platform

To improve the mobile platform more efficiently and effectively, all the moving frames are determined based on the 2-D kinematic model of the mobile platform. Fig 4.1 depicts conditions of these frames. The mechanism of the mobile platform consists of two links. Like a rocker-bogie mechanism, these two links can be called by rocker and bogie, which are articulated with each other and connected. But their joint is a hybrid joint which created by combining passive revolute joint and active prismatic joint, instead of a passive revolute joint. The robot's main body is connected to the *Link 2*, and it is expressed in the moving frame {B}. Two moving frames are located at the joint between *Link 1* and *Link 2*, {H} is fixed on the *Link 2* while the another frame {S} is located on the *Link 1*, but it can move by using the mechanism and defined by the slide distance variable *S*. Each wheel axis also has the moving frame, which located at both *Link 1* and *Link 2*, expressed in $\{A_i\}(i=1, 2, 3)$. The frames placed on the same link are parallel to each other, so {B}, {H} and $\{A_3\}$ at *Link 2* are parallel, as well as {S}, $\{A_1\}$ and $\{A_2\}$ are parallel too. Also, the environment is expressed in the fixed frame of {F}.

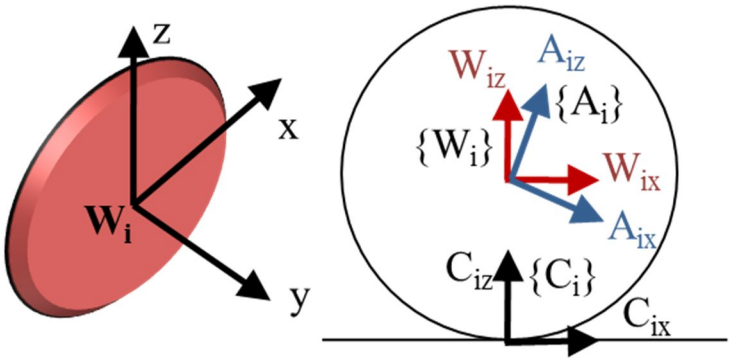

Figure 4.2: Kinematics model of wheels

As shown in the planar kinematics model of the Fig. 4.1, wheels are attached to all links, *Link 1* has two wheels (W_1 and W_2), and *Link 2* has one wheel (W_3). Fig. 4.2 depicts the detailed kinematics model of wheels. As described before, frames $\{A_i\}$ (i=1, 2, 3) are attached to the links. Frames $\{W_i\}$ (i=1, 2, 3) are attached to the center of wheels, so when the wheels are rotating with respect to the links, the frames $\{A_i\}$ (i=1, 2, 3) are stationary, while the frames $\{W_i\}$(i=1, 2, 3) are keep rotating with wheels. The frames $\{C_i\}$ (i=1, 2, 3) are located at the contact point between wheels and the ground, and remain stationary.

4.2 Position transformation graph

All relations between the frames of kinematic model can be expressed by using the position transformation graph. As shown in Fig. 4.3, each relationship of frames can be expressed by its unique corresponding matrix. These corresponding matrices can be classified in variable or constant transformation matrix. For example, if frame A and B are fixed on the same link, the transformation matrix is 'constant one' and expressed in ${}^{A}T_{B}$. Besides, when these frames are fixed on the different link, its transformation matrix is 'variable one' and expressed in ${}^{A}\Phi_{B}$. Matrix $\overline{C}_i$ is an instantaneously coincident frame,

which is stationary relative to the fixed frame [40].

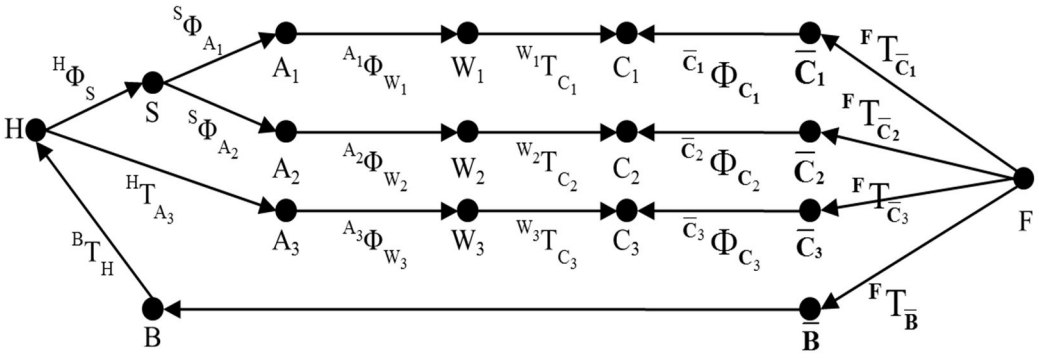

Figure 4.3: Position transformation graph of the kinematics model

4.3 Transformation matrices

As described in the section 4.2, all relationships between frames can be expressed by using the transformation matrices. In this section, all the transformation matrices are derived from the kinematic model of the mobile platform.

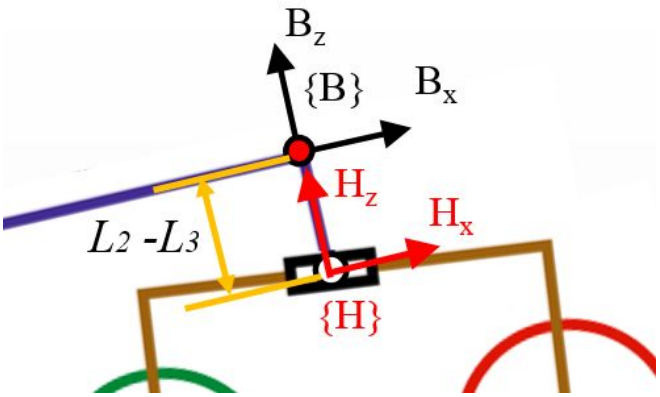

Figure 4.4: The kinematic model for ${}^{B}T_{H}$

$$ {}^{B}T_{H} = \begin{bmatrix} 1 & 0 & 0 & 0 \\ 0 & 1 & 0 & 0 \\ 0 & 0 & 1 & L_2 - L_3 \\ 0 & 0 & 0 & 1 \end{bmatrix} \tag{4.1} $$

Fig. 4.4 shows how the transformation matrix ${}^{B}T_{H}$ can be formulated from the kinematics model. Frame {B} and {H} are fixed to the same link and this makes these frames parallel. So the transformation matrix ${}^{B}T_{H}$ is defined by the distance between the centers of both frames. The distance is fixed constant which is parallel to Z axis and rotation can't affect to this. From this condition, the matrix is described in Eqn. (4.1).

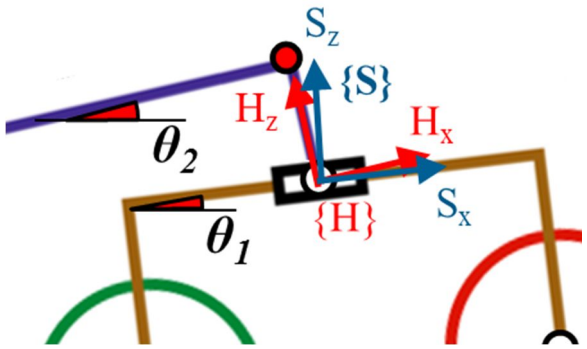

Figure 4.5: Kinematic model for ${}^{H}\Phi_{S}$

The transformation matrix ${}^{H}\Phi_{S}$ can be explained from Fig 4.5. Firstly, centers of both frames {S} and {H} are identical, so the transformation matrix needs to know exact angle between the frames {S} and {H}. ${}^{H}\theta_{S}$ is the angle between frames {S} and {H}, which can be obtained from angles of the two links. θ_1 and θ_2 are the angles between horizontal line and the *link 1* and *link 2*. Derived transformation matrix based from link angles are shown in Eqn. (4.2).

$$ {}^{H}\phi_{S} = \begin{bmatrix} \cos {}^{H}\theta_{S} & 0 & \sin {}^{H}\theta_{S} & 0 \\ 0 & 1 & 0 & 0 \\ -\sin {}^{H}\theta_{S} & 0 & \cos {}^{H}\theta_{S} & 0 \\ 0 & 0 & 0 & 1 \end{bmatrix}, \quad {}^{H}\theta_{S} = \theta_1 - \theta_2 \tag{4.2} $$

${}^{S}T_{A1}$, ${}^{S}T_{A2}$, and ${}^{H}T_{A3}$ are the transformation matrices to define the location of wheel axles on each links. Fig. 4.6 is the kinematics model of *Link 1* to derive the transformation matrices ${}^{S}T_{A1}$ and ${}^{S}T_{A2}$. As described earlier, Frame {S} can be changed, since the slide distance variable *S* can be increased or decreased. The range of the variable *S* is 0 to L_1, so the distances between {S} and $\{A_2\}$ or $\{A_1\}$ can be derived. Both displacements of Z-axis direction are same: L_2, the height of joint from wheel axles to joint frame {S}. Displacements of Z-axis direction also calculated from the full-link length and *S*. Fig. 4.7 is the kinematics model of *Link 2* to derive the transformation matrices ${}^{H}T_{A3}$. As *Link 2* don't have variable like S, this transformation requires only fixed displacement elements to be defined, like link length parameters which already known. From the process described above, these transformation matrices for wheel axles can be obtained, as shown in Eqn. (4.3).

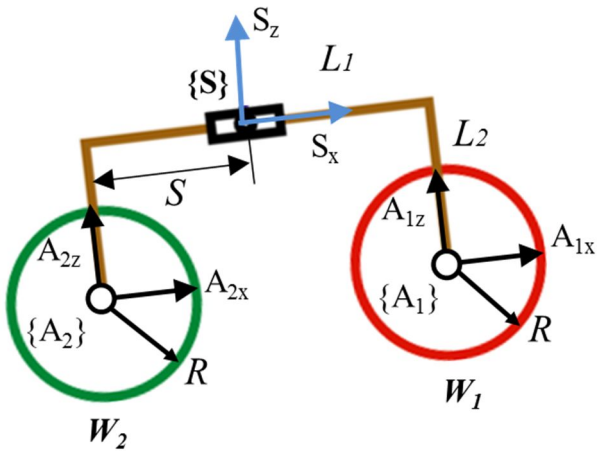

Figure 4.6: *Link 1* kinematic model for ${}^{S}T_{A1}$ and ${}^{S}T_{A2}$

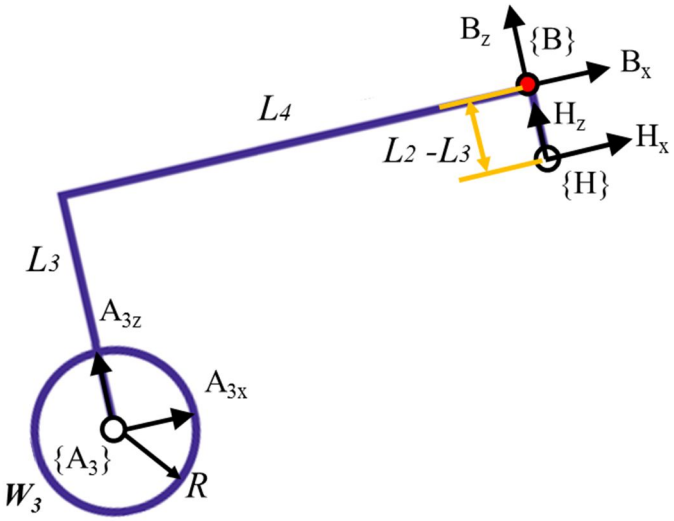

Figure 4.7: *Link 2* kinematic model for ${}^{H}T_{A3}$

$$
{}^{S}\phi_{A_1} = \begin{bmatrix} 1 & 0 & 0 & L_1 - S \\ 0 & 1 & 0 & 0 \\ 0 & 0 & 1 & -L_2 \\ 0 & 0 & 0 & 1 \end{bmatrix} \quad {}^{S}\phi_{A_2} = \begin{bmatrix} 1 & 0 & 0 & -S \\ 0 & 1 & 0 & 0 \\ 0 & 0 & 1 & -L_2 \\ 0 & 0 & 0 & 1 \end{bmatrix}
$$

$$
{}^{H}T_{A_3} = \begin{bmatrix} 1 & 0 & 0 & -L_3 \\ 0 & 1 & 0 & 0 \\ 0 & 0 & 1 & L_2 \\ 0 & 0 & 0 & 1 \end{bmatrix} \tag{4.3}
$$

Derivation process of the transformation matrix ${}^{A1}\Phi_{W1}$, ${}^{A1}\Phi_{W1}$ and ${}^{A1}\Phi_{W3}$ can be explained from Fig. 4.2. Frame $\{W_i\}$ (i=1, 2, 3) are fixed to wheels and maintain inclinations, while the angles of Frame $\{A_i\}$ (i=1, 2, 3) are subjected to the link angles, θ_1 and θ_2. The formulations are given by Eqn. (4.4).

$$
{}^{A_1}\phi_{W_1} = \begin{bmatrix} \cos\theta_1 & 0 & -\sin\theta_1 & 0 \\ 0 & 1 & 0 & 0 \\ \sin\theta_1 & 0 & \cos\theta_1 & 0 \\ 0 & 0 & 0 & 1 \end{bmatrix}
$$

$$
{}^{A_2}\phi_{W_2} = \begin{bmatrix} \cos\theta_1 & 0 & -\sin\theta_1 & 0 \\ 0 & 1 & 0 & 0 \\ \sin\theta_1 & 0 & \cos\theta_1 & 0 \\ 0 & 0 & 0 & 1 \end{bmatrix} \tag{4.4}
$$

$$
{}^{A_3}\phi_{W_3} = \begin{bmatrix} \cos\theta_2 & 0 & -\sin\theta_2 & 0 \\ 0 & 1 & 0 & 0 \\ \sin\theta_2 & 0 & \cos\theta_2 & 0 \\ 0 & 0 & 0 & 1 \end{bmatrix}
$$

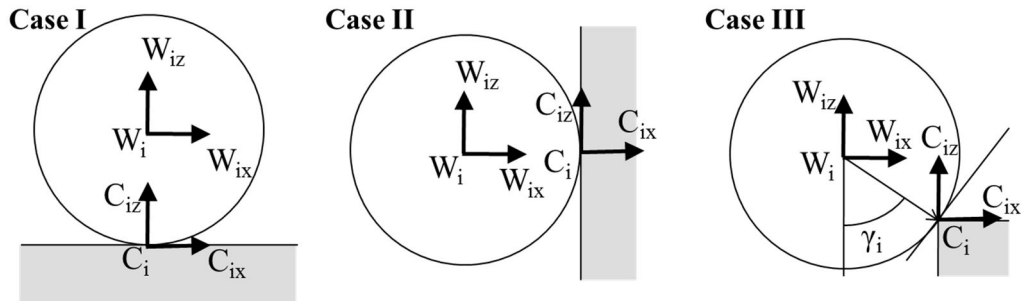

Figure 4.8: Kinematic model of contact angle between wheels and ground

The transformation matrices ${}^{W_1}T_{C_1}$, ${}^{W_1}T_{C_1}$ and ${}^{W_1}T_{C_1}$ are changed by the condition of the contact angle as shown in Fig. 4.8 The contact angle means an angle between a wheel and ground. When a wheel is on horizontal even terrain (as in case I in Fig 4.8), its contact angle is 0°. On the other hand, if a wheel is touched to wall (as in case II in Fig 4.8) its contact angle is 90°. Likewise, when the contact angle is between 0 to 90°, the wheel's contact situation will be likely case III in Fig. 4.8. Based on this contact angle idea, the

transformation matrices ${}^{W_1}T_{C_1}$, ${}^{W_1}T_{C_1}$ and ${}^{W_1}T_{C_1}$ are formulated as described in Eqn. (4.5). γ_i (i=1, 2, 3) are contact angles between each wheel and ground.

$$ {}^{W_i}T_{C_i} = \begin{bmatrix} 1 & 0 & 0 & R\sin\gamma_i \\ 0 & 1 & 0 & 0 \\ 0 & 0 & 1 & R\cos\gamma_i \\ 0 & 0 & 0 & 1 \end{bmatrix}, \quad (i = 1, 2, 3) \tag{4.5} $$

4.4 Jacobian matrices

The Jacobian matrix can be derived from the first-order partial derivatives of a vector-valued function. In the mobile platform cases, the Jacobian matrix can be obtained by differentiation of position transformation matrices [40]. Likewise, the formulation of the Jacobian for W1 can be obtained as Eqns. (4.6) and (4.7).

$$ {}^{\bar{B}}\dot{p}_B = \begin{bmatrix} {}^{\bar{B}}V_{Bx} \\ {}^{\bar{B}}V_{Bz} \\ {}^{\bar{B}}\omega_B \end{bmatrix} = \begin{bmatrix} \cos\theta_2 & \sin\theta_2 & -{}^{B}d_{A_1 z} & \cos{}^{B}\theta_S & -{}^{B}d_{Hz} \\ -\sin\theta_2 & \cos\theta_2 & -{}^{B}d_{A_1 x} & -\sin{}^{B}\theta_S & -{}^{B}d_{Hx} \\ 0 & 0 & -1 & 0 & -1 \end{bmatrix} \begin{bmatrix} {}^{\bar{C}_i}V_{C_1 x} \\ {}^{\bar{C}_i}V_{C_1 z} \\ {}^{A_i}\omega_{W_1} \\ V_S \\ {}^{H}\omega_S \end{bmatrix} \tag{4.6} $$

$$ \textit{where,} \quad \begin{bmatrix} {}^{\bar{C}_1}V_{C_1 x} \\ {}^{\bar{C}_1}V_{C_1 z} \\ {}^{A_1}\omega_{W_1} \\ V_S \\ {}^{H}\omega_S \end{bmatrix} = \begin{bmatrix} R\cos\gamma_1 & 0 & 0 \\ R\sin\gamma_1 & 0 & 0 \\ 1 & 0 & 0 \\ 0 & 1 & 0 \\ 0 & 0 & 1 \end{bmatrix} \begin{bmatrix} {}^{A_i}\omega_{W_1} \\ V_S \\ {}^{H}\omega_S \end{bmatrix} $$

$$\therefore J_1 = \begin{bmatrix} R\cdot\cos\gamma_1\cdot\cos\theta_2 + R\cdot\sin\gamma_1\cdot\sin\theta_2 + {}^{B}d_{A_1z} & \cos{}^{B}\theta_S & -{}^{B}d_{Hz} \\ -R\cdot\cos\gamma_1\cdot\sin\theta_2 + R\cdot\sin\gamma_1\cdot\cos\theta_2 + {}^{B}d_{A_1x} & -\sin{}^{B}\theta_S & -{}^{B}d_{Hx} \\ -1 & 0 & -1 \end{bmatrix}$$

$$\textit{where,} \quad \begin{cases} {}^{B}d_{A_1x} = {}^{B}\prod_{A_1}(1,4) = {}^{B}T_H \cdot {}^{H}\Phi_S \cdot {}^{S}T_{A_1}(1,4) \\ {}^{B}d_{A_1z} = {}^{B}\prod_{A_1}(3,4) = {}^{B}T_H \cdot {}^{H}\Phi_S \cdot {}^{S}T_{A_1}(3,4) \\ {}^{B}d_{Hx} = {}^{B}T_H(1,4) \\ {}^{B}d_{Hz} = {}^{B}T_H(3,4) \\ {}^{B}\theta_S = \theta_1 - \theta_2 \end{cases} \tag{4.7}$$

In Eqn. (4.7), ${}^{B}T_{H}$ (3,4) represents the element of the matrix ${}^{B}T_{H}$, located at third row, forth column. Likewise, ${}^{B}T_{H}$ (1,4) means the element of the matrix ${}^{B}T_{H}$, located at first row, forth column. These expressions can also be applied to the other matrices to formulate other Jacobian matrices, such as J_1 and J_2.

In case of J_2(the Jacobian matrix for W_2) also can be formulated by using very similar process of the Jacobian matrix J_1. The formulation of the Jacobian matrix J_2 for W_2 is expressed in Eqns. (4.8).

$$J_2 = \begin{bmatrix} R\cdot\cos\gamma_2\cdot\cos\theta_2 + R\cdot\sin\gamma_2\cdot\sin\theta_2 + {}^{B}d_{A_2z} & \cos{}^{B}\theta_S & -{}^{B}d_{Hz} \\ -R\cdot\cos\gamma_2\cdot\sin\theta_2 + R\cdot\sin\gamma_2\cdot\cos\theta_2 + {}^{B}d_{A_2x} & -\sin{}^{B}\theta_S & -{}^{B}d_{Hx} \\ -1 & 0 & -1 \end{bmatrix}$$

$$\textit{where,} \quad \begin{cases} {}^{B}d_{A_2x} = {}^{B}\prod_{A_1}(1,4) = {}^{B}T_H \cdot {}^{H}\Phi_S \cdot {}^{S}T_{A_2}(1,4) \\ {}^{B}d_{A_2z} = {}^{B}\prod_{A_1}(3,4) = {}^{B}T_H \cdot {}^{H}\Phi_S \cdot {}^{S}T_{A_2}(3,4) \\ {}^{B}d_{Hx} = {}^{B}T_H(1,4) \\ {}^{B}d_{Hz} = {}^{B}T_H(3,4) \\ {}^{B}\theta_S = \theta_1 - \theta_2 \end{cases} \tag{4.8}$$

In case of J_3(the Jacobian matrix for W_3), the formulation process is different with the other Jacobian matrices, .W_3 is attached on the *link 2*, but W_1 and W_2 are attached on the *Link* 1. So the configurations of transformation matrices for W3 are slightly different with

the other wheels, W_1, and W_2. Based on these conditions, the formulation result of the Jacobian matrix J_3 for W_3 is expressed by Eqns. (4.9) and (4.10).

$$
{}^{\bar{B}}\dot{p}_B = \begin{bmatrix} {}^{\bar{B}}V_{Bx} \\ {}^{\bar{B}}V_{Bz} \\ {}^{\bar{B}}\omega_B \end{bmatrix} = \begin{bmatrix} \cos\theta_2 & \sin\theta_2 & -{}^{B}d_{A_3 z} \\ -\sin\theta_2 & \cos\theta_2 & -{}^{B}d_{A_3 x} \\ 0 & 0 & -1 \end{bmatrix} \begin{bmatrix} {}^{\bar{C}_3}V_{C_3 x} \\ {}^{\bar{C}_3}V_{C_3 z} \\ {}^{A_3}\omega_{W_3} \end{bmatrix}
$$

$$
where, \quad \begin{bmatrix} {}^{\bar{C}_3}V_{C_3 x} \\ {}^{\bar{C}_3}V_{C_3 z} \\ {}^{A_3}\omega_{W_3} \end{bmatrix} = \begin{bmatrix} R\cos\gamma_3 \\ R\sin\gamma_3 \\ 1 \end{bmatrix} \left[{}^{A_3}\omega_{W_3} \right] \tag{4.9}
$$

$$
\therefore J_3 = \begin{bmatrix} R\cdot\cos\gamma_3\cdot\cos\theta_2 + R\cdot\sin\gamma_3\cdot\sin\theta_2 - {}^{B}d_{A_3 z} \\ -R\cdot\cos\gamma_3\cdot\sin\theta_2 + R\cdot\sin\gamma_3\cdot\cos\theta_2 - {}^{B}d_{A_3 x} \\ 1 \end{bmatrix}
$$

$$
where, \quad \begin{cases} {}^{B}d_{A_3 x} = {}^{B}\prod_{A_3}(1,4) = {}^{B}T_H \cdot {}^{H}\Phi_S \cdot {}^{S}T_{A_3}(1,4) \\ {}^{B}d_{A_3 z} = {}^{B}\prod_{A_3}(3,4) = {}^{B}T_H \cdot {}^{H}\Phi_S \cdot {}^{S}T_{A_3}(3,4) \end{cases} \tag{4.10}
$$

Following Eqns. (4.11) can be derived from combination of the Jacobian matrices for each wheel by utilizing Eqn. described above.

$$
\begin{aligned}
{}^{\bar{B}}\dot{p}_B &= \begin{bmatrix} {}^{\bar{B}}V_{Bx} \\ {}^{\bar{B}}V_{Bz} \\ {}^{\bar{B}}\omega_B \end{bmatrix} \\
&= \begin{bmatrix} R\cdot\cos\gamma_1\cdot\cos\theta_2 + R\cdot\sin\gamma_1\cdot\sin\theta_2 + {}^{B}d_{A_1z} & \cos{}^{B}\theta_S & -{}^{B}d_{Hz} \\ -R\cdot\cos\gamma_1\cdot\sin\theta_2 + R\cdot\sin\gamma_1\cdot\cos\theta_2 + {}^{B}d_{A_1x} & -\sin{}^{B}\theta_S & -{}^{B}d_{Hx} \\ -1 & 0 & -1 \end{bmatrix} \cdot \begin{bmatrix} {}^{A_1}\omega_{W_1} \\ V_S \\ {}^{H}\omega_S \end{bmatrix} \\
&= J_1\cdot\dot{q}_1 \\
&= \begin{bmatrix} R\cdot\cos\gamma_2\cdot\cos\theta_2 + R\cdot\sin\gamma_2\cdot\sin\theta_2 + {}^{B}d_{A_2z} & \cos{}^{B}\theta_S & -{}^{B}d_{Hz} \\ -R\cdot\cos\gamma_2\cdot\sin\theta_2 + R\cdot\sin\gamma_2\cdot\cos\theta_2 + {}^{B}d_{A_2x} & -\sin{}^{B}\theta_S & -{}^{B}d_{Hx} \\ -1 & 0 & -1 \end{bmatrix} \cdot \begin{bmatrix} {}^{A_2}\omega_{W_2} \\ V_S \\ {}^{H}\omega_S \end{bmatrix} \\
&= J_2\cdot\dot{q}_2 \\
&= \begin{bmatrix} R\cdot\cos\gamma_3\cdot\cos\theta_2 + R\cdot\sin\gamma_3\cdot\sin\theta_2 - {}^{B}d_{A_3z} \\ -R\cdot\cos\gamma_3\cdot\sin\theta_2 + R\cdot\sin\gamma_3\cdot\cos\theta_2 - {}^{B}d_{A_3x} \\ 1 \end{bmatrix} \cdot \begin{bmatrix} {}^{A_3}\omega_{W_3} \end{bmatrix} \\
&= J_3\cdot\dot{q}_3
\end{aligned}
\tag{4.11}
$$

where,

$$
\begin{cases}
{}^{B}\theta_S = \theta_1 - \theta_2 \\
{}^{B}d_{Hx} = {}^{B}T_H(1,4) \\
{}^{B}d_{Hz} = {}^{B}T_H(3,4) \\
{}^{B}d_{A_1x} = {}^{B}\prod_{A_1}(1,4) = {}^{B}T_H\cdot{}^{H}\Phi_S\cdot{}^{S}T_{A_1}(1,4) \\
{}^{B}d_{A_1z} = {}^{B}\prod_{A_1}(3,4) = {}^{B}T_H\cdot{}^{H}\Phi_S\cdot{}^{S}T_{A_1}(3,4) \\
{}^{B}d_{A_2x} = {}^{B}\prod_{A_1}(1,4) = {}^{B}T_H\cdot{}^{H}\Phi_S\cdot{}^{S}T_{A_2}(1,4) \\
{}^{B}d_{A_2z} = {}^{B}\prod_{A_1}(3,4) = {}^{B}T_H\cdot{}^{H}\Phi_S\cdot{}^{S}T_{A_2}(3,4) \\
{}^{B}d_{A_3x} = {}^{B}\prod_{A_3}(1,4) = {}^{B}T_H\cdot{}^{H}\Phi_S\cdot{}^{S}T_{A_3}(1,4) \\
{}^{B}d_{A_3z} = {}^{B}\prod_{A_3}(3,4) = {}^{B}T_H\cdot{}^{H}\Phi_S\cdot{}^{S}T_{A_3}(3,4)
\end{cases}
$$

As shown in Eqn. (4.11), relationship between each wheel velocity can be arranged. Matrix $\dot{q}_i$ (i = 1, 2, 3) represents the velocity of the corresponding wheel. Based on

these results, velocity ratio of each wheel can be derived by using Jacobian matrices and inverts Jacobian matrices. Eqn. (4.12) shows the calculation process of matrix $\dot{q}_i$ (i = 1, 2, 3).

$$\begin{cases} \dot{q}_1 = (J_1^T \cdot J_1)^{-1} \cdot J_1^T \cdot {}^{\bar{B}}\dot{p}_B \\ \dot{q}_2 = (J_2^T \cdot J_2)^{-1} \cdot J_2^T \cdot {}^{\bar{B}}\dot{p}_B \\ \dot{q}_3 = (J_3^T \cdot J_3)^{-1} \cdot J_3^T \cdot {}^{\bar{B}}\dot{p}_B \end{cases} \tag{4.12}$$

The kinematic analysis including wheel Jacobian matrices can be applied to construct a control strategy of the mobile platform during ascending and descending stairs safely as well as efficiently. The detailed control strategy will be discussed later through the chapter 6 to 7.

Chapter 5

Design and development of the platform

In the previous chapter, the kinematic design parameters of the hybrid-link mechanism mobile platform are optimized by MATLAB optimization algorithms. Based on this optimized result, the mobile platform is designed and constructed. When designing the mobile platform from a kinematic concept to a detailed one, preventing interference between the mobile platform and ground structure or between the mobile platform's parts themselves is essential, so all the predicted cases are checked before manufacturing process.

Sensors and actuators are selected based on the detailed requirements. And all related parts are installed in hallow space of the robot body and links to achieve the durability during operation. These instruments are controlled by main controller(Compact RIO), and it is located at main body. By this structure, mobile platform can communicate with the laptop or personal computer with LAN cable or Wi-Fi signal. Power is supplied by AC cable to SMPS which attached to the mobile platform′s body.

5.1 Outline of the mobile platform

The CAD model is created based on the optimized kinematic design parameters obtained from the section 3. Fig. 5.1 shows the CAD model and its kinematic model. As shown in the Fig 5.1, the kinematic model and CAD model has the coincidence layout. Ready-made wheels which have same radius of the kinematic optimization result are applied to the real mobile platform construction.

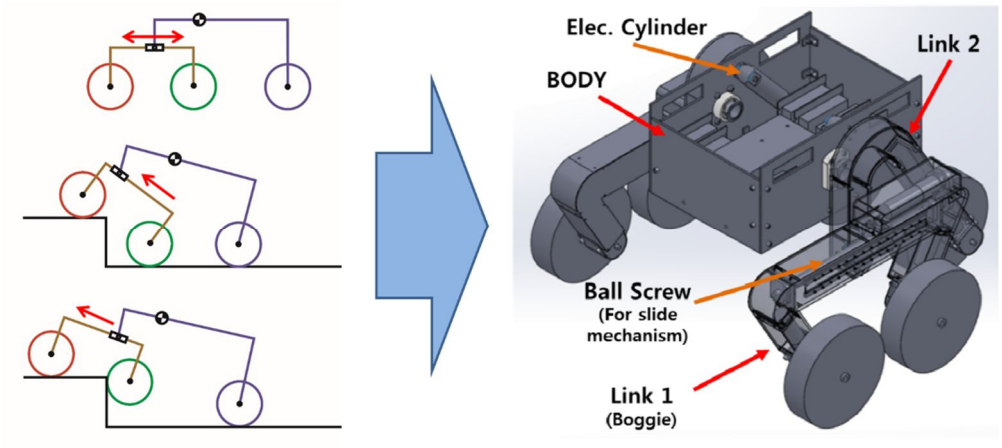

Figure 5.1: Comparison between the kinematics model and the CAD model of the mobile platform

The constructed prototype of the hybrid-link mechanism mobile platform is shown in Fig 5.2. The mobile platform is constructed based on the CAD model depicted in Fig 5.1. The size of the mobile platform is 650 mm (W) X 600 mm (L) X 460mm (H). And the weight of the real mobile platform is 35.5 kg. Most parts of the mobile platform are made of aluminum alloy to reduce weight for efficient stairs-climbing. Steel materials applied to the parts where high strength and rigidity are required, such as wheel shafts or joints. The maximum speed of the mobile platform is limited to 2 m/sec considering safety and stability. Still this mobile platform can move with faster speed by using the maximum performance of the wheel driving motors.

When the mobile platform needs to change its direction, it does not use additional steering mechanism. Instead of that, the mobile platform can enable steering by using its separated wheel speed control. This All-Wheel-Drive control grants the ability of 360 degree turn on a fixed spot. As mentioned before, electrical power is supplied from outside via cable, while the communication signal between the terminal laptop is established via Wi-Fi.

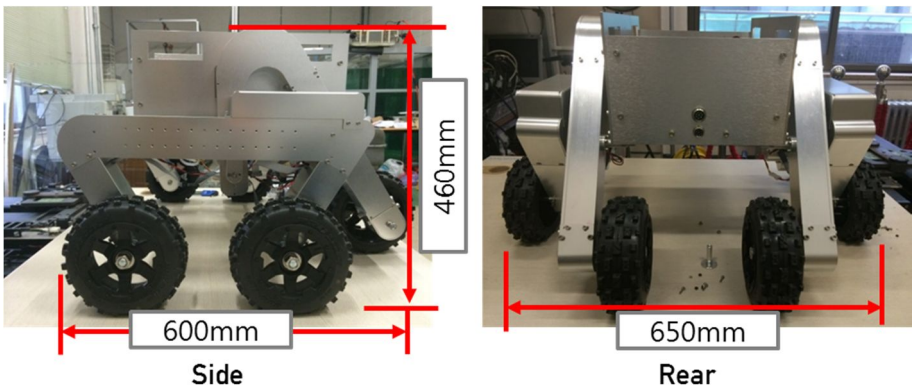

Figure 5.2: Manufactured mobile platform and its size

5.2 Mechanical parts

In this section, mechanical parts which consists the mobile platform are introduced and explained. Body and links are designed based on the kinematic optimized result. Also, preventing interferences between the mobile platform and ground structure or between the mobile platform parts during operation on the stairs was considered during process. Counter-weights and safety legs are calculated based on the simulation so that they can be utilized effectively. 2D-drawings are created by using AUTOCAD, based on the 3D models created by SOLIDWORKS.

5.2.1 Body

The main body contains various electrical components as shown in Fig. 5.3. Firstly, CompactRIO, the main controller is installed at center of the body, while EPOS2s, the

eight actuator drivers for wheels and slide joint position actuators are placed around the CompactRIO. Also inclinometer for body angle sensing and 2-D laser scanner is installed at body. The pitch angle is controlled by two linear actuators, connected between *Link 2* and body. Also Two SMPS are installed to supply DC power to the whole mobile platform components. The connections between *link 2* and body are protected by hollow shaft for connections and preventing interference between parts.

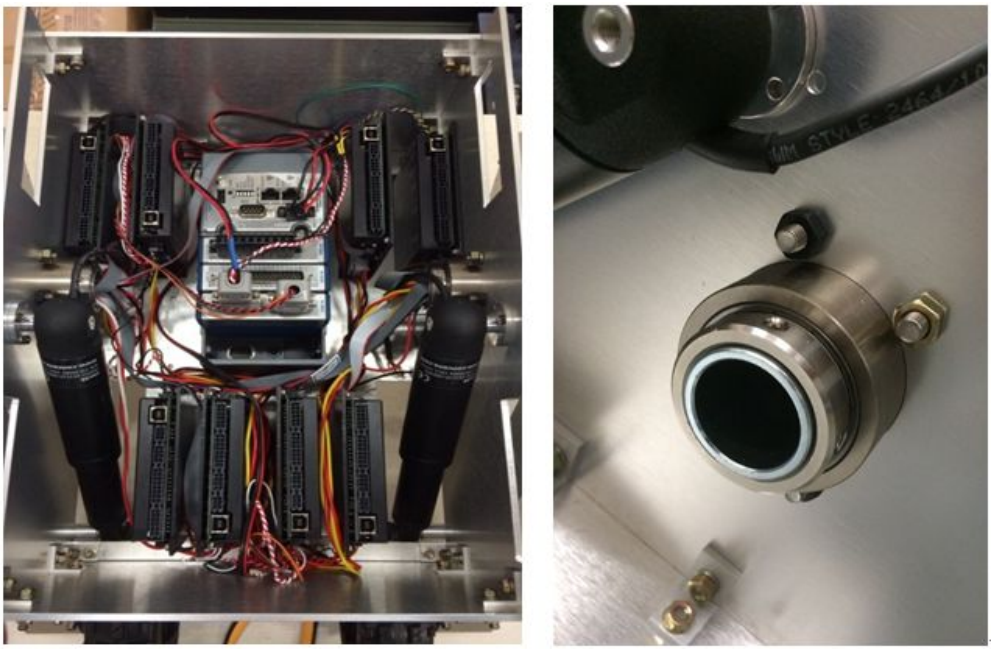

Figure 5.3: (a) Inside of the mobile platform body (b) The hollow shaft between body and *link 2*

Also Fig. 5.4 shows the upper cover of the mobile platform body, which are made of ABS and aluminum. This shape of the upper structure expresses utilization capability of the platform as a telepresence mobile platform controlled remotely, as well as extensibility by attaching various modules.

Figure 5.4: The mobile platform with upper cover parts attached

5.2.2 *Link 1* and *Link 2*

Inclinometers and slide/wheel actuators are installed in *Link 1* and *Link 2*. Most of wire, inclinometers and motors are located at inside of the hollow area of links, so that they can be protected from external risks. The joint between *Link 1* and *Link 2* is not fixed to grant free movement, because of that connection wire between *Link 1* and *Link 2* is exposed, so plastic outer cases are applied to cover the wires. *Link 2* is connected with body by using the hollow shafts and linear actuators while *Link 1* and *Link 2* are connected with moveable rotational joint as described before. The rotational joint between *Link 1* and *Link 2* can move their position on the *Link 1* by using the ball-screw mechanism. Slide motors are connected parallel to the ball screw axles by pinion gears. Fig 5.5 shows these configurations.

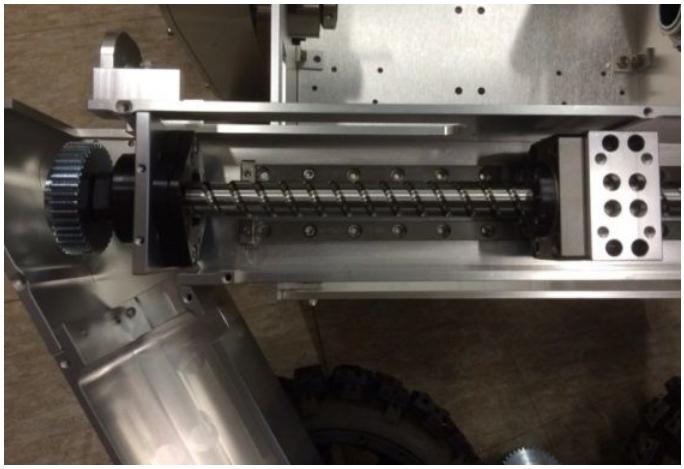

(a)

(b)

Figure 5.5: The inside configuration of the links. (a) *Link 1* (b) *Link 2*

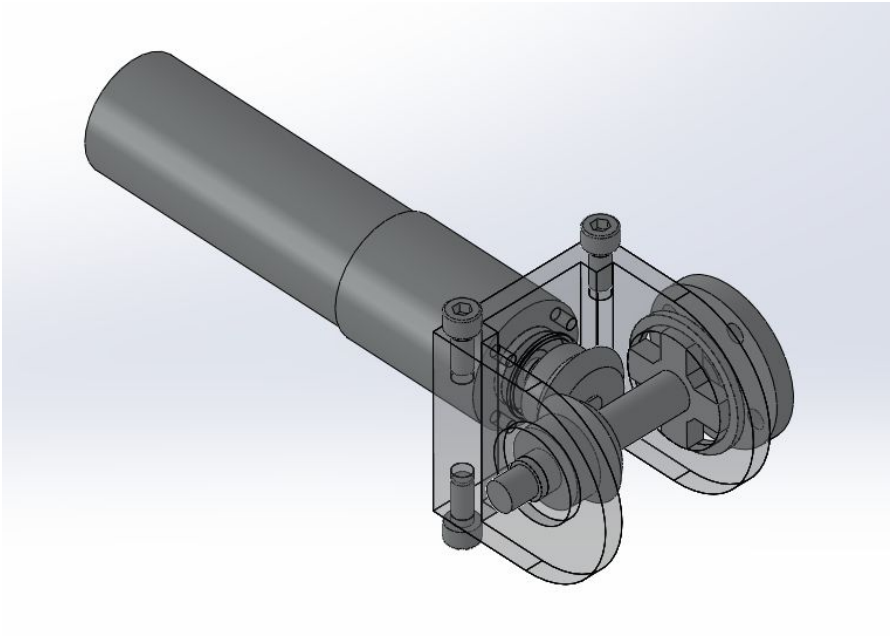

(a)

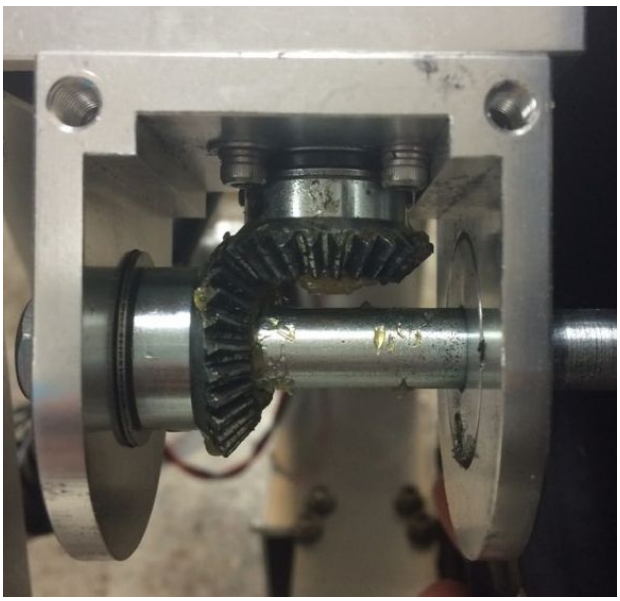

(b)

Figure 5.6: The driving motor module (a) 3-D modeling (b) bevel gear area close-up

5.2.3 Driving motor module

Every driving motors consists a driving motor module. Motor and wheel axles are connected perpendicularly by bevel gears while all axles are supported by bearings. These gear compositions are covered by U-shaped thin shell, to be protected from external environments. Fig.5.6 shows the 3-D model and close-up of the driving motor modules gear area.

5.2.4 Counter weight

A center of mass calculation during the mobile platform production indicates that the center of mass is biased towards backward. As depicted in Fig. 5.7, the center of mass before adjustment is stable on plane surface, but it can be dangerous when climbing staircases. This can be solved fundamentally when the new mobile platform is constructed based on the feedback from the tests, so counter-weight installation is performed based on the calculation to move the center of mass forward enough to secure the stability in the proto-type stage.

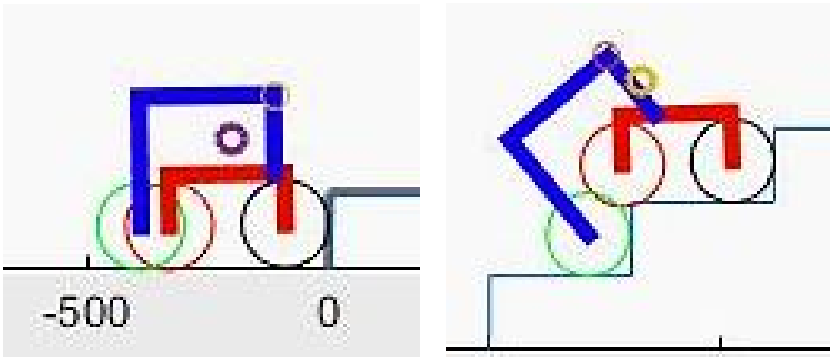

(a) (b)

Figure 5.7: The center of mass of the mobile platform before installing counter-weights (a) on a plane surface (b) Critical posture while climbing stairs

Counter-weight conditions

To install counter-weight to the mobile platform effectively, calculation process based on the install condition identification is essential. A detailed counter-weight install conditions are depicted in Fig.5.8. Firstly, the aim of the counter-weight installation is moving the center of mass forward as much as possible. When the center of mass is relocated to the forward direction, this will prevents front wheel lifting situation which can cause falling down, the most critical failure of the mobile platform. On the other hand, available counter-weight installation position is limited to two areas: front area of body frame and hollow area around wheel 1 axis of *Link 1*, and available maximum weight are different based on the volume limitations. As the last calculation constraints, maximum installation weights are derived from the motor load limitation and body weight balance condition to prevent falling prone of the body and *link 2*. Based on these constraints, appropriate counter weight setting value can be calculated.

Counter-weight installation

By using the constraints determined above, the maximized counter-weight values for body and *Link 1* area can be derived. The center of mass of the mobile platform while climbing stairs can be calculated from MATLAB simulation. By applying this process with the constraints, the optimized counter-weight value is obtained, as shown in Fig. 5.9.

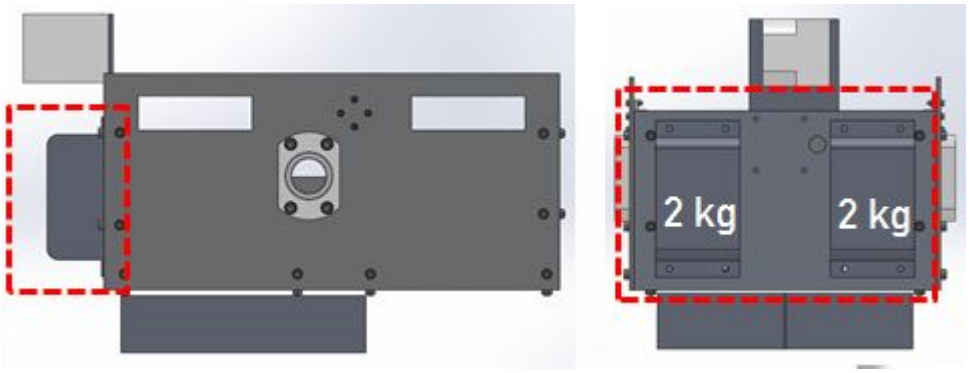

(a)

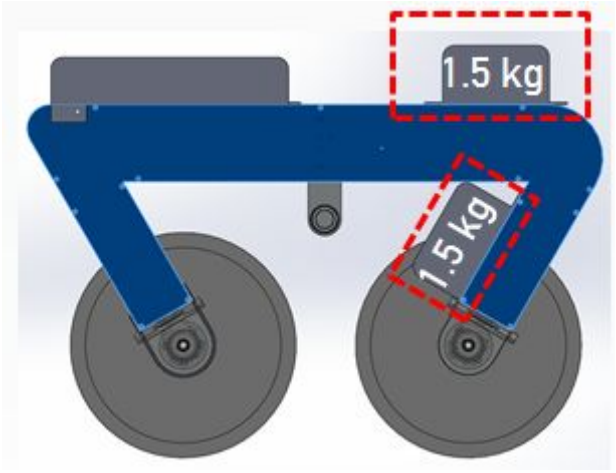

(b)

Figure 5.8: Possible Counter weight installation positions and maximum weight (a) body area (b) *Link 1* area

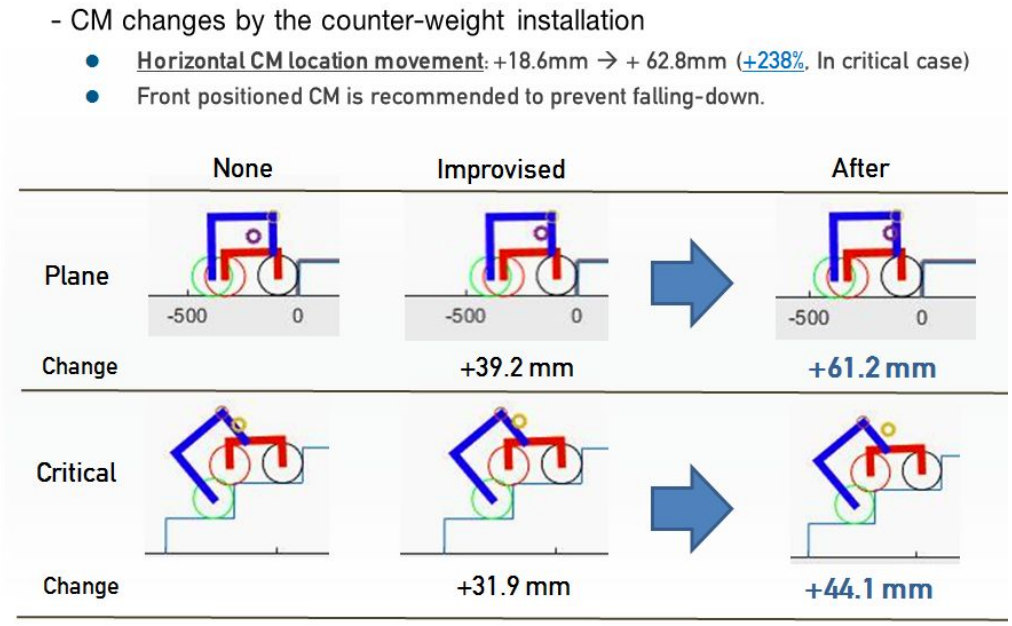

Figure 5.9: Change of the center of mass by applying the optimized counter weight value

Fig. 5.10 shows installation of the counter-weight to the mobile platform. Each counter-weight modules are made of lead material, covered by aluminum cases, installed at the outside of the mobile platform body and *Link 1*. The calculated results are used as the exact weight of each counter weight modules.

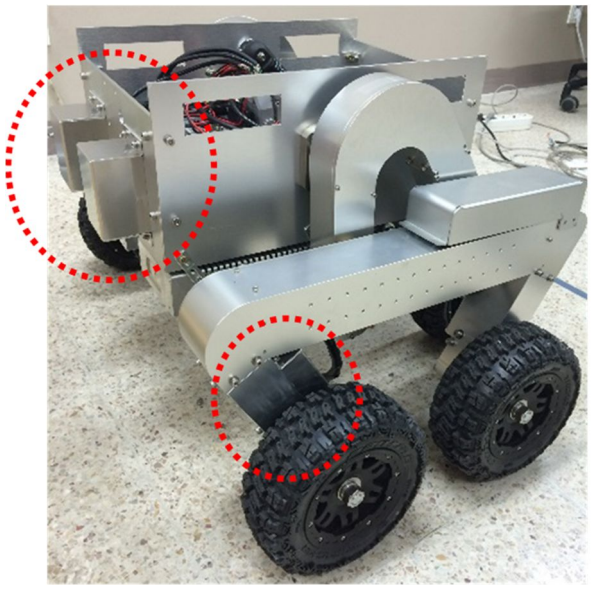

(a)

(b)

Figure 5.10: Installation of the counter-weight to the mobile platform: (a) Overall (b) detailed view of *Link 1* counter-weight

5.2.5 Safety legs

The mobile platform must prepare occurrences of the failure situations during the stair ascending and descending process. The worst case of the failure is falling down of the mobile platform, caused by the front wheel lifted posture. As a countermeasure of this case, Safety legs are designed and attached to *link 2*.

The safety legs are designed based on the conditions listed below: A. Simple, light-weight structure and independent from actuators. B. Do not interfere with staircases or other mobile platform components during stair climbing. C. When the falling down imminent, make contact with stair surface before other structures do and support the mobile platform from behind of the rear wheels to prevent further damage.

The safety legs are designed and manufactured based on the conditions explained above. The safety legs are made of 3t aluminum plate to obtain both light-weight and rigidness characteristics. And by applying statically analyzed result from Solidworks simulation module, each leg can endure more than 150N while under its yield strength, as shown in the Fig 5.11 (a). Also Fig. 5.11 (b) depicts its displacement calculation result, displacement is less than 0.7mm when 150N applied to one safety leg. As the final step of the process, the manufactured safety legs are installed on *link 2* as shown in Fig. 5.12.

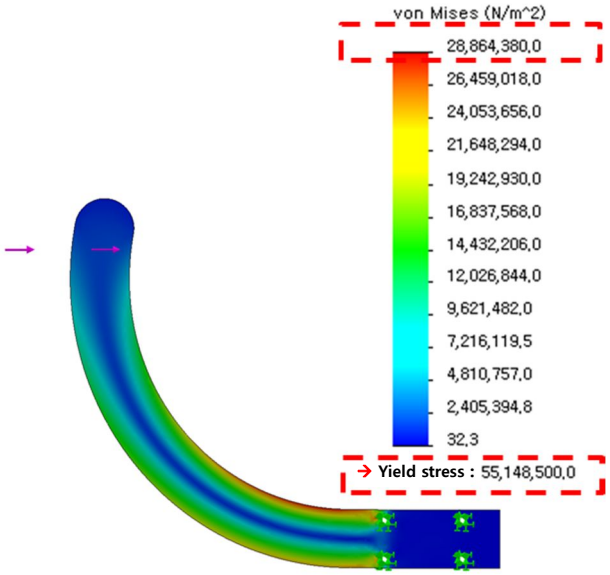

(a)

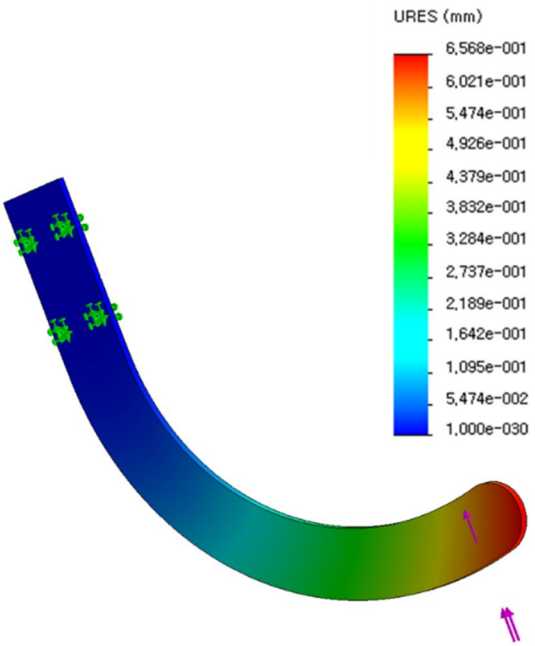

(b)

Figure 5.11: Design and analysis of the safety legs (a) Stress analysis (b) Strain analysis

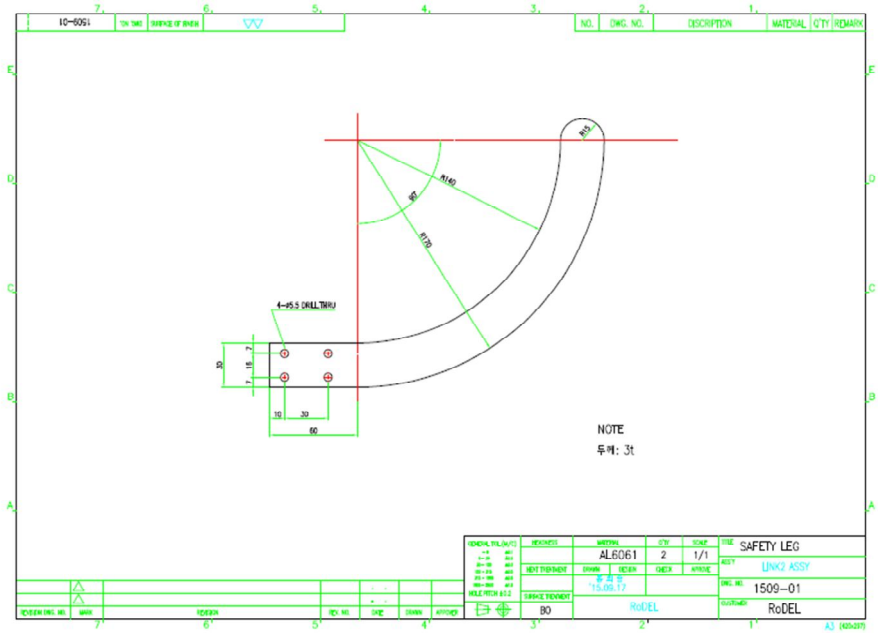

(a)

(b)

Figure 5.12: Production of the safety legs (a) Drawing (b) Installed safety legs on *link 2*.

5.3 Electrical parts

The electrical parts for the mobile platform are consisted with main control units, actuators, sensors, and power supply. These electrical parts are selected based on the performance requirement. The detailed list of the electrical parts will be shown in section 5.4.

5.3.1 Main control components and software

Compact Rio functions as central controller, as it governs the most of electrical components by communicating with sensors and controlling except for the power supply. This controller communicates with the terminal laptop, with a wireless AP unit connected with a LAN cable. CompactRIO connected with dedicated modules such as analog inputs and outputs for sensors and linear actuators, as well as CAN communication module to establish CAN communication between DC servo motors and their drivers.

Basically LABVIEW functions as major control software, but MATALB is also applied as a processing module for specific calculation section to implement complicated algorithm. Control algorithm software is constructed and compiled by LABVIEW, and it is installed to CompactRIO. Instruments with LABVIEW installed such as laptops and personal computers are act as terminals through LAN cables or Wi-Fi. Fig.5.13 depicts the communication scheme between the terminal laptop and CompactRIO control center module.

Figure 5.13: LABVIEW Monitoring by laptop and communication establishment with CompactRIO module.

5.3.2 Motors & Actuators

DC servo motors and dedicated drivers shown in Fig. 5.14 (a) are selected components for slide joint and wheel actuator. 6 units are selected for wheels, the other 2 units are applied slide joints, and communicate with CAN module of CompactRIO. These servo motors and drivers are supplied from MAXON. These motors are selected based on the requirements list suggested in chapter 2.

Electric linear actuators are connected between body and *Link 2* so that the body can maintain its horizontal profile during stair climbing process by controlling pitch angle of body frame. They receive voltage signals from CompactRIO's analog output module, and can stretch its length up to 51mm. The linear actuators are shown in Fig 5.14 (b).

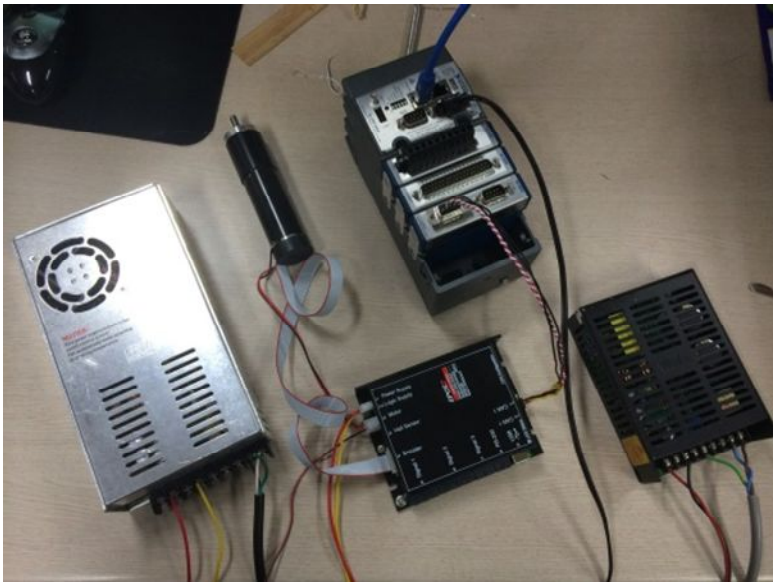

(a)

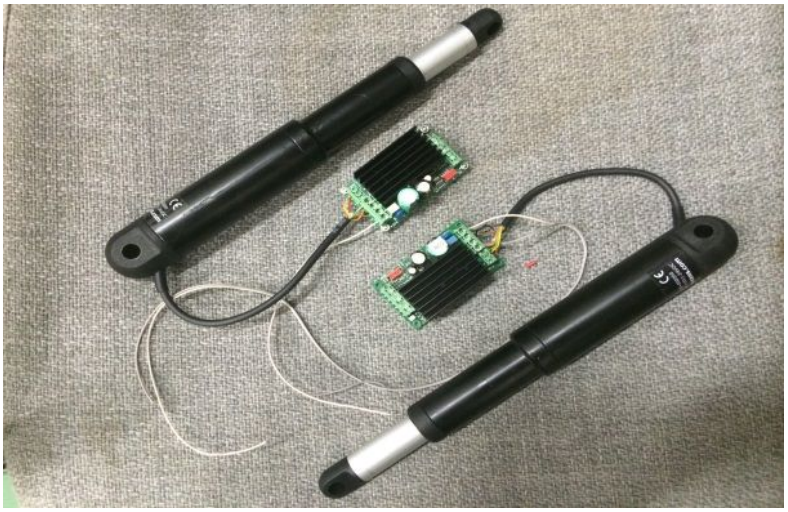

(b)

Figure 5.14: Actuator units (a) DC servo motors and drivers for slide and wheel movements (testing scene) (b) Electrical linear actuator for body stabilizer

5.3.3 Power supply

To maximize the mobile platform's mobility, adopting charged batteries for the power supply is the optimal solution for mobile platform. But the mobile platform constructed in this research is a prototype and focused on the implementing mechanism and control algorithm verification. Therefore SMPS is selected for alternative power supply for the mobile platform. Two 350W SMPS are installed at underneath of body, as shown in the Fig. 5.15. This is the only wired connection between the mobile platform and external circumstances.

Figure 5.15: Installing SMPS to the body frame

5.3.4 Sensors

Total five inclinometers are installed at each link and body to identify the actual angles of the links and the body during stair climbing process. Voltage output is changed from 0.5 V to 4.5 V due to inclinometers angle change from -90 to 90 degrees. From the voltage signal explained above, Body can maintain its horizontal position while climbing stairs, as well as the posture can be identified from link angles. Fig. 5.16 shows the installed inclinometers on links.

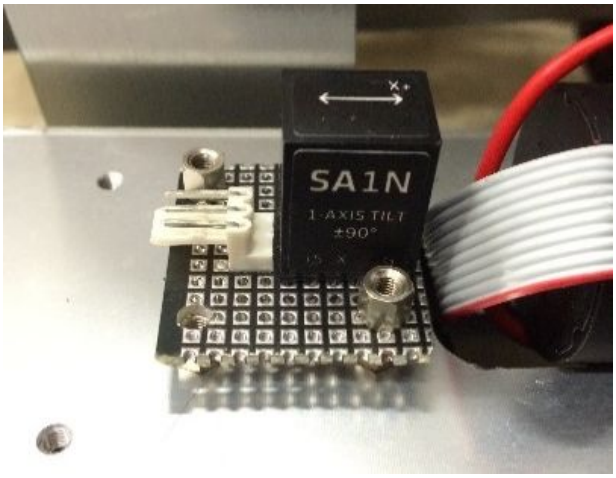

(a)

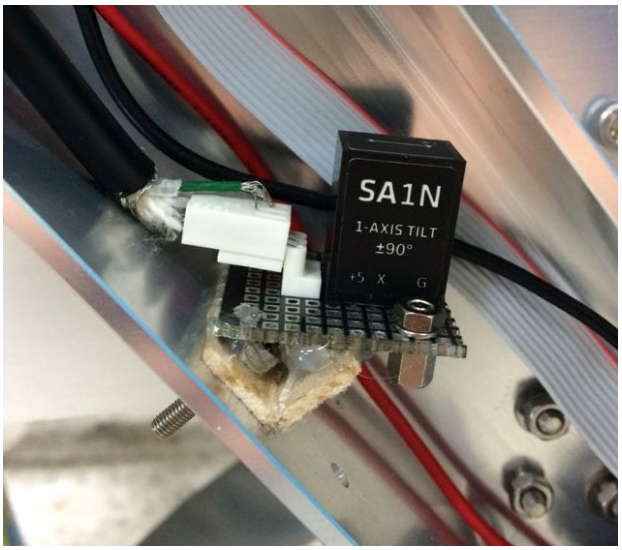

(b)

Figure 5.16: Inclinometers installed on links (a) *Link 1* (b) *Link 2*

2-D laser scanner is a product from Hokuyo Inc., selected as a scanning instrument to obtain stair shape for the mobile platform. The laser scanner can communicate with other instruments by RS-232 or USB 2.0. As shown in Fig. 5.17, the laser scanner installed

perpendicular, in front case of the body case. The scanning range of this laser scanner is from 50mm to 10 meters, with the under 1% of scanning error.

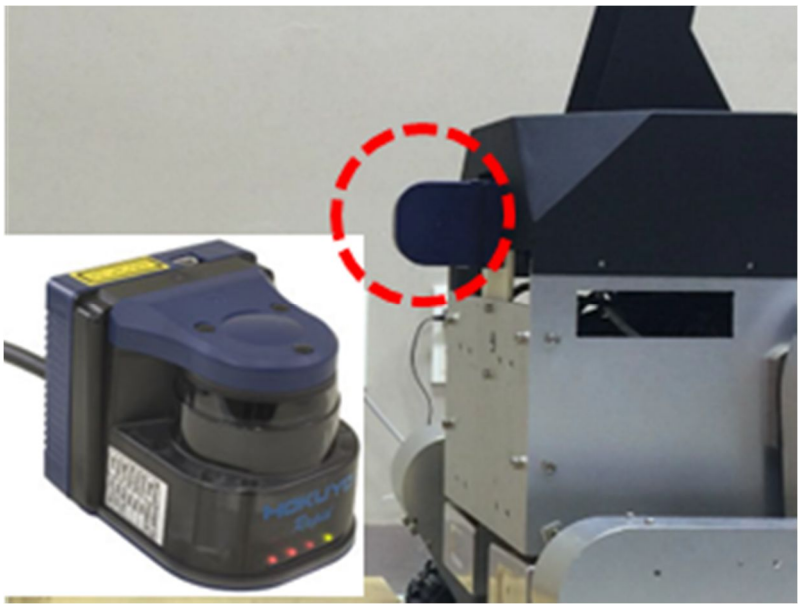

Figure 5.17: Hokuyo 2D Laser scanner at the front of the mobile platform body

5.4 Detailed design of the mobile platform

Based on the explained mechanical and electrical components above, detailed design of the mobile robot is completed. In this section, the assembly drawings and electrical parts list are presented. Detailed assembly drawings are shown in Fig. 5.18 through Fig. 5.24. Table 5.1 shows an electrical parts list including sensors and actuators.

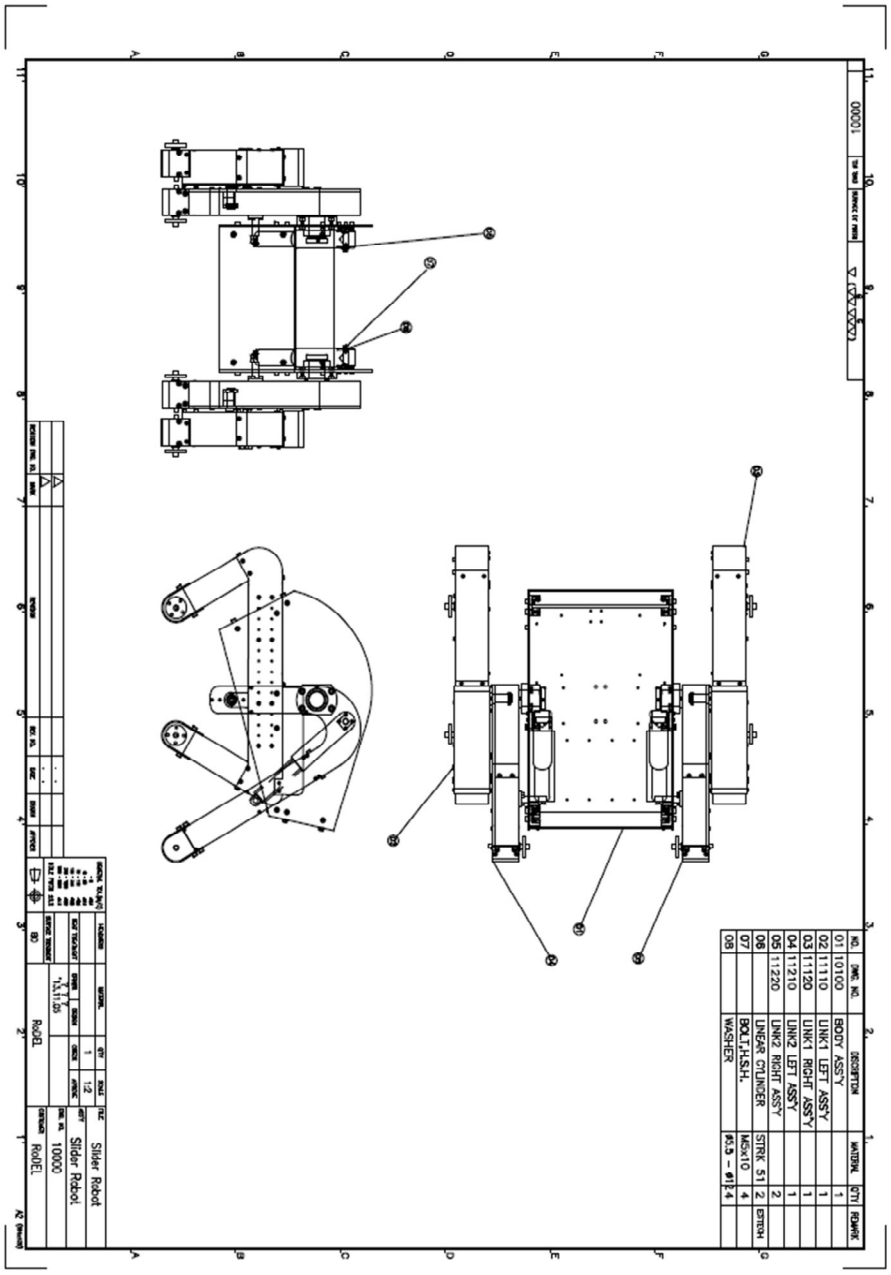

Figure 5.18: The detailed drawing of the mobile platform assembly

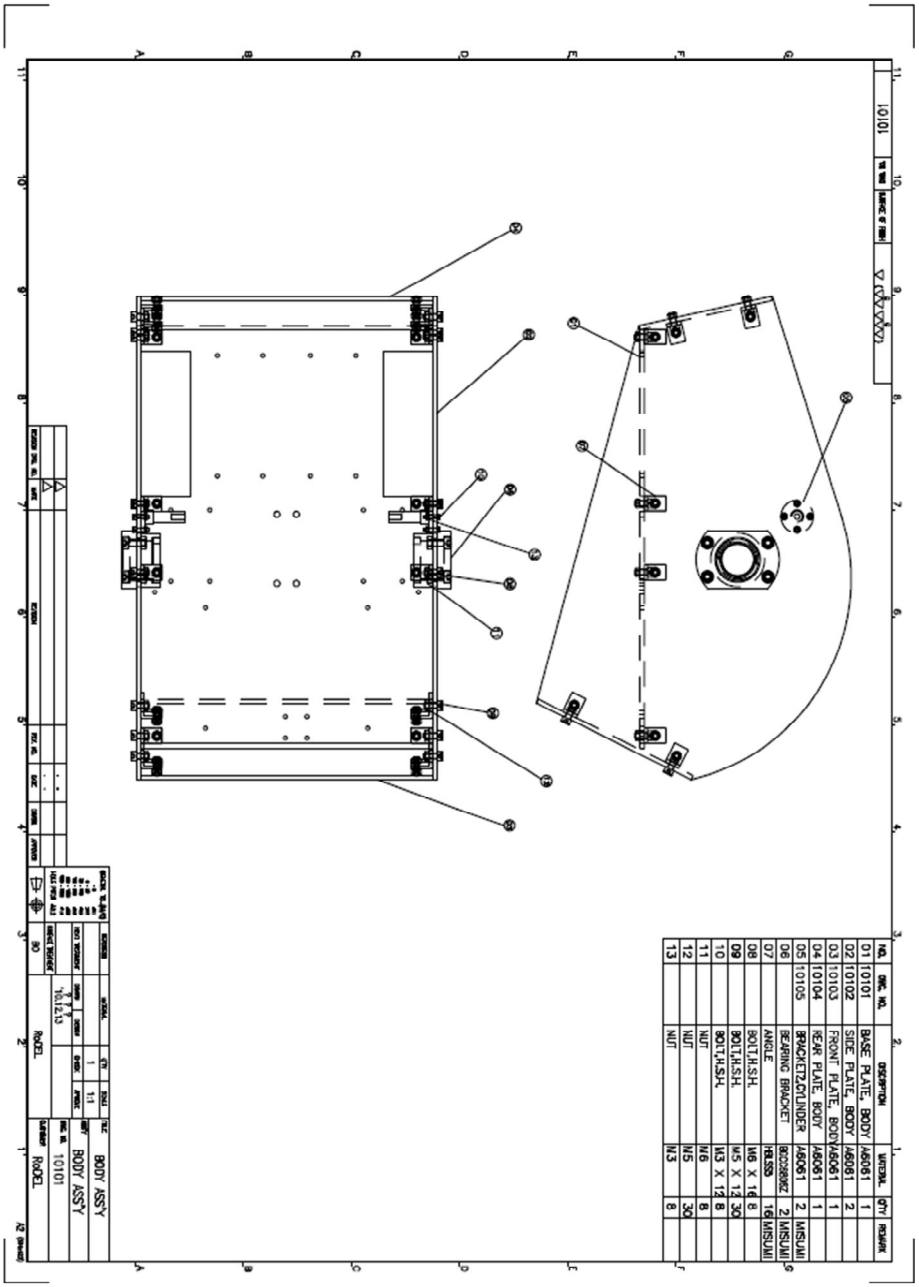

Figure 5.19: The detailed drawing of the mobile platform's body frame

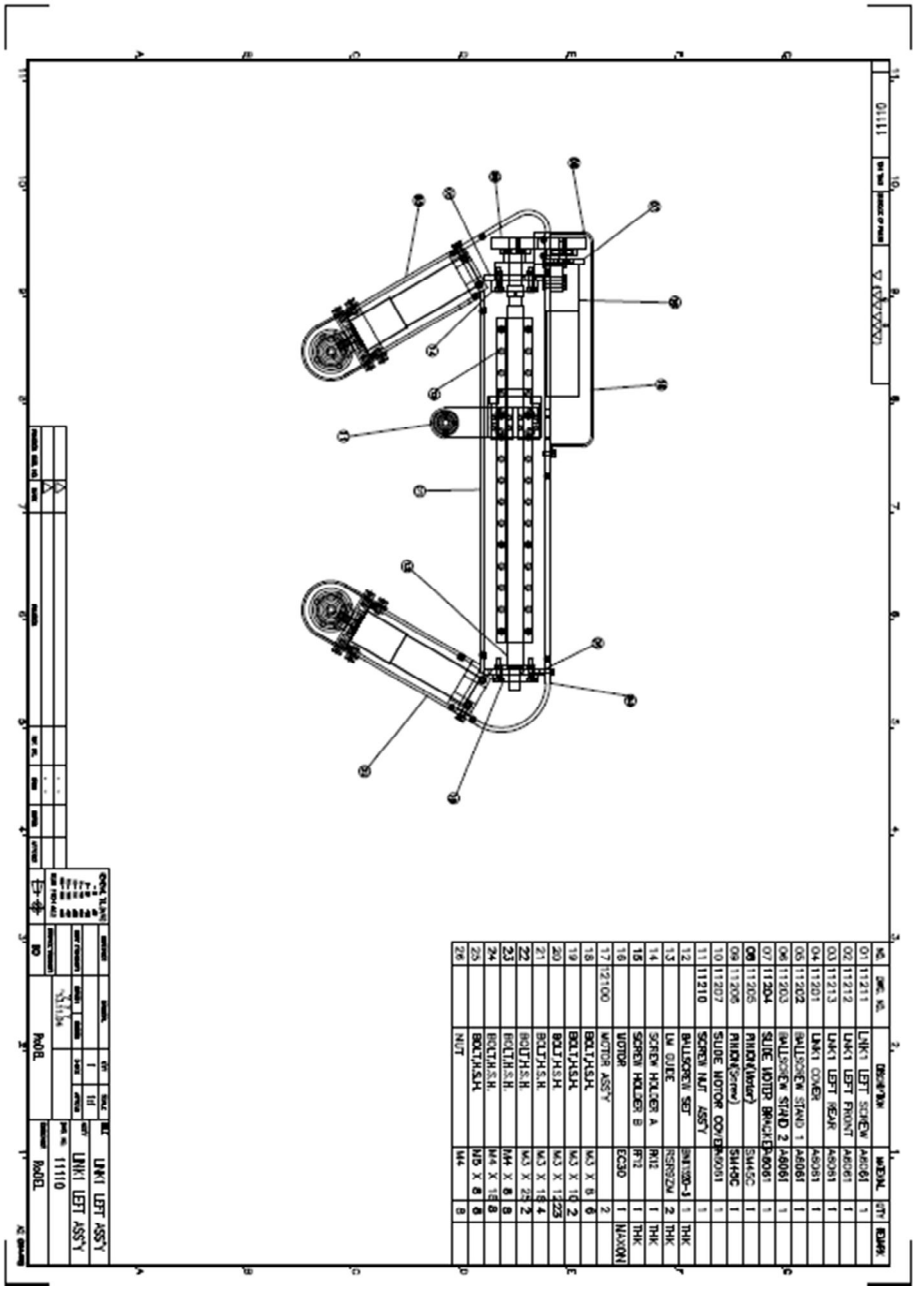

Figure 5.20: The detailed drawing of the mobile platform's left *Link 1*

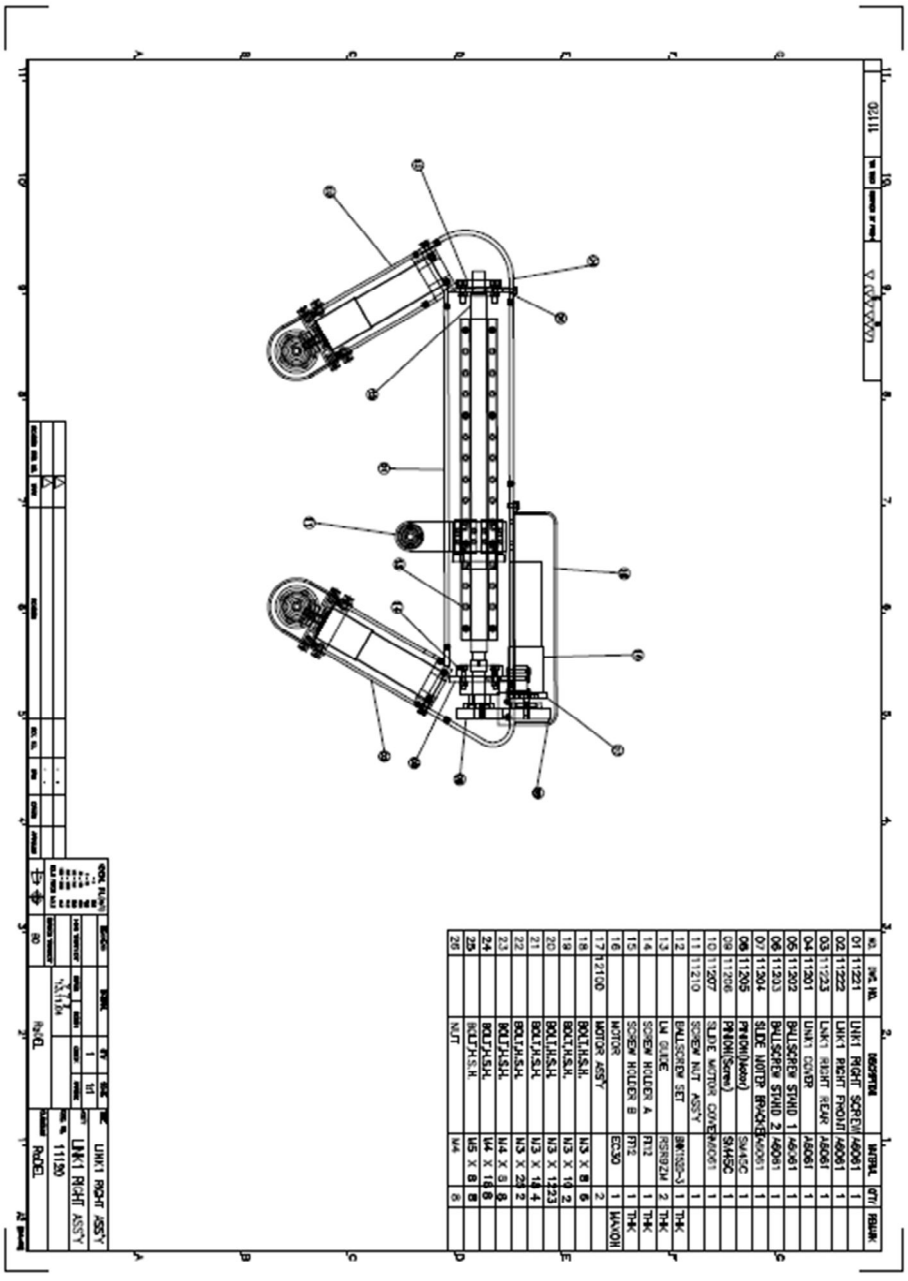

Figure 5.21: The detailed drawing of the mobile platform's right *Link 1*

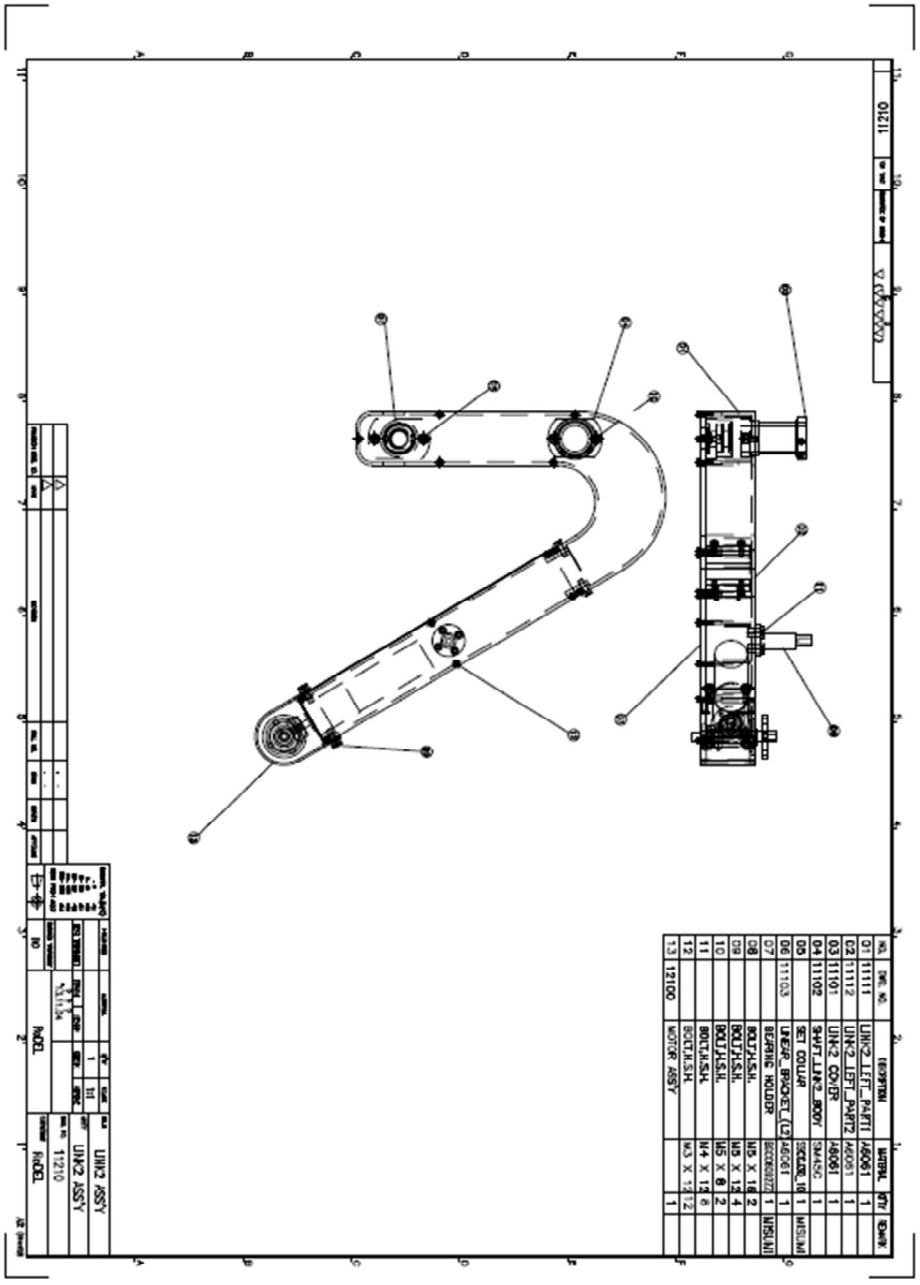

Figure 5.22: The detailed drawing of the mobile platform's left *Link 2*

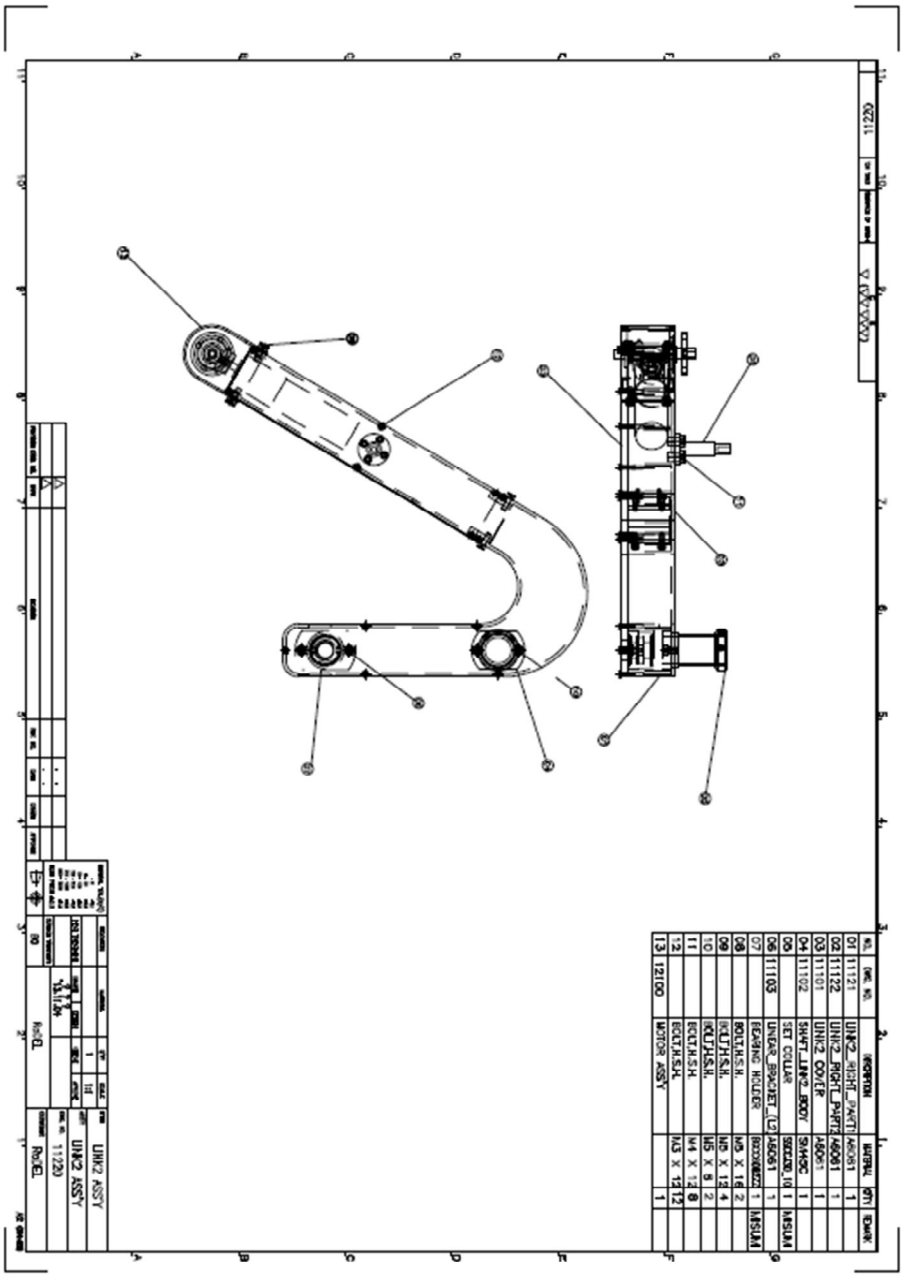

Figure 5.23: The detailed drawing of the mobile platform's right *Link 2*

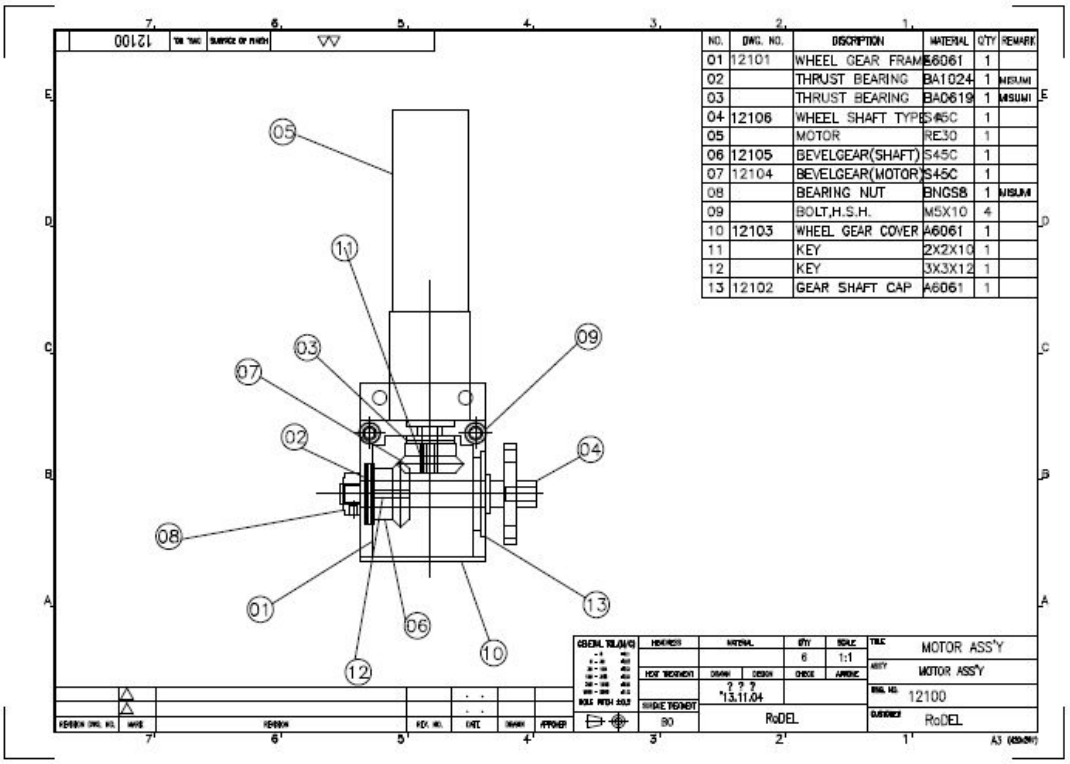

Figure 5.24: The detailed drawing of the motor assembly

Table 5.1: Electrical parts list of the mobile robot

Name	Specification	Number
Main controller	National Instruments cRIO-9024 w/ modules	1 EA
Motor (Wheel driving)	Maxon RE30, 60W, 111:1, 3-ch encoder	6 EA
Motor (Slide joint)	Maxon RE30, 60W, 51:1, 3-ch encoder	2 EA
Motor driver	Maxon EPOS2 50/5	8 EA
Electrical cylinder	CONCENS con35, 50 mm stroke	2 EA
Electrical cylinder driver	CONCENS C2-20, position controller	2EA
SMPS	Meanwell NES-350-24	2 EA
2D Laser Scanner	Hokuyo UBG-04LX-F01, 60 to 4000 scan range, 28ms scan time	1 EA
Inclinometer	DAS SA1N 1-axis, ±90°	5 EA

Chapter 6

Unknown stair climbing strategy with Basic drive control

It is highly predictable situation that the mobile platform will encounter stairs with unknown dimensions during its movement. In the previous research, Look-up tables for specific stairs are created and applied to the rocker-bogie robot to determine the wheel speed direction [21], this method failed to overcome the new staircases with unknown dimensions. To solve this problem, stair climbing process including unknown stairs is created by adopting 2-D scanner to obtain stair dimensions in this chapter.

Appropriate movement direction for wheels and slide actuators are essential for successfully performing stair climbing ability. Individual speed direction for each wheels and contact angle estimation result between each wheel and stair structure are obtained from calculated wheel Jacobian matrices. Meanwhile, maintaining slide joint position is also important to keep the mobile platform's stability in best condition while ascending or descending staircases. Concept idea, detailed process of the basic actuator control architecture including stair dimension detection process for unknown stairs and climbing

ability test result of the mobile platform when the control architecture is applied will be presented in this chapter.

Section 6.1 introduces the overall stair ascending and descending process. Acquisition methodology for stair dimension, its application and test result are shown in section 6.2. Section 6.3 explains the process of the obtaining slide joint movement trajectory. Finally, stair climbing ability verification test with the control algorithm is performed in section 6.4.

6.1 Stair climbing process outline

Fig. 6.1 depicts the whole control structure of the mobile platform. Firstly, basic movement with certain direction and monitoring is executed by a Laptop or Personal Computer which communicating with CompactRIO of the mobile platform. LABVIEW must be installed on Laptop or Personal Computer to maintain appropriate communication condition. All the electric components installed in the mobile platform are supervised by CompactRIO, including the CAN communication between slide and wheel actuator and their drivers. Based on the calculation process, Speed directions are given to every wheel actuators individually, while position directions are given to the slide actuators. CompatRIO can recognize each actuator condition from the encoder signals. Actual position and posture of the mobile robot can be obtained from the inclinometer sensors, by comparing these values with the look-up table which created right before climbing stairs.

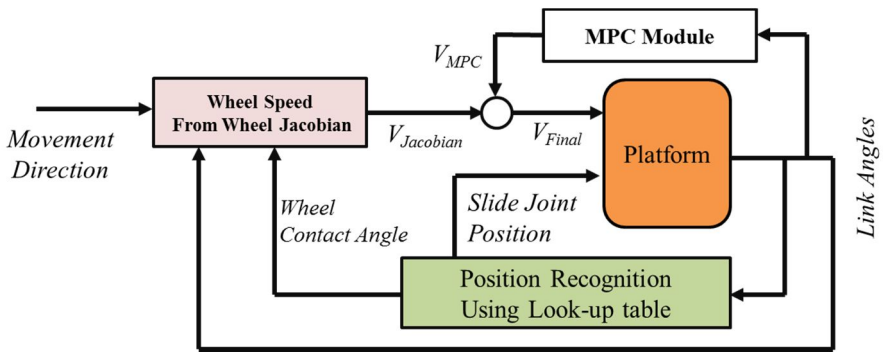

Figure 6.1: Mobile platform control structure

The overall flow while the stair climbing process is shown in Fig. 6.2. Firstly, the mobile platform approaches to a staircase. Before starting climbing process, dimensions of staircase are obtained by 2-D laser scanner of the mobile platform. Based on the stair size detection result, a look up table is created which including slide joint movement trajectory and wheel contact angle for every stair climbing stage. Once mobile platform starts the climbing process, CompactRIO compares the table and angle data obtained from the inclinometers of links in every sampling time (for instance, 30ms when the test is done in this chapter) after the appropriate position is confirmed from the table, CompatRIO commands actuators to perform calculated wheel speeds and slide joint position.

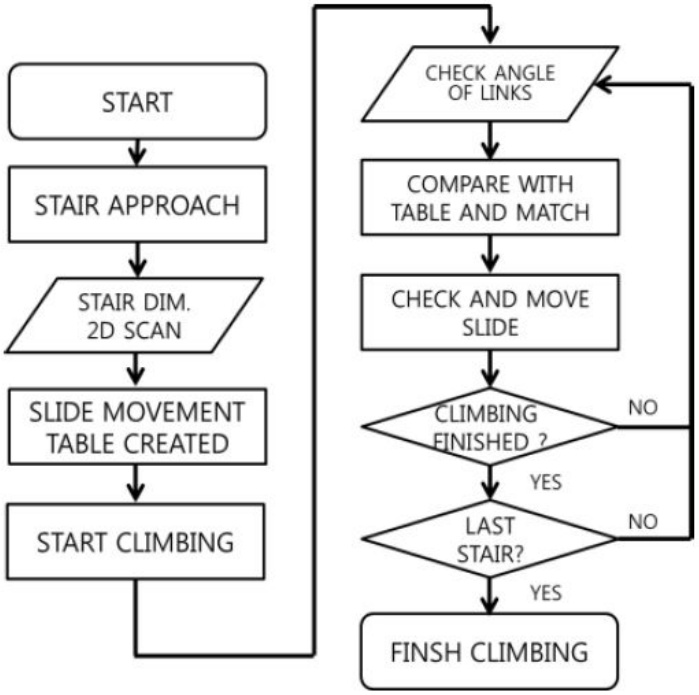

Figure 6.2: Stair climbing process

Eqn. (6.1) shows the factor used to evaluate which is the exact position of the table and suitable to be used as an actual position of the mobile platform. The previous position is applied as a center point of searching range. Each candidate position in the table compares

its link angles with the real data obtained from the inclinometers, and the factor can be calculated as shown in the Eqn. (6.1). The candidate which has the minimum factor is chosen as a step in the table for the actual position.

$$(\text{Error Distnace}) = \sqrt{(\theta_{1,Table} - \theta_{1,Sensor})^2 + (\theta_{2,Table} - \theta_{2,Sensor})^2} \tag{6.1}$$

Slide movement direction

After the actual position is matched with the step of the look up table, slide direction is executed by using slide joint position value of the step. During the climbing process, deformation of wheels make the tire into ellipse (horizontally long), so the wheel contacts earlier than the expected when table production process. To minimize its negative effect to the mobile platform's stability, anticipated position is directed to the slide joint actuator. This method helps the mobile platform to evade the posture detection failure or stair climbing process failure so that can maintain more accurate movement trajectory.

Meanwhile, the slide joints can't change its position instantly - limitations from such as maximum speed and acceleration of slide joint motors, so slide joint position direction error is inevitable. To minimize this effect, maximum slide movement distance between steps in the look up table is set to 20 mm, so that the maximum error of slide joint position is less than 20mm.

Wheel movement direction

Accurate wheel speed direction of the mobile platform is essential to maintain high-level stair climbing ability, such as minimizing wheel slip as well as torque and energy consumption minimization. As explained with kinematic analysis performed in Chapter 4, accurate wheel speed direction requires wheel contact angles and link angles to calculate the wheel Jacobian matrices. Angles of links can be obtained from the inclinometers from each links, but another method is required to obtain the wheel contact angles. To solve this problem, the contact angles are obtained from the look-up table, which calculated during the look-up table production process. By applying this data after the exact position of the

mobile platform is confirmed from the look-up table, the mobile platform can calculate and command exact wheel speeds to each wheel individually.

Besides, the movement speed of the slide joint actuator can effect to inaccurate movement of W_3. This can cause the failure condition such as wheel lifted situations, as depicted in Fig. 6. 3, also can cause whole stair climbing process failure. To prevent this situation, W_3 speed calibration process is produced. The process of the W_3 speed calibration is shown in the Fig. 6.4. Instantaneous speed caused by the slide joint's movement, it can be calculated from the posture conditions.

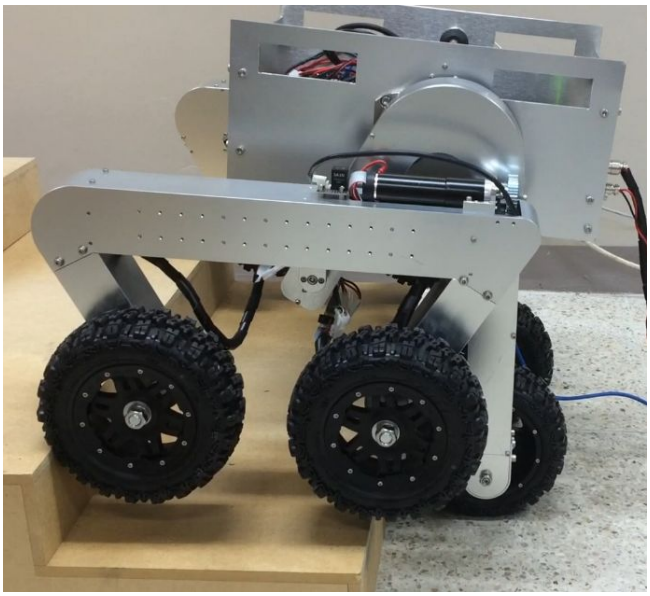

Figure 6.3: Wheel lifted situation

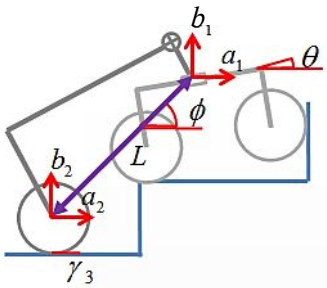

- Rear wheel driving speed correction

[1] L : Slide joint position (1) to Wheel 3 center (2) distance → fixed

[2] Slide movement speed derivation from link angle (θ) and joint

[3] Wheel 3 center moving direction calculated from the contact angle(γ_3)

[4] Wheel 3 center is set to origin for calculation

[5] Wheel 3 center speed obtained from [1,2,3,4]

[6] Converted into wheel 3 motor speed

$$\{(x_1 + a_1) - (x_2 + a_2)\}^2 + \{(x_1 + b_1) - (x_2 + b_2)\}^2 = L^2 \quad [1]$$

$$\begin{matrix} a_1 = V_{sld}\cos\theta \\ b_1 = V_{sld}\sin\theta \end{matrix} \quad [2] \qquad \begin{matrix} a_2 = V_3\cos\gamma_3 \\ b_2 = V_3\sin\gamma_3 \end{matrix} \quad [3] \qquad \begin{matrix} (x_2, y_2) = (0,0) \\ (x_1, y_1) = (L\cos\phi, L\sin\phi) \end{matrix} \quad [4]$$

$$V_3^2 - 2A \times V_3 + V_s^2 + 2B = 0$$

$$\begin{pmatrix} A = V_s\cos\theta \times \cos\gamma_3 + L\cos\phi \times \cos\gamma_3 + V_s\sin\theta \times \sin\gamma_3 + L\sin\phi \times \sin\gamma_3 \\ B = L\cos\phi \times V_s\cos\theta + L\cos\phi \times V_s\cos\theta \end{pmatrix} \quad [5]$$

$$V_3 = \omega_{3,motor} \times (\text{gear ratio}_{wheel}) \times R_3 \quad [6]$$

$$V_{sld} = \omega_{slide,motor} \times (\text{gear ratio}_{slide}) \times (\text{Ballscrew pitch})$$

Figure 6.4: W3 speed calibration process based on the slide Joint movement speed

Most idea of the primal actuator control for the mobile platform is explained above, but some parts require more explanations. Stair dimension acquisition and look-up table creation process will be shown with more details in section 6.2 and 6.3

6.2 Stair dimension acquisition

The stair dimension acquisition process is an important step, as it is the major basis of the look-up table production process for accurate slide joint and wheel actuator movement directions. To achieve this, a 2-D laser scanner is installed to the mobile platform, in front of the body structure as shown in chapter 5. Law data obtained from the 2-D laser scanner must be processed to get appropriate stair dimension data. An algorithm to acquire stair dimensions and test result with discussions are shown in the section 6.2.1.

6.2.1 Dimension acquisition with Ramer–Douglas–Peucker algorithm

The law data from the 2-D laser scanner is consisted of range data from the each unit angles. Firstly, this bundle of range data must be transformed into point data with X-Y coordinates. After the transformation process, 'Filtering' process is required to simplify the data. Basically, the data is full of points, but only vertex points are utilized to identify the stair dimensions. To accomplish this aim, the Ramer–Douglas–Peucker algorithm [41] is applied to the simplification process.

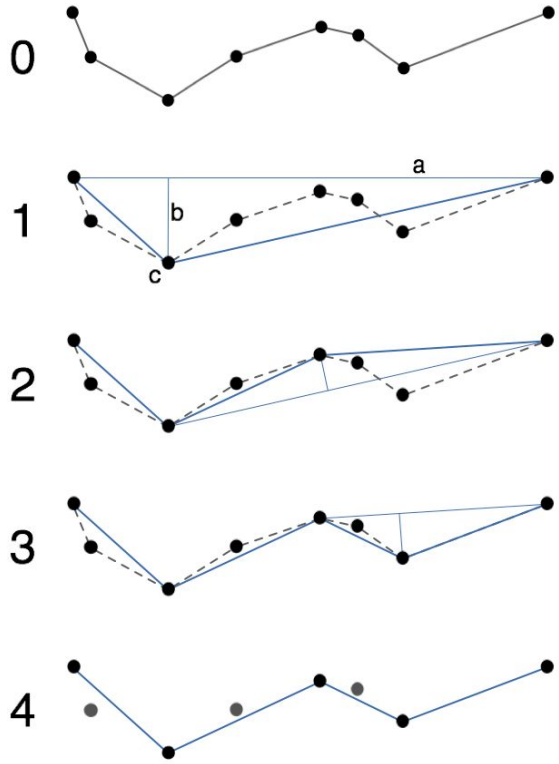

Figure 6.5: Ramer–Douglas–Peucker Algorithm process

The process of the algorithm can be visualized as Fig. 6.5. A point data set is ready before the process (Step 0 in fig. 6.5). After that, create line '**a'** by connecting between first and last points and calculate distances of the most far-away point '**c'** (Step 1 in 6.5). If the distance '**b'** is larger than a pre-set value, the point will not be eliminated for simplification

(Step 2 in fig. 6.5). And then repeat step 1, by using the point (instead of first one) c and the last one and compare distance again (Step 3 in fig. 6.5). Finally, Simplification is finished by repeating this process (Step 4 in fig. 6.5).

From the favor of the Ramer–Douglas–Peucker algorithm, the process data has only the vertex points, so line data with lengths are obtained. Finally, Stair dimension can be acquired.

6.2.2 Stair dimension acquisition test and result

In this section, stair dimension acquisition test is performed, based on the process explained in section 6.2.1. The aim of this test is to confirm accuracy of the stair dimension acquisition result, before applying in the whole stair climbing process. The test is executed with the stair structures, made with MDF material and has various stair shapes. The test is performed while the 2-D laser scanner is attached to the mobile platform. As shown in the Fig. 6.6, maximum acquired dimension error is less than 5mm, which can be ignored since relatively small to total sizes of the stair structures.

Point #	Width (mm)	Height (mm)	Angle (deg)
5	300	102	88.16
6	300	97	88.58

	Width (mm)	Height (mm)
Avg	300	99.5
Actual	300	100
Error	0	-0.5

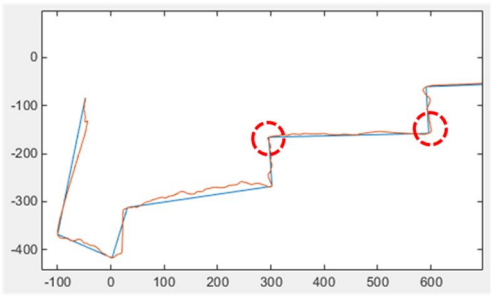

(a)

Point #	Width (mm)	Height (mm)	Angle (deg)
6	317	130	91.24
7	317	124	89.40

	Width (mm)	Height (mm)
Avg	317	127
Actual	315	130
Error	+2	-3

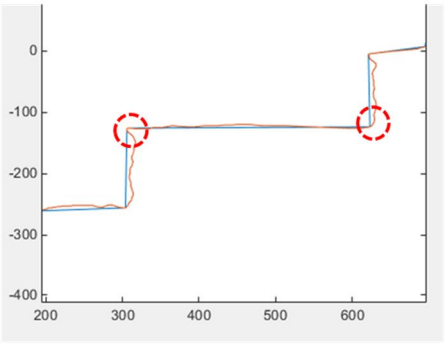

(b)

Point #	Width (mm)	Height (mm)	Angle (deg)
4	306	139	91.84
5	306	161	90.4
6	315	161	91.0
7	315	159	90.2

	Width (mm)	Height (mm)
Avg	300	99.5
Actual	300	100
Error	0	-0.5

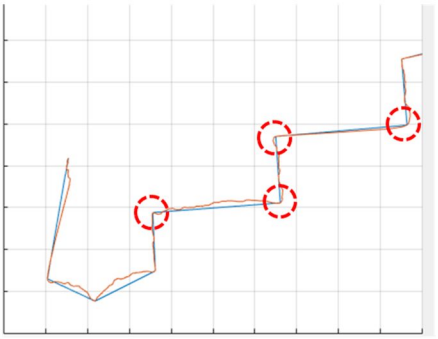

(c)

Figure 6.6: Stair shape acquisition test result (a) 300X100 (b) 315X130 (c) 310X160

To verify the effect during the look-up table creation process for these errors, look-up tables are created based on the variable stair dimension values and compared together. Fig. X depicts the comparison between created look-up table for three stair shapes, 300X100, 315X130 and 310X160. In each tables, X and Y axis represents the link angle value, θ_2 and θ_1, respectably. Black line shows result created from the actual stair dimension value, while blue line and red line are the result from the +5mm and -5mm data. To simplify the comparison data visually, slide joint is fixed during table creation process. As shown in the Fig. 6.7, angular trajectory errors caused by the stair dimension error are notified. But considering the error value applied to the test is the maximum error and the global trends are still maintained, the effect caused from the dimension detection error can be ignored. So the stair dimension acquisition algorism tested in this section can be applied to the stair ascending and descending process for the mobile platform

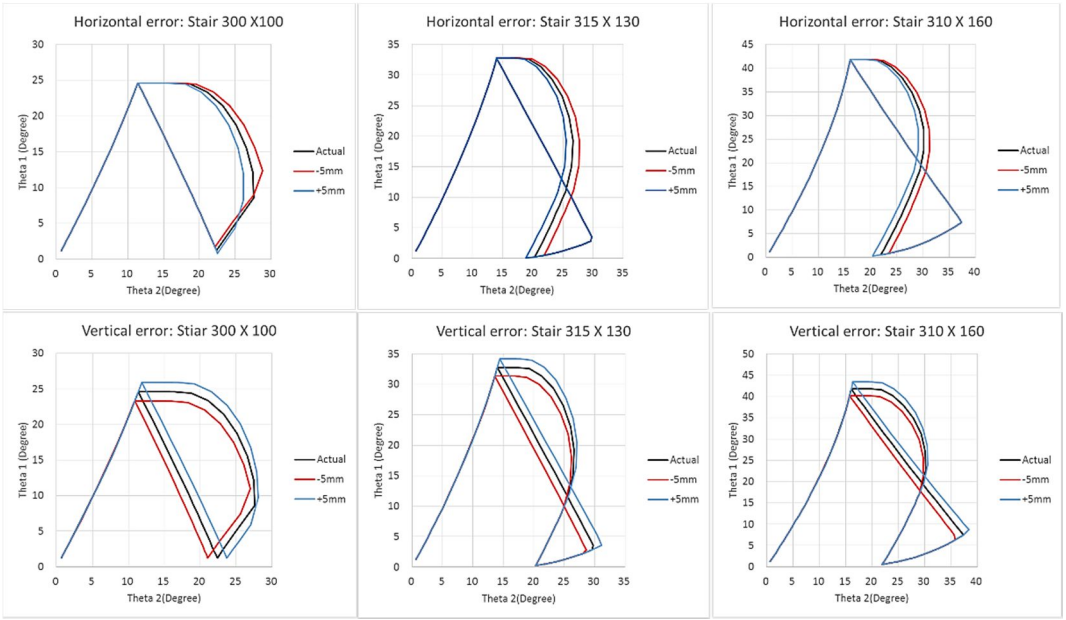

Figure 6.7: Table error caused by stair dimension sensing error

6.3 Look-up table creation process

The look up tables created from the obtained stair dimensions are essential to recognize the current position and posture of the mobile platform. Every look up table is created form the specific stair dimension and each look up table is unique. So the look-up table must be created before starting the stair climbing process when the mobile platform encounters a new stair structure. The look-up table includes angles of links, slide joint position, and wheel contact angles corresponding to the position of *Wheel 1* while moving on the stair surface.

After the stair dimension is obtained by using the method described in section 6.2, the look-up table creation process is started. *Wheel 1* starts climbing stair surfaces, and safety factors, link angles and wheel contact angles of every slide joint position are calculated. After the calculation for all positions of *Wheel 1* on the stair surface is finished, the best slide joint position for each *Wheel 1* location is selected, which has the largest stability factor. From this result, slide joint position trajectory is created which can maintain stability of the mobile platform while climbing staircase. The stability factor, the core element of the slide joint movement trajectory selection process is described in section 6.3.1 and 6.3.2

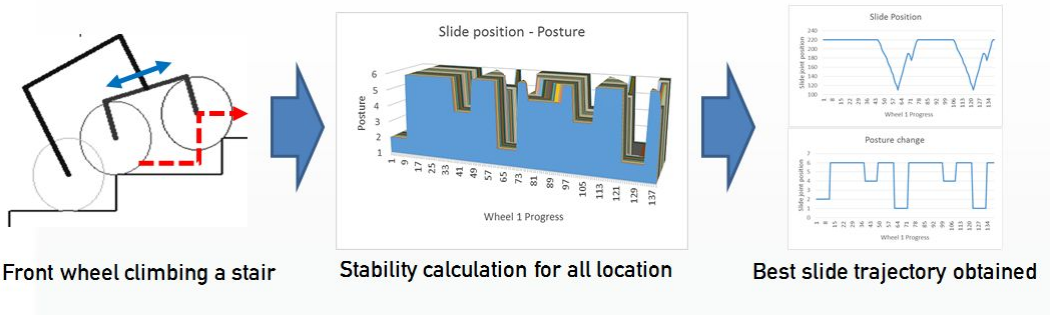

Figure 6.8: Schematic process of the slide joint movement trajectory selection for the look-up table

6.3.1 Force-closure based strategy

The early suggested idea of the stability factor for selecting the best position of the slide joint is based on the 'Force Closure' idea from robotics [42]. In a grasping problem, a positive span area is obtained from combination of reaction forces caused by current contact conditions. Fig. 6.9 shows examples of a positive span area. When external force within the positive span area is applied, actual grasp condition can be maintained.

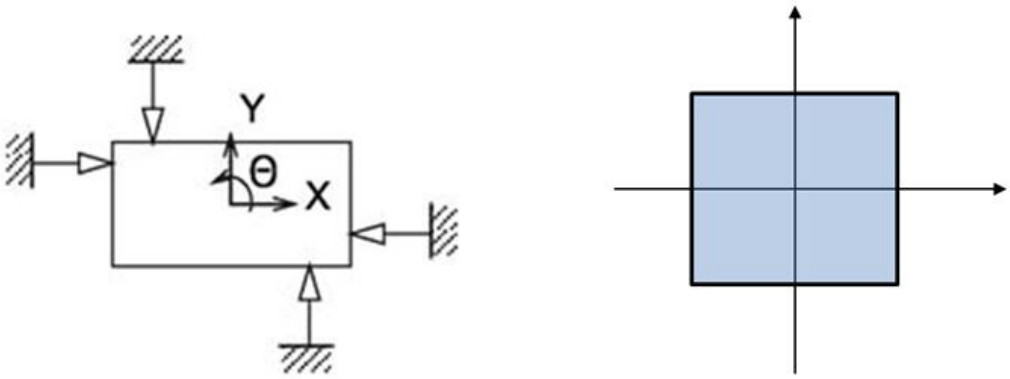

(a) (b)

Figure 6.9: Force closure example (a) A grasping condition (b) Positive span

When applying this idea to the mobile platform on staircases, external forces which a mobile platform can tolerate can be obtained based on its positive span. As a result, radius of inscribed circle is selected as the stability factor. Fig. 6.10 explains how this stability factor can be derived by using its positive span created from actual contact status.

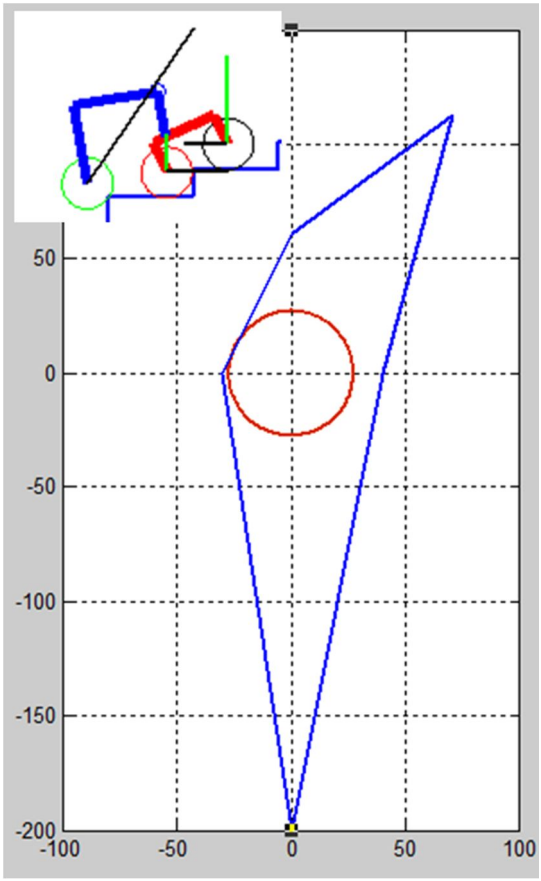

Figure 6.10: Stability factor derivation through positive span of the force closure theory

Based on the idea explained above, slide position is selected as a stability factor, as shown in the Fig. 6.11. But failures are occurred during the ascending and descending process on the most stairs when the slide joint trajectory is applied to the movement of the mobile platform, as well as the limits of the idea also verified as listed below:

A. Slide movement trajectory can be obtained through the calculation and simulation using MATLAB, but the process uses complicated optimization algorithm when the reaction forces of each wheels are calculated. This process increases total process time from 5 to 10 minutes and it is too long time for climbing preparation process.

B. To verify the calculation result, such as reaction forces of each wheels. Complicated method is required, especially wheels need force detection instruments for all tires' surface.

C. The obtained results are too complicate to visualize, as well as the idea for this result is not intuitive. By combining B, this causes the non-intuitive characteristic of the process.

D. More intuitive, direct and critical characteristics, such as Center of mass and wheel position are not considered.

New strategy is selected, due to a limitations of the strategy using the 'force-closure' theory are verified as shown above, another new strategy is selected.

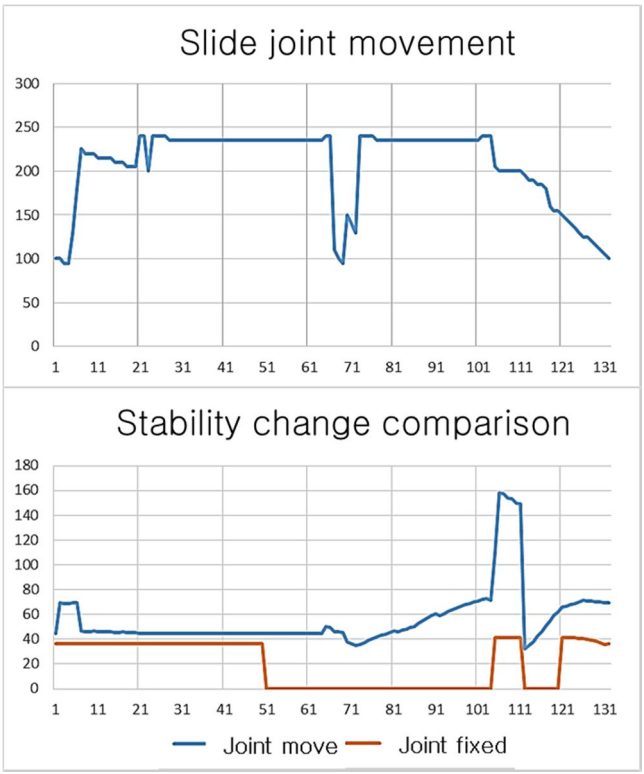

Figure 6.11: Slide movement trajectory and stability progress using the force-closure theory

6.3.2 Case-based strategy

In this section, a new stability calculation strategy using the 'case selection' idea is introduced which adopted to resolve the problems of the former stability calculation strategy based on the 'force-closure' theory.

As mentioned in the previous section, the wheel reaction forces acquisition process from the calculation including the optimization algorithm is complicated, uncertain, slow to use and hard to understand and/or verify. To clear these limits, the new stability factor calculation strategy is focused on improving intuitiveness and calculation process speed. In the previous stability calculation process, optimization algorithm is applied to solve undetermined system problems to obtain the wheel reaction forces, so that the process time is drastically increased, approximately from five to ten minutes to finish. In the newly suggested strategy, stability factors are obtained based on the posture and center of mass of the mobile platform, so any optimization algorithm used in the previous strategy is not required. From the modification of the calculation process, total look-up table creation process time is decreased into less than 10 seconds.

The detailed process of the new safety factor derivation is shown as below:

1. Firstly, wheel – stair contact conditions for each wheels are recognized, whether in either horizontal or vertical contact state. Edge-contacted cases are included to horizontal contact state, as the tires of wheels are deformed so that can use the tread surface of the stair. Basically, each wheels (W_1, W_2 and W_3) can have two contact cases, so 8 contact cases can be obtained. But when W_1 is in a vertical contact state, vertical contact between W_2 and stair is impossible, due to a kinematic constraint explained in chapter 3. Therefore the 6 cases are selected based on the wheel contact conditions. Fig. 6.12 shows the detail of posture variations. The most critical posture among these cases is the posture when W_2 and W_3 are contacted vertically to stair, where the mobile platform can't maintain its stability and collapse will be caused. When W_1 and W_3 are contacted vertically to

stair, the mobile platform can maintain its posture stably, while the center of mass keep its position forward to the mobile platform. The former posture #3 described above will be evaded in the slide joint position selection stage.

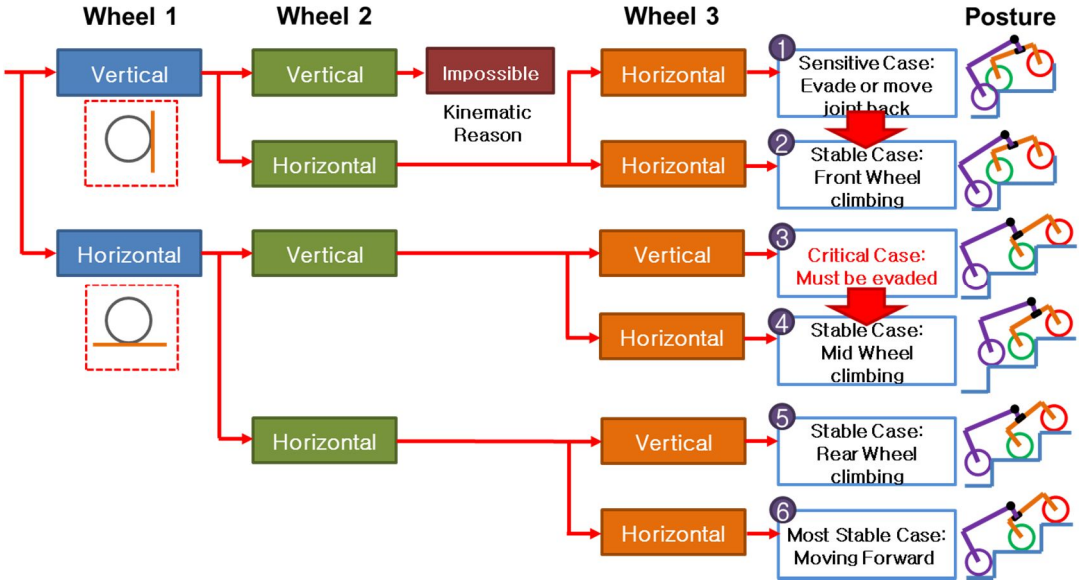

Figure 6.12: Posture classification based on the wheel contact conditions

2. After the posture classification stage has been completed based on the wheel contact conditions, critical posture can be evaded. In this stage, the position of slide joint for each W_1 position is selected to maintain the center of mass position to forefront of the mobile robot. To express this aim, the distance from the center of mass to the axis of the climbing wheel is selected as the stability factor. In this process, dynamic change caused by the change of the posture and the position slide joint are implemented to the calculation of the location of the center of mass of the mobile robot.

3. While selecting the position of the slide joint, special conditions are created for exceptional cases as below:

   A. It is obvious that the posture #6, where the all wheels on the horizontal

surface is the most stable condition, so it is the most desirable case for the mobile platform. The stability factor will be maximized for the posture to be selected preferentially.

B. Critical posture #3 (when W_2 and W_3 are contacted vertically to stair) will be evaded at all cost, the stability factor will be minimized to evade the selection of this posture.

Based on the calculation algorithm explained above, stability factors for each slide joint position of every W_1 position is obtained, and the slide position which maximizing the stability factor is selected. Factors are affected by the exceptional cases mentioned before, so that the selection preference can be controlled. Finally, the slide movement trajectory to for maximizing its stability factor while climbing stair is determined, and created into the look-up table, including the wheel contact angles and link angles.

To apply the reality to the movement of the slide joint with the movement trajectory of the slide joint, more algorithms must be added to the process. An available movement speed of the slide joint is added to the limitation of the selection process, as the searching range of the slide joint position for the next W_1 position. Fig. 6.13 describes the algorithm for adding real movement range as the limitation for the slide joint position selection process.

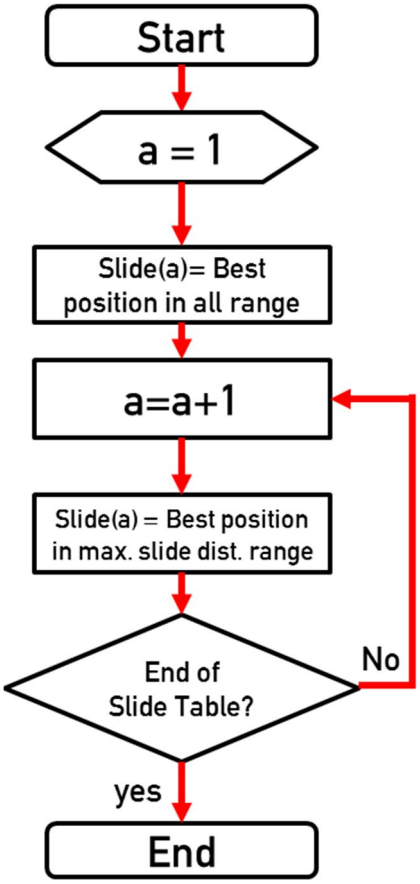

Figure 6.13: Slide joint position selecting algorithm to apply reality on the movement of the slide joint

6.4 Basic stair-climbing ability verification test

In this section, stair climbing test is proceeded to verify the stair climbing ability of the mobile platform. Various stair structures are created as a test benches for the mobile platform to ascend and descend. All the hardware and software, including the basic control algorithm explained are applied as components of the ability verification test. The details of test setting and the result are shown in section 6.4.1 and 6.4.2.

6.4.1 Test circumstance set-up

Before starting the ability verification test for the mobile platform, components for the test are prepared. The test components, the mobile platform prototype as a test subject, stair structures for the test benches and circumstances and a laptop for monitoring and AC power supply are prepared.

The hybrid-link mobile platform

The mobile platform is created as the prototype for the hybrid mechanism. The hardware and software of the mobile platform are ready for the ability verification test. 220V AC power is supplied from the cable to the mobile platform. Also, the mobile platform communicates with the laptop, which functions as a monitoring terminal.

Stair structures

To proceed the stair climbing ability verification test, stair structures which have various dimensions are constructed. The dimensions of stair structures and created stair structure based on the dimensions are shown in Fig. 6.14. As shown in the picture, every stair structure has three steps, while the last step plane is large enough to the mobile platform can stay in plain posture. All these staircases are made of MDF material.

(a) (b) (c)

Figure 6.14: Three stair structures for climbing test (a) 300X100 (b) 315X130 (c) 310X160

Monitoring terminal laptop

To monitor the state of the mobile platform and direct basic motion of the mobile platform,

maintaining control of the mobile platform while the stair climbing process is essential. To establish this, a laptop is utilized as a monitoring and communication terminal. LABVIEW is installed to the laptop to secure the better communication status with the mobile platform. Also, Wi-Fi communication is established between the laptop terminal and CompactRIO on the mobile robot instead of LAN cable so that the mobile platform can move freely.

Power supply

To supply DC power to the whole components of the mobile platform, it has two 350W SMPS units under the body compartment. A 220V AC cable from the external power source is connected to these SMPS units, so that power supply requirement can be satisfied.

Fig. 6.15 show the test circumstance, ready to start, which composed with the components described above. By using the test set-ups, the stair climbing ability verification test is performed for each staircase structure. The result of the ability verification test and its discussion is shown in section 6.4.2.

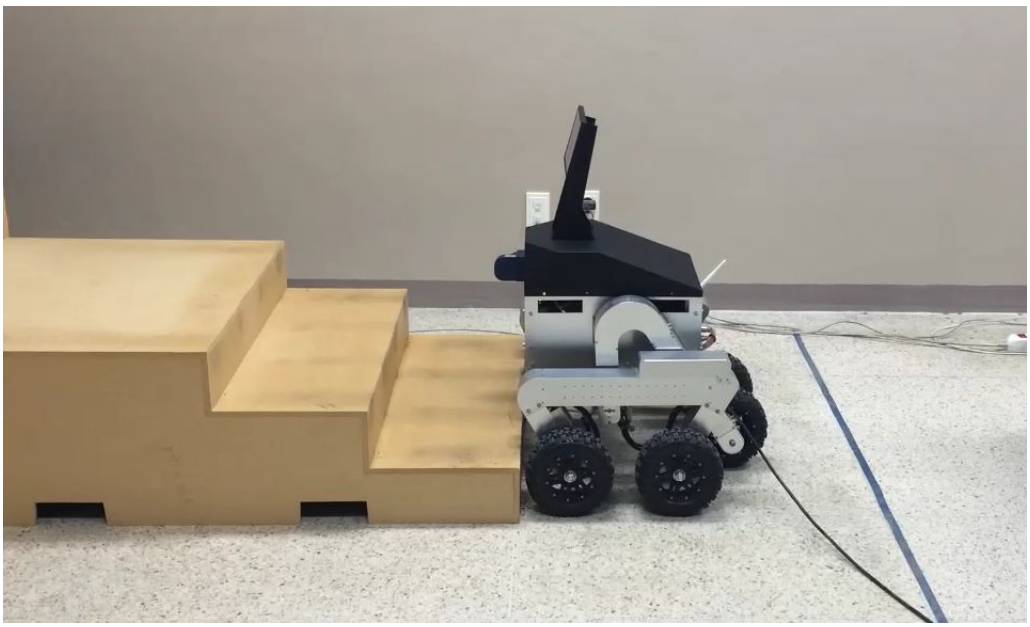

Figure 6.15: Test circumstance set-up

6.4.2 Test result and discussion

The climbing test results for three stair structure examples are shown in Fig. 6.16 to Fig. 6.18.As shown in these results, successful stair climbing performances are verified with no failure situations as well as its posture recognition process. Fig. 6.19 shows the detailed climbing process on stair 310 X 160.

Also, look-up tables for three staircases are shown in Table 6.1 to 6.6. These tables are express the progress during the front wheel(W_1) is climbing the first and second step of the stair structures After that, progress between the first and second stair is repeated when the mobile platform still has stair steps to climb. Repeated steps are from step 16 to 46 (in Table 6.1 and 6.2 for stair 300 X 100), step 21 to 63 (in Table 6.1 and 6.2 for stair 315 X 130) and step 27-79 (in Table 6.1 and 6.2 for stair 310 X 160), respectively.

Although the stair climbing ability based upon the mobile platform and posture recognition process are verified in this section, posture inaccuracy can be occurred by imbalance between left and right link angles. This imbalance can even bring unstable and climbing failure if it is serious. It is highly possible which may can be caused by stair and wheel conditions, or other non-ideal condition related reasons.

To handle this problem, more control element is required to improve its posture accuracy during climbing process. This will be discussed in the next chapter including implementation and stair climbing tests.

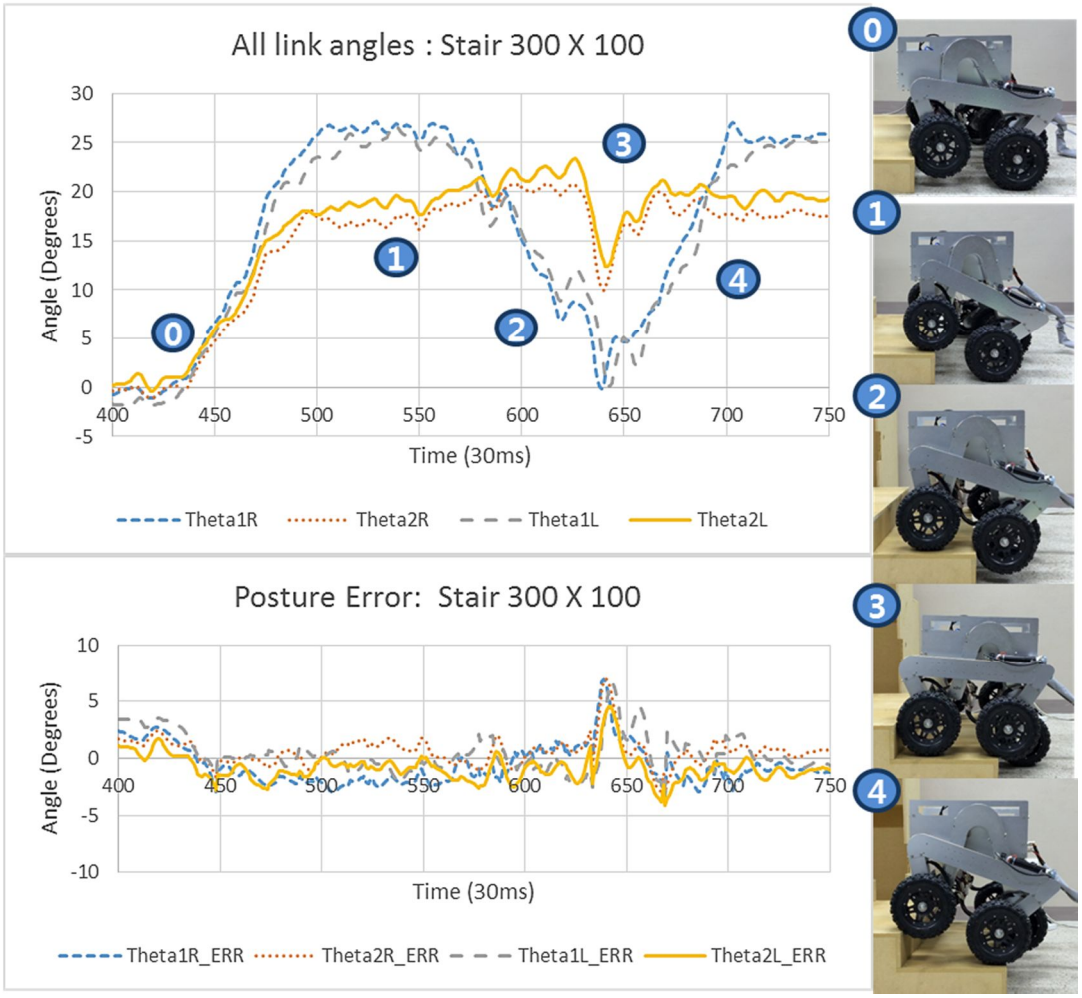

Figure 6.16: Test result for stair: 300 X 100

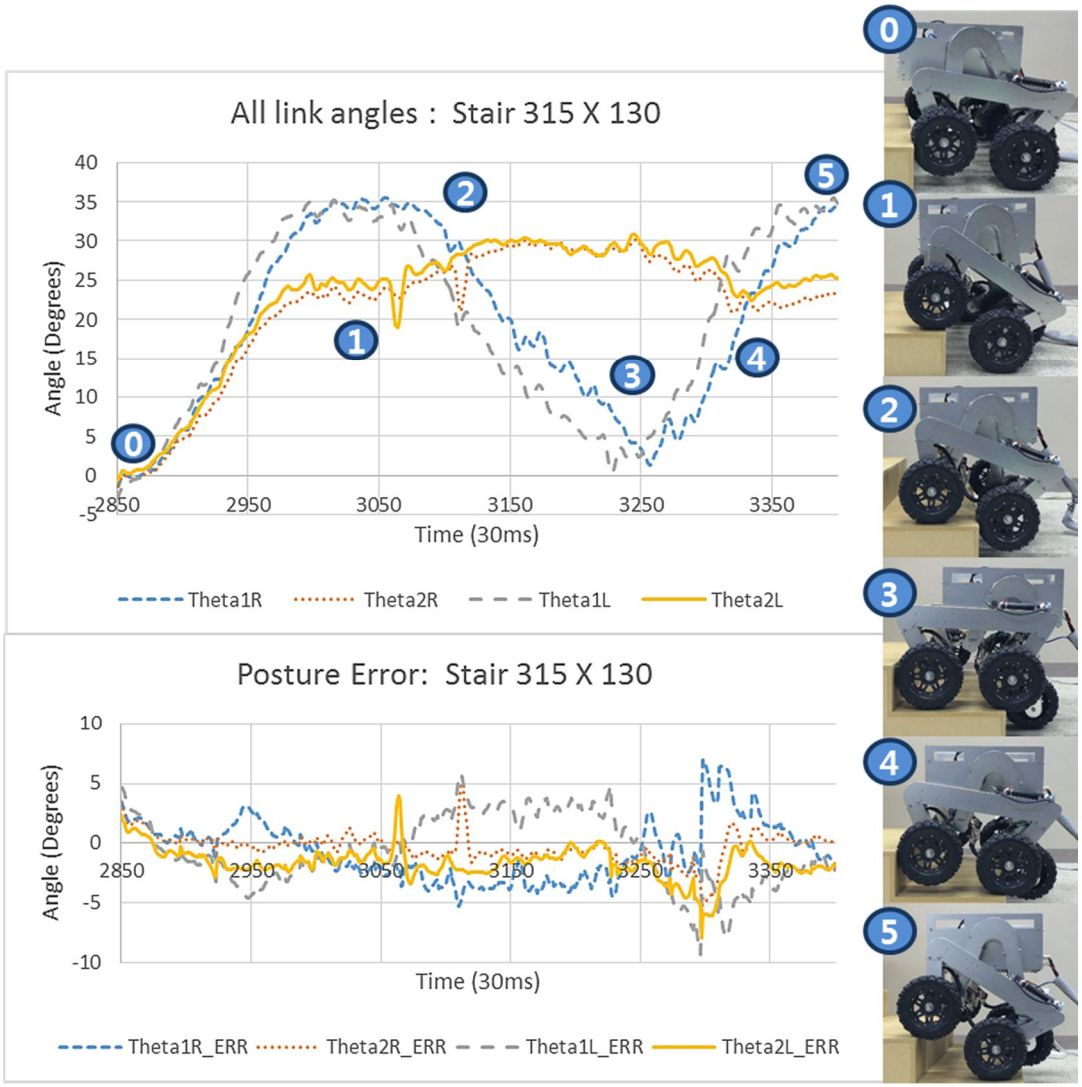

Figure 6.17: Test result for stair: 315 X 130

Figure 6.18: Test result for stair: 310 X 160

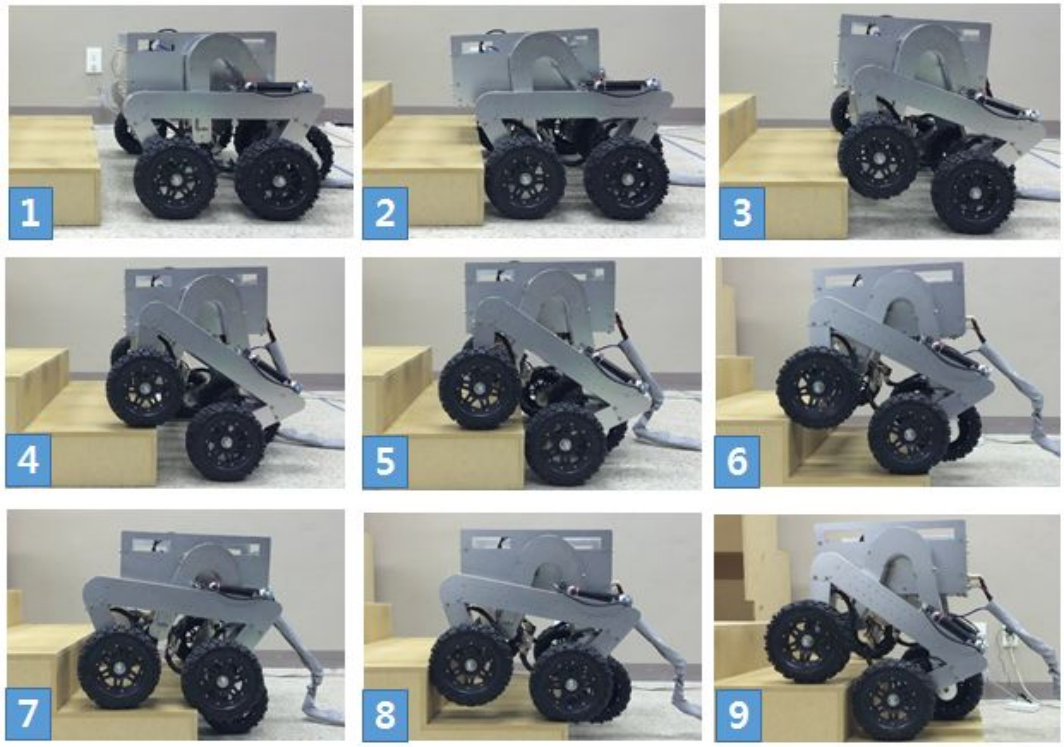

Figure 6.19: Full climbing procedure (for stair 310 X 160)

Table 6.1: A look-up table of the stairs, for stair 300 X 100

Step	θ_1[˚]	θ_2[˚]	γ_1[˚]	γ_2[˚]	γ_3[˚]
1	1.19	0.94	90	0	0
2	2.39	1.88	90	0	0
3	3.58	2.81	90	0	0
4	7.77	6.05	76	0	0
5	11.79	9.10	64	0	0
6	15.50	11.84	53	0	0
7	18.76	14.19	42	0	0
8	21.41	16.06	31	0	0
9	23.34	17.39	19	0	0
10	24.42	18.13	8	0	0
11	24.62	18.26	-3	0	0
12	24.62	18.26	0	0	0
13	24.62	18.26	0	0	0

Table 6.2: A look-up table of the stairs, for stair 300 X 100 - continued

Step	θ_1[˚]	θ_2[˚]	γ_1[˚]	γ_2[˚]	γ_3[˚]
14	24.62	18.26	0	0	0
15	24.62	18.26	0	0	0
16	23.56	18.55	0	90	0
17	20.50	19.33	0	86	0
18	17.86	19.95	0	79	0
19	15.66	20.44	0	74	0
20	13.87	20.81	0	69	0
21	12.48	21.08	0	64	0
22	11.44	21.28	0	61	0
23	10.67	21.42	0	57	0
24	10.07	21.30	0	54	0
25	9.54	21.18	0	51	0
26	9.00	21.10	0	47	0
27	8.38	21.05	0	44	0
28	7.67	21.05	0	40	0
29	6.86	20.95	0	35	0
30	5.96	21.09	0	31	0
31	4.99	21.28	0	26	0
32	3.98	21.44	0	22	0
33	5.10	19.94	90	22	90
34	6.20	17.82	90	21	82
35	7.29	16.15	90	21	74
36	10.50	16.19	76	16	63
37	13.04	18.86	64	10	62
38	15.57	18.76	53	2	48
39	18.76	19.00	42	0	34
40	21.41	19.02	31	0	22
41	23.34	18.70	19	0	13
42	24.42	18.26	8	0	4
43	24.62	18.26	-3	0	0
44	24.62	18.26	0	0	0
45	24.62	18.26	0	0	0
46	24.62	18.26	0	0	0

Table 6.3: A look-up table of the stairs, for stair 315 X 130

Step	θ_1[˚]	θ_2[˚]	γ_1[˚]	γ_2[˚]	γ_3[˚]
1	1.19	0.94	90	0	0
2	2.39	1.88	90	0	0
3	3.58	2.81	90	0	0
4	4.78	3.74	90	0	0
5	5.98	4.67	90	0	0
6	7.18	5.59	90	0	0
7	8.38	6.52	90	0	0
8	9.59	7.44	90	0	0
9	10.81	8.35	90	0	0
10	15.08	11.54	76	0	0
11	19.23	14.53	64	0	0
12	23.10	17.23	53	0	0
13	26.52	19.53	42	0	0
14	29.34	21.34	31	0	0
15	31.41	22.63	19	0	0
16	32.58	23.34	8	0	0
17	32.80	23.47	-3	0	0
18	32.80	23.47	0	0	0
19	32.80	23.47	0	0	0
20	32.80	23.47	0	0	0
21	31.34	23.98	0	90	0
22	28.95	24.78	0	90	0
23	26.38	25.61	0	90	0
24	23.56	26.48	0	90	0
25	20.50	27.37	0	86	0
26	17.86	28.10	0	79	0
27	15.66	28.66	0	74	0
28	13.87	28.73	0	69	0
29	12.48	28.76	0	64	0
30	11.44	28.45	0	61	0
31	10.67	28.41	0	57	0
32	10.07	28.35	0	54	0
33	9.54	28.29	0	51	0
34	9.00	28.26	0	47	0
35	8.38	28.07	0	44	0
36	7.67	28.18	0	40	0
37	6.86	28.37	0	35	0

Table 6.4: A look-up table of the stairs, for stair 315 X 130 - continued

Step	θ_1[˚]	θ_2[˚]	γ_1[˚]	γ_2[˚]	γ_3[˚]
38	5.96	28.48	0	31	0
39	4.99	28.86	0	26	0
40	3.98	29.19	0	22	0
41	2.98	29.62	0	18	0
42	2.03	30.16	0	14	0
43	1.20	30.65	0	10	0
44	2.37	29.40	90	10	90
45	3.53	27.38	90	10	90
46	4.68	25.28	90	9	90
47	5.81	23.10	90	9	90
48	6.94	21.04	90	9	83
49	8.06	19.35	90	8	75
50	9.18	18.03	90	8	68
51	10.29	17.11	90	7	62
52	11.40	17.83	90	7	61
53	15.18	20.46	76	3	61
54	19.23	22.81	64	0	62
55	23.10	22.54	53	0	50
56	26.52	22.60	42	0	36
57	29.34	22.36	31	0	21
58	31.41	22.26	19	0	6
59	32.58	23.34	8	0	0
60	32.80	23.47	-3	0	0
61	32.80	23.47	0	0	0
62	32.80	23.47	0	0	0
63	32.80	23.47	0	0	0

Table 6.5: A look-up table of the stairs, for stair 310 X 160

Step	θ_1[˚]	θ_2[˚]	γ_1[˚]	γ_2[˚]	γ_3[˚]
1	1.19	0.94	90	0	0
2	2.39	1.88	90	0	0
3	3.58	2.81	90	0	0
4	4.78	3.74	90	0	0
5	5.98	4.67	90	0	0
6	7.18	5.59	90	0	0
7	8.38	6.52	90	0	0
8	9.59	7.44	90	0	0
9	10.81	8.35	90	0	0
10	12.02	9.27	90	0	0
11	13.25	10.18	90	0	0
12	14.48	11.09	90	0	0
13	15.71	11.99	90	0	0
14	16.96	12.90	90	0	0
15	18.21	13.80	90	0	0
16	22.66	16.93	76	0	0
17	27.03	19.86	64	0	0
18	31.15	22.47	53	0	0
19	34.86	24.68	42	0	0
20	37.95	26.39	31	0	0
21	40.25	27.58	19	0	0
22	41.57	28.23	8	0	0
23	41.81	28.35	-3	0	0
24	41.81	28.35	0	0	0
25	41.81	28.35	0	0	0
26	41.81	28.35	0	0	0
27	41.41	28.52	0	90	0
28	39.57	29.33	0	90	0
29	37.66	30.15	0	90	0
30	35.66	31.01	0	90	0
31	33.56	31.89	0	90	0
32	31.34	32.81	0	90	0
33	28.95	33.78	0	90	0
34	26.38	34.78	0	90	0
35	23.56	35.86	0	90	0
36	20.50	35.72	0	86	0
37	17.86	35.67	0	79	0
38	15.66	35.66	0	74	0
39	13.87	36.06	0	69	0
40	12.48	35.96	0	64	0

Table 6.6: A look-up table of the stairs, for stair 310 X 160 - continued

Step	θ_1[˚]	θ_2[˚]	γ_1[˚]	γ_2[˚]	γ_3[˚]
41	11.44	36.16	0	61	0
42	10.67	36.26	0	57	0
43	10.07	35.98	0	54	0
44	9.54	36.02	0	51	0
45	9.00	36.10	0	47	0
46	8.38	36.26	0	44	0
47	7.67	36.29	0	40	0
48	6.86	36.69	0	35	0
49	5.96	37.03	0	31	0
50	4.99	37.54	0	26	0
51	3.98	38.22	0	22	0
52	2.98	39.02	0	18	0
53	2.03	39.90	0	14	0
54	3.18	39.10	90	14	90
55	4.32	37.29	90	13	90
56	5.45	35.43	90	13	90
57	6.56	33.53	90	13	90
58	7.66	31.57	90	12	90
59	8.76	29.56	90	12	90
60	9.84	27.49	90	11	90
61	10.92	25.36	90	10	90
62	12.00	23.49	90	10	81
63	13.08	21.99	90	9	73
64	14.16	20.87	90	8	66
65	15.24	20.81	90	8	63
66	16.33	21.47	90	7	62
67	17.43	22.13	90	6	61
68	18.54	22.79	90	5	60
69	22.66	25.62	76	0	63
70	27.03	27.46	64	0	64
71	31.15	26.94	53	0	52
72	34.86	26.89	42	0	39
73	37.95	26.67	31	0	24
74	40.25	26.45	19	0	9
75	41.57	28.23	8	0	0
76	41.81	28.35	-3	0	0
77	41.81	28.35	0	0	0
78	41.81	28.35	0	0	0
79	41.81	28.35	0	0	0

Chapter 7

Model Predictive Control based posture correction process

So far the new hybrid link mechanism is suggested and the mobile platform prototype is created and tested on the test beds with its wheel posture based case selecting stability. Basic performance of the mobile platform is verified in chapter 6, but to obtain the integrity of the mobile platform, it requires additional control to maintain its accurate posture, especially left-right angular equality.

To achieve this, MPC (Model Predictive Control) can be applied to the control. MPC is the optimal control technique for deriving optimized input values via the near-future prediction based on the MIMO (Multi- In, Multi-Out) plant model which satisfy the cost function maintaining technique. By implementing MPC to predict the condition of the mobile platform and direct the compensation movements to actuators, better movement ability such as accuracy, stability can be obtained.

In this chapter, MPC components for the mobile platform are configured, followed by its implement process and implementation verification process. After that, final implement

test to the mobile platform prototype and discussions are done.

7.1 Model predictive control

MPC is a control strategy for specific cases based on the optimal control theory with the time instants k. The purpose of this optimization process is to calculate new control input vector u(k) based on input and output constraints. The basic conceptual architecture of the MPC depicted in Fig. 7.1.

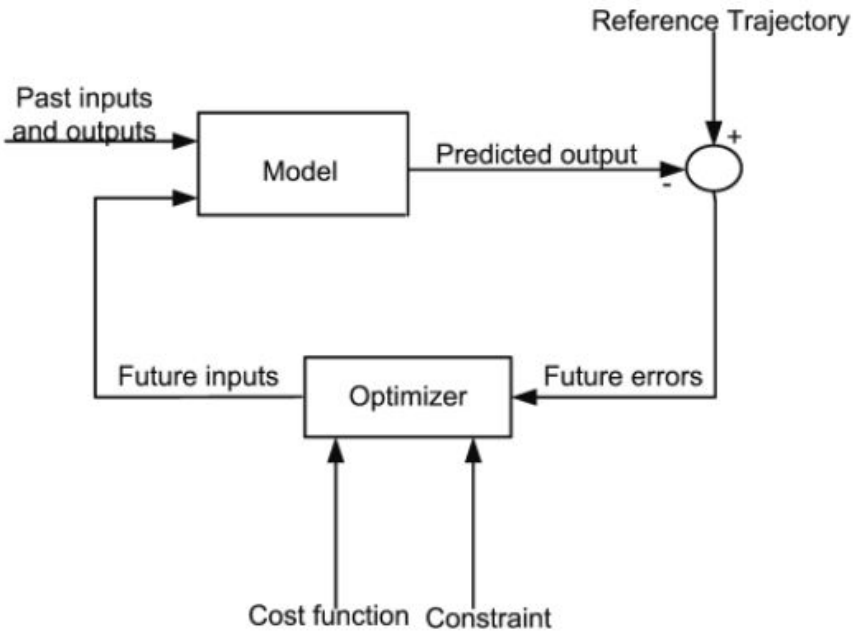

Figure 7.1: The basic conceptual architecture of the MPC [43]

The main components of the Model predictive control are listed below. To implement MPC to the mobile platform control, all the components set-ups will be followed.

Prediction and Control horizons

Prediction horizon is the sampling interval during the plant output is predicted by the MPC controller. Control horizon is the sampling interval during control action is implied during

the prediction of the MPC controller. So the prediction horizon must be bigger than the control horizon. Fig. 7.2 shows the relationship of both control and prediction horizon. At the time k, MPC predicts the plant output up to time $k+N_p$, but the control action changes till the time $k+N_c$.

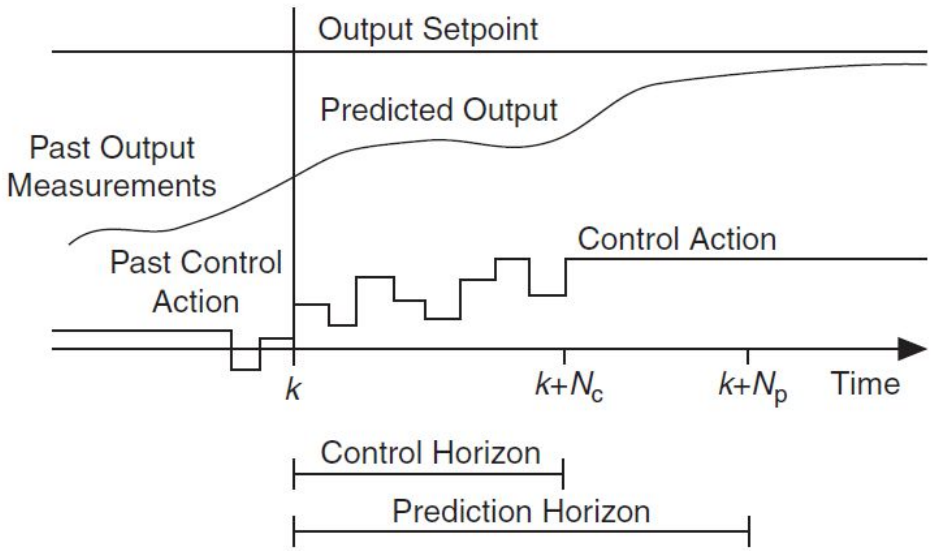

Figure 7.2: Control Horizon & Prediction Horizon [44]

Model

Unlike PID or other ordinary control technique, a model which expresses the relationship between the input u, state x and output y are essential to implement MPC. The state-space model of MPC has discrete characteristics. Eqn. (7.1) shows an ordinary state-space model scheme for MPC

$$\begin{aligned} x(k+1) &= Ax(k) + Bu(k) \\ y(k) &= Cx(k) + Du(k) \end{aligned} \tag{7.1}$$

Cost function

As described above, MPC includes the optimization problem, so the cost function is

required. In many cases, minimizing output errors and control efforts are selected as the cost function. Also, cost function can be altered by adjusting the weight factors.

Constraints

All physical systems have its constraints. For instance, maximum speed or acceleration of actuators can be translated into the input constraints, while maximum temperature or pressure of controlled instrument can be considered as output constraints. To implement MPC with more accurate input direction, careful set-up of the constraints is essential.

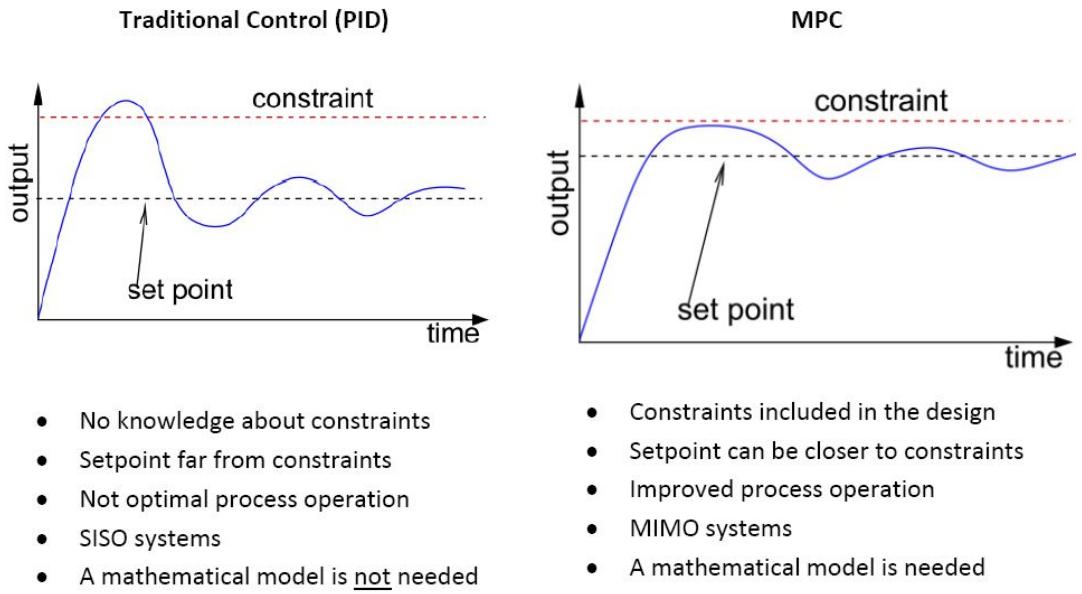

Figure 7.3: Comparison between PID control and MPC [43]

In many cases, MPC used as an alternative solution of ordinary control technics, such as PID control and so on. The characteristics of MPC compared to PID can be stated as below: Firstly, PID uses a Single-Loop control, but MPC is act as an overall system. Also, PID uses SISO (Single-Input, Single-Output) system, but MIMO (Multiple-Inputs, Multiple-Output) system is applied to MPC, so that more complicated and advanced control can be achieved. In addition, Model is essential to MPC to reflect dynamical characteristics to MPC, unlike PID. Instead, the model enhances MPC's adaptability to long delay time or

high-order dynamics. Fig. 7.3 summarizes the comparison between PID control and MPC [43].

Based on the contents explained above, implement of MPC to the mobile platform is proceeded in the next section. To follow the look-up table (which created uniquely from specific stair dimension) accurately and obtain better efficient movement of wheel actuators, accurate actuator direction calibration is done by the MPC module so that stair ascending and descending performance of the mobile robot can be maximized.

To apply the movement direction by MPC to the mobile platform, all of the MPC elements are defined for the mobile platform, and the basic verification is done by the simulation. After that, The verified MPC module is implied to the real mobile platform to compare the result between with MPC and without MPC. Also the discussion about the comparison result is followed.

7.1.1 State-variable equation

From the open-loop direction from the stair climbing strategy which introduced in chapter 6, slide position is assumed that it maintains ideal position. So to handle left-right angular difference minimization during the stair climbing process, the MPC implementation must be focused to wheel speed regulation for each wheel. As the first step of the implement process, a state-variable equation is created in this section.

Firstly, wheel speed regulation values for six wheels are selected as the input u(k), so that each value can be differently calculated. As state x(k) and output y(k), angular difference values are chosen. Basically, using angular values such as degrees or radians for these expressions is the most direct way to understand, but they are expressed as x-y length value of the triangle, which oblique side is its link length. By applying this expression, complicated trigonometric function combination in the state-variable equation can be evaded. Fig. 7.4 explains this angle – length expression conversion process. Also, the relationship between wheel speeds and angular changes can be expressed by this, as

intended.

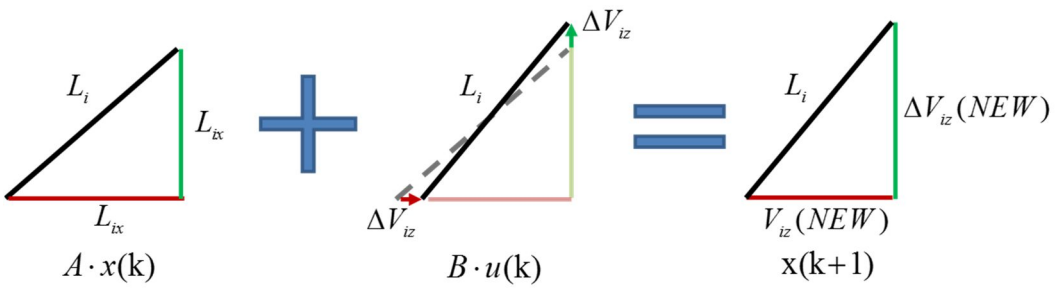

Figure 7.4: Angle – length expression conversion process

Eqns. (7.2) shows the relationship between the wheel speeds and link angle changes. By adding changing values which calculated by wheel speed to previous state/output value, next state/output value can be expressed. Based on these elements, the state-variable equation for the mathematical model of the mobile platform is can be expressed as Eqns. (7.3).

$$
\begin{aligned}
L_{1x,new} &= L_{1x,\mathrm{prev}} + (TR\omega_1 \cos\gamma_1 - TR\omega_2 \cos\gamma_2) \\
L_{1z,new} &= L_{1z,\mathrm{prev}} + (TR\omega_1 \sin\gamma_1 - TR\omega_2 \sin\gamma_2) \\
L_{2x,new} &= L_{2x,\mathrm{prev}} + (V_{Sx} - TR\omega_3 \cos\gamma_3) \\
L_{2z,new} &= L_{2z,\mathrm{prev}} + (V_{Sz} - TR\omega_3 \sin\gamma_3) \\
V_{Sx} &= (\mathrm{R}_3 \cos\gamma_3 \cos\theta_2 + \mathrm{R}_3 \sin\gamma_3 \sin\theta_2 - L_2) \cdot \omega_3 \\
V_{Sz} &= (-\mathrm{R}_3 \cos\gamma_3 \sin\theta_2 + \mathrm{R}_3 \sin\gamma_3 \cos\theta_2 + L_3) \cdot \omega_3
\end{aligned}
\tag{7.2}
$$

$$\begin{bmatrix} L_{1x}(\mathrm{k+1}) \\ L_{1z}(\mathrm{k+1}) \\ L_{2x}(\mathrm{k+1}) \\ L_{2z}(\mathrm{k+1}) \end{bmatrix} = \begin{bmatrix} 1 & 0 & 0 & 0 \\ 0 & 1 & 0 & 0 \\ 0 & 0 & 1 & 0 \\ 0 & 0 & 0 & 1 \end{bmatrix} \cdot \begin{bmatrix} L_{1x}(\mathrm{k}) \\ L_{1z}(\mathrm{k}) \\ L_{2x}(\mathrm{k}) \\ L_{2z}(\mathrm{k}) \end{bmatrix}$$

$$+ \begin{bmatrix} TR\cos\gamma_1 & -TR\cos\gamma_2 & 0 \\ TR\sin\gamma_1 & -TR\sin\gamma_2 & 0 \\ 0 & 0 & -TR\cos\gamma_3 + TK_{sx} \\ 0 & 0 & -TR\sin\gamma_3 + TK_{sz} \end{bmatrix} \cdot \begin{bmatrix} \omega_1 \\ \omega_2 \\ \omega_3 \end{bmatrix} \tag{7.3}$$

$$\therefore A = \begin{bmatrix} 1 & 0 & 0 & 0 \\ 0 & 1 & 0 & 0 \\ 0 & 0 & 1 & 0 \\ 0 & 0 & 0 & 1 \end{bmatrix}, \quad B = \begin{bmatrix} TR\cos\gamma_1 & -TR\cos\gamma_2 & 0 \\ TR\sin\gamma_1 & -TR\sin\gamma_2 & 0 \\ 0 & 0 & -TR\cos\gamma_3 + TK_{sx} \\ 0 & 0 & -TR\sin\gamma_3 + TK_{sz} \end{bmatrix}$$

$$where, \quad \begin{cases} K_{sx} = \mathrm{R}_3\cos\gamma_3\cos\theta_2 + \mathrm{R}_3\sin\gamma_3\sin\theta_2 - L_2 \\ K_{sz} = -\mathrm{R}_3\cos\gamma_3\sin\theta_2 + \mathrm{R}_3\sin\gamma_3\cos\theta_2 + L_3 \end{cases}$$

7.1.2 Conditions

Cost function

To minimize left and right link angular difference, these angular difference values are set as the cost functions set which to be minimized. Since the *Link 1* angular difference is more sensitive than *Link 2* angular difference caused by its mechanical characteristic, to reflect this fact weighting factor of the *Link 1* angular difference is four times bigger than *Link 2* angular difference.

Constraints

Maximum and minimum value of the constraints for input u(k) is defined based on the wheel motor characteristics. Although the motors are controlled by its own driver with speed direction mode including safety measures, these constraints will give more realistic directions to wheel motors

7.2 Implementation test and result

Implementation test is performed, based on the contents described in the previous chapter. The implemented MPC module is installed at laptop to minimize system load to CompactRIO. Other test setting is corresponding with the previous test.

For three stair shapes, 300X100, 315X130 and 310X160. To compare the performance of the MPC implementation, PI control implemented case and basic open loop direction only case are also tested. To utilize PI control appropriately, PI gains are changed as when the mobile platform climbing different stairs.

Fig. 7.5 shows the summary of the control performance comparison. Significant improvements are observed in these graphs. Firstly, left and right difference average is slightly reduced. Average reduced value is -64% when compared to basic control only case. On the other hand, Posture error average when comparing with the look-up table also reduced, which average is 33% lower than the basic control only case. Also, PI control implemented cases are also show the improvement by using its specific gain value, but less effective than the MPC implementation. In Fig. 7.6 depicts representative comparison result between each control case for stair 315 X 130 while Fig. 7.7 shows stair climbing experiment in a test circumstance. The detailed experiment result for each stair of all control implementations are depicted in Fig. 7.8 to 7.12.

It is important that the MPC method don't need gain tuning like PI or other ordinary control method, since the mobile robot has to climb unknown stairs therefore cannot prepare gain settings. Also, no gain setting means less set-up or related process is unnecessary, so the MPC implementations is more simple way to support the mobile robot movement.

Based on the result above, the MPC implementation to the hybrid mobile platform is successfully done more effectively, it is considered as a convenient way to enhance the accuracy and left-right balance of the mobile platform when compared to other traditional control way.

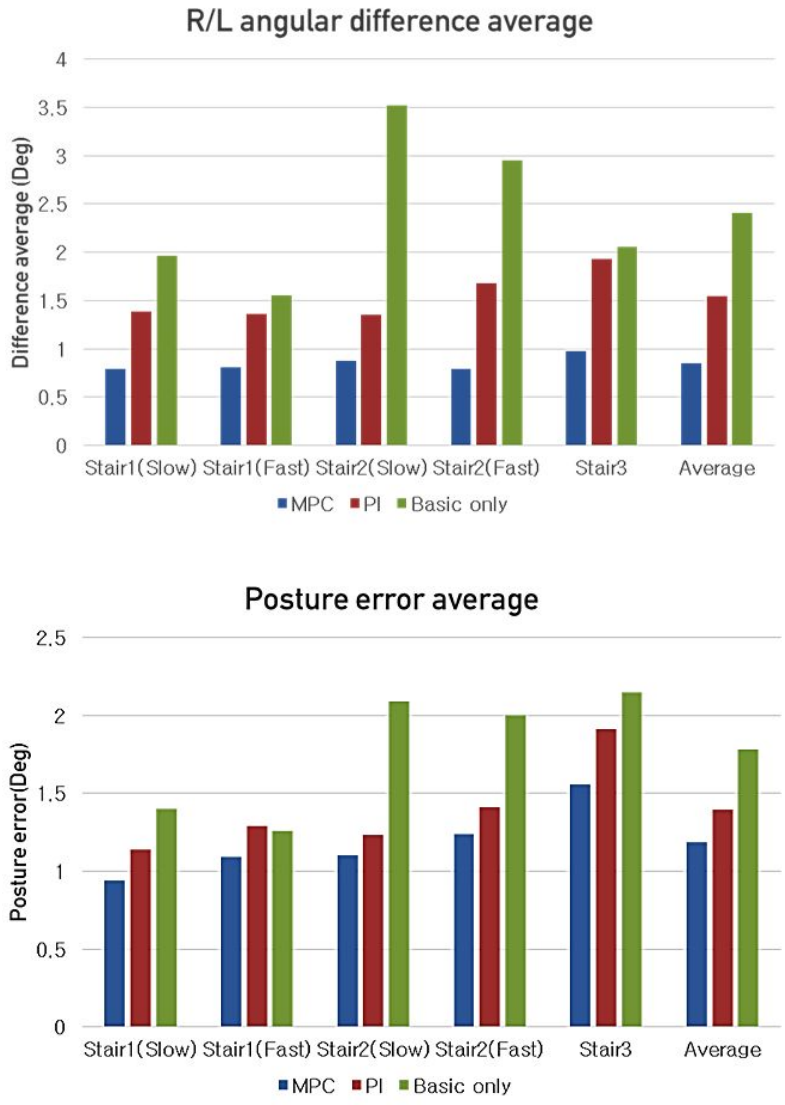

Figure 7.5: Control performance comparison summary

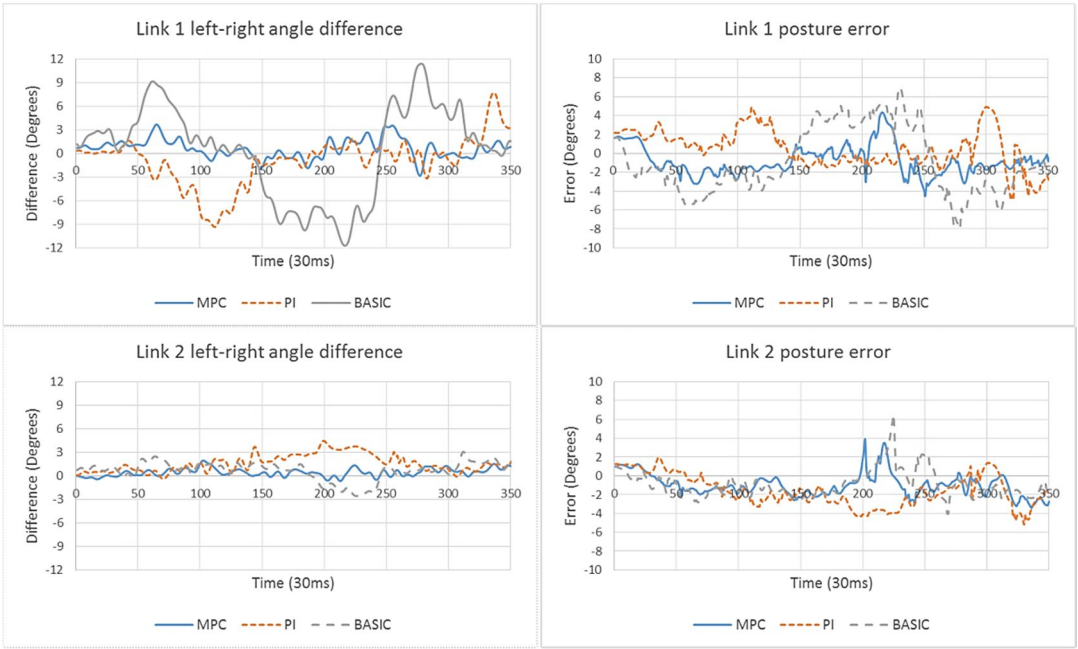

Figure 7.6: Control performance verification result, detailed – 315 X 130

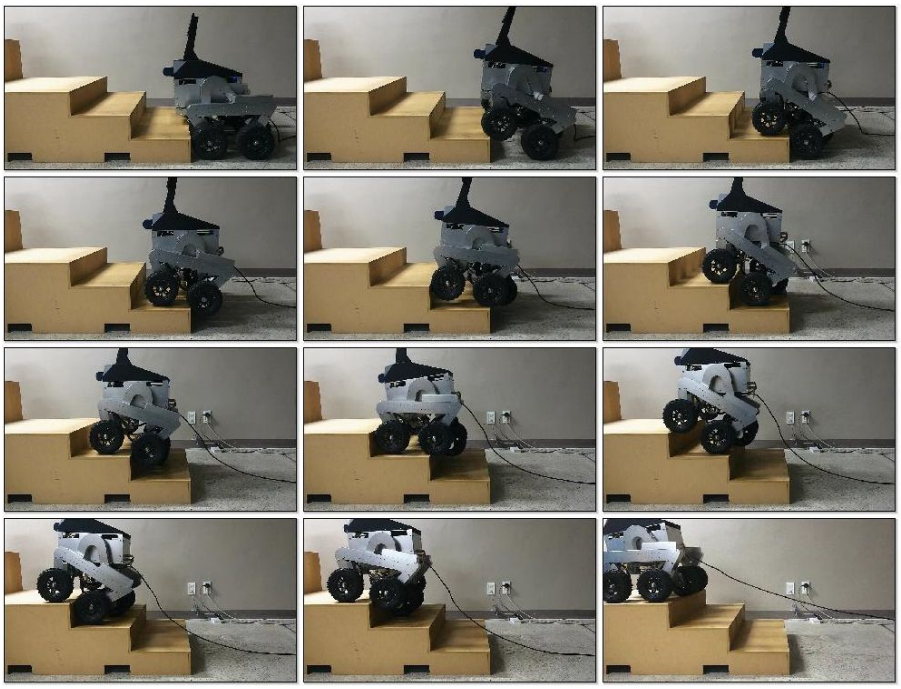

Figure 7.7: Stair climbing process - 315 X 130

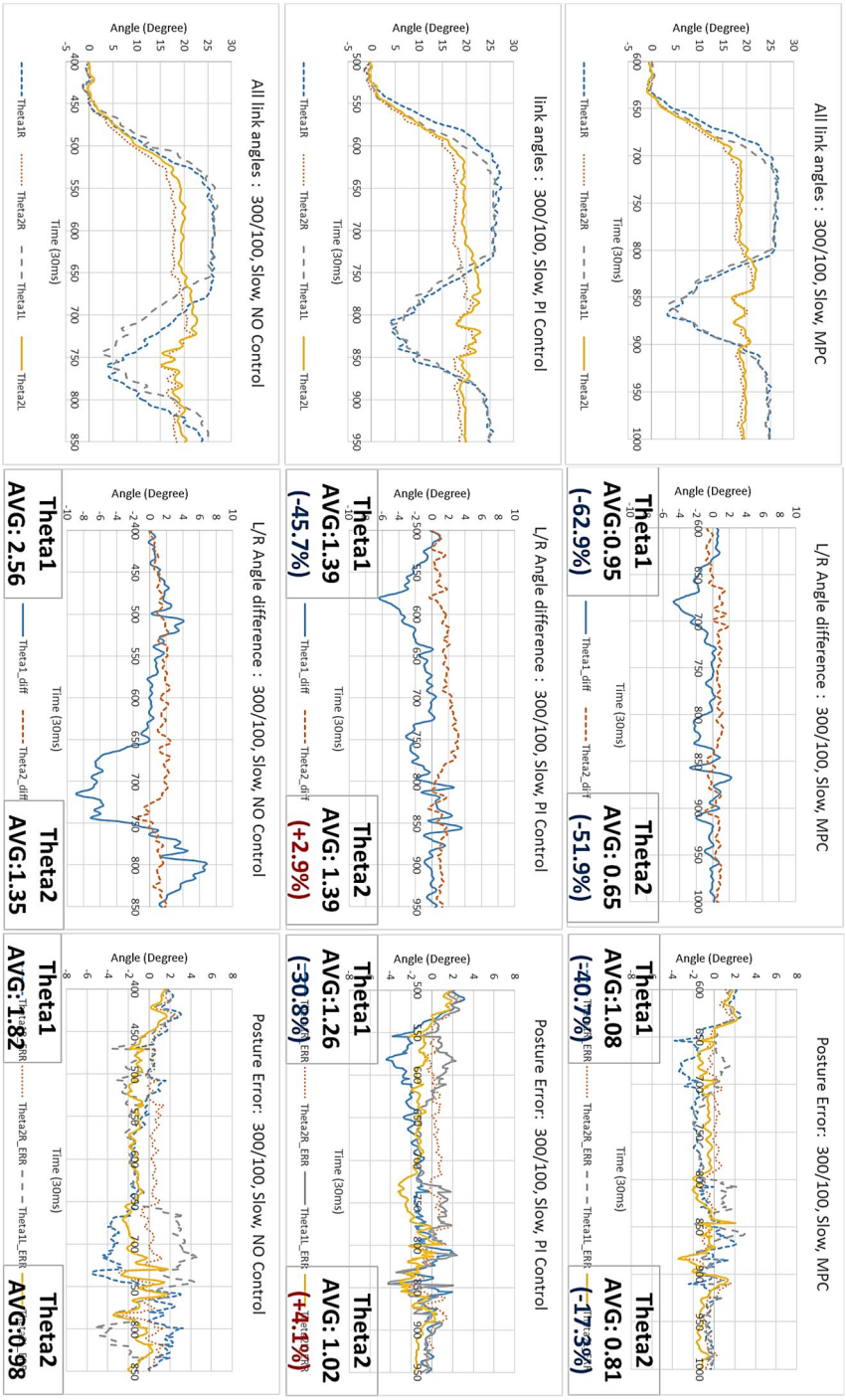

Figure 7.8: Control performance comparison summary – 300X100 (Slow)

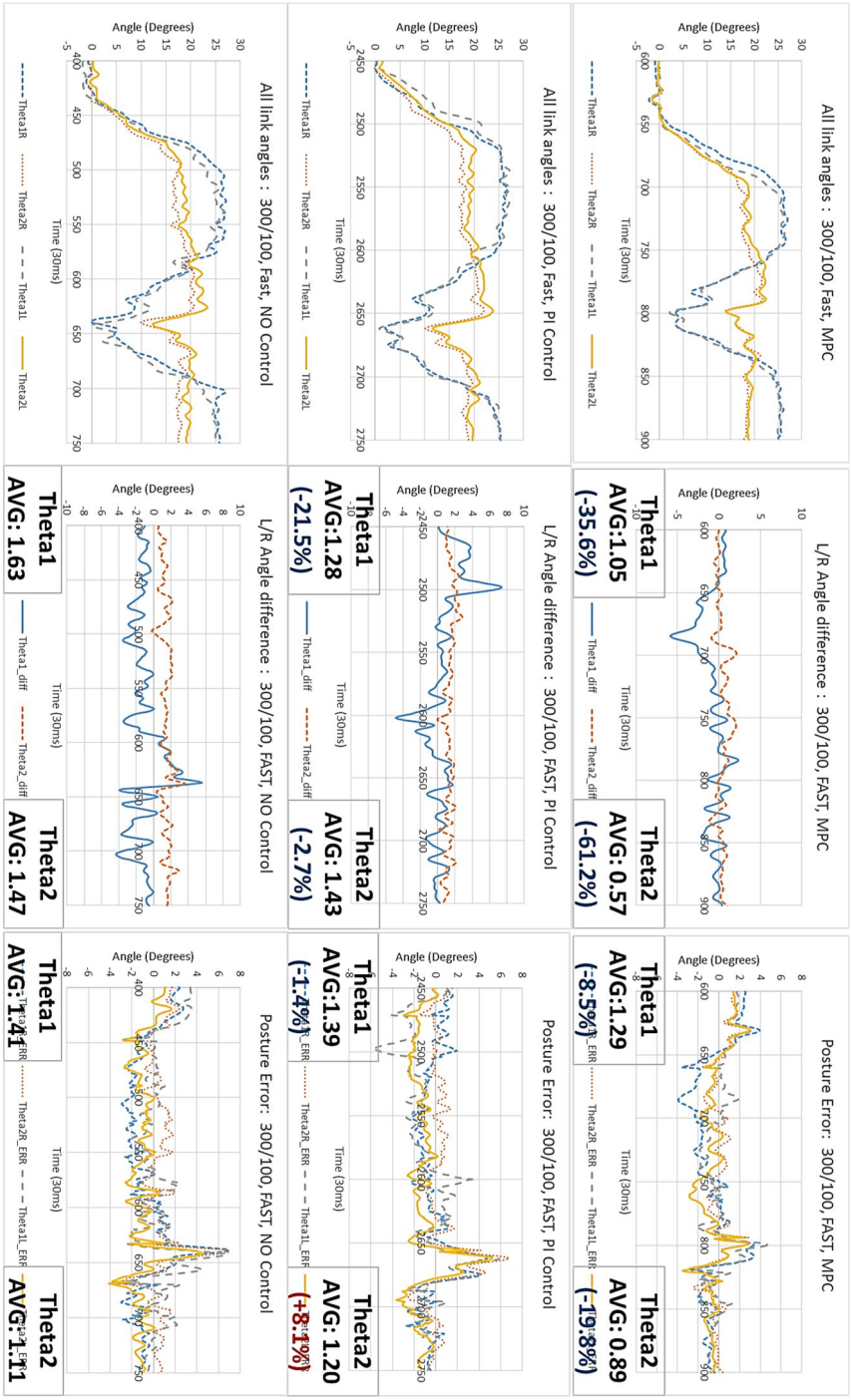

Figure 7.9: Control performance comparison summary – 300X100 (Fast)

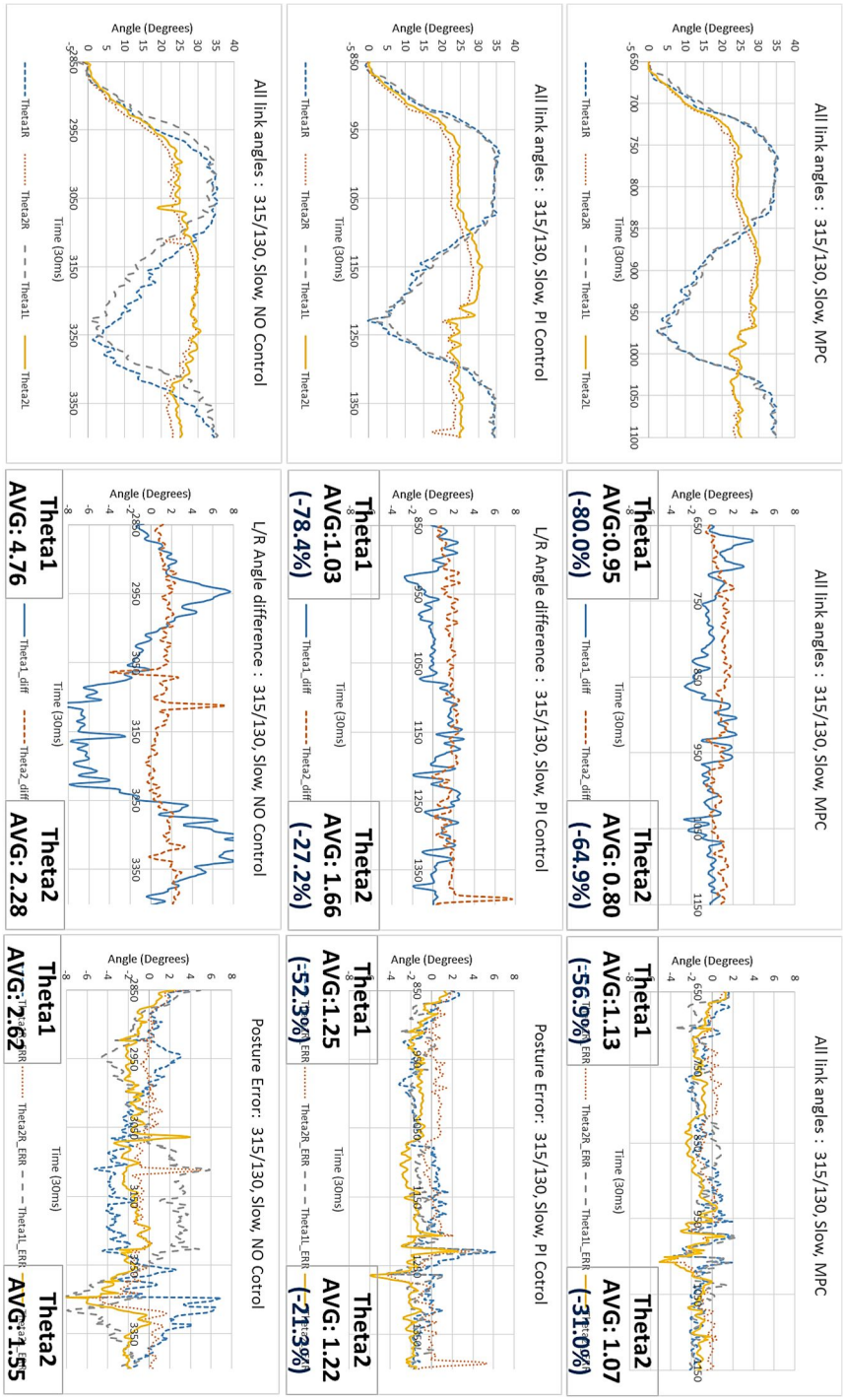

Figure 7.10: Control performance comparison summary – 315X130 (Slow)

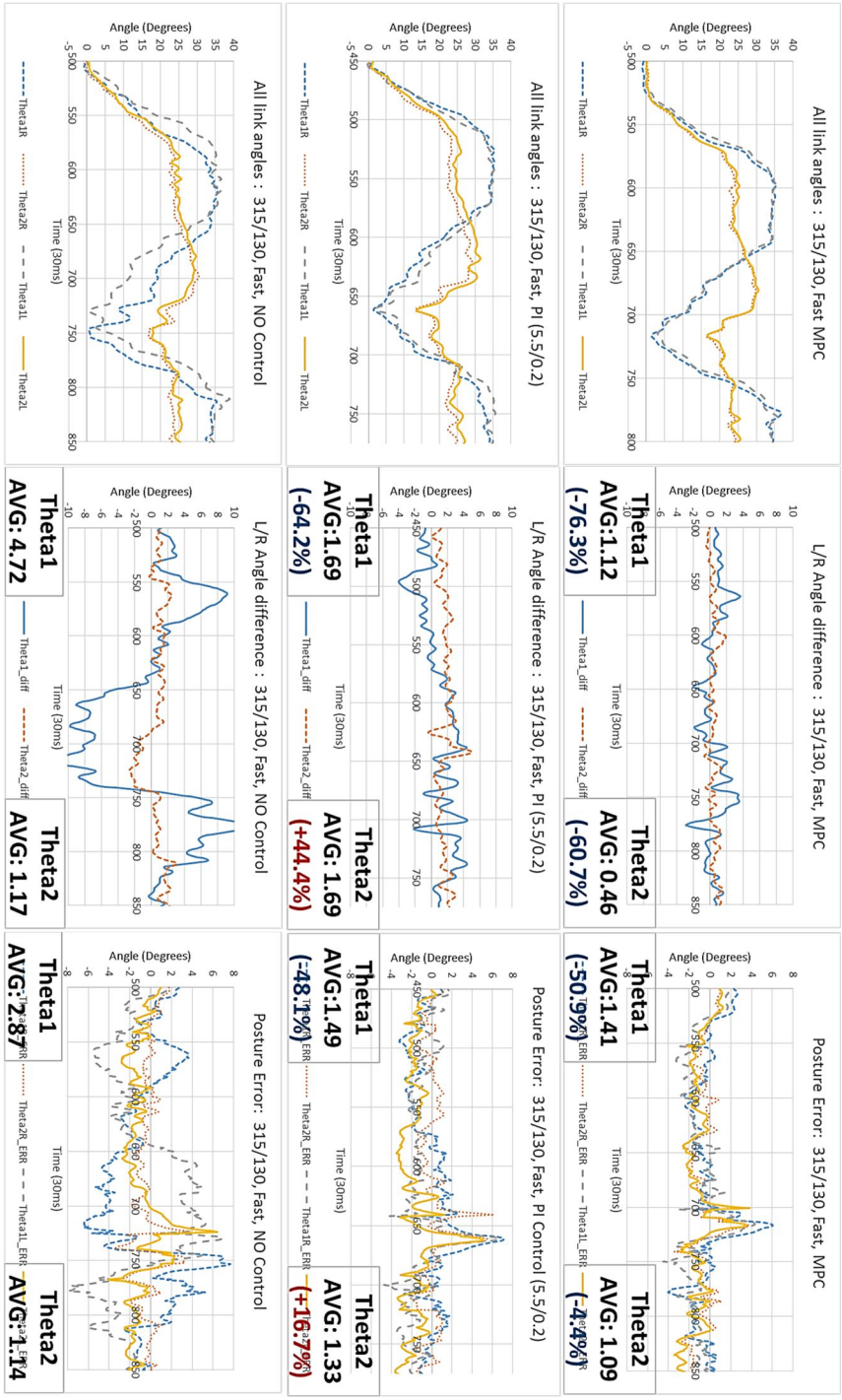

Figure 7.11: Control performance comparison summary – 315X130 (Fast)

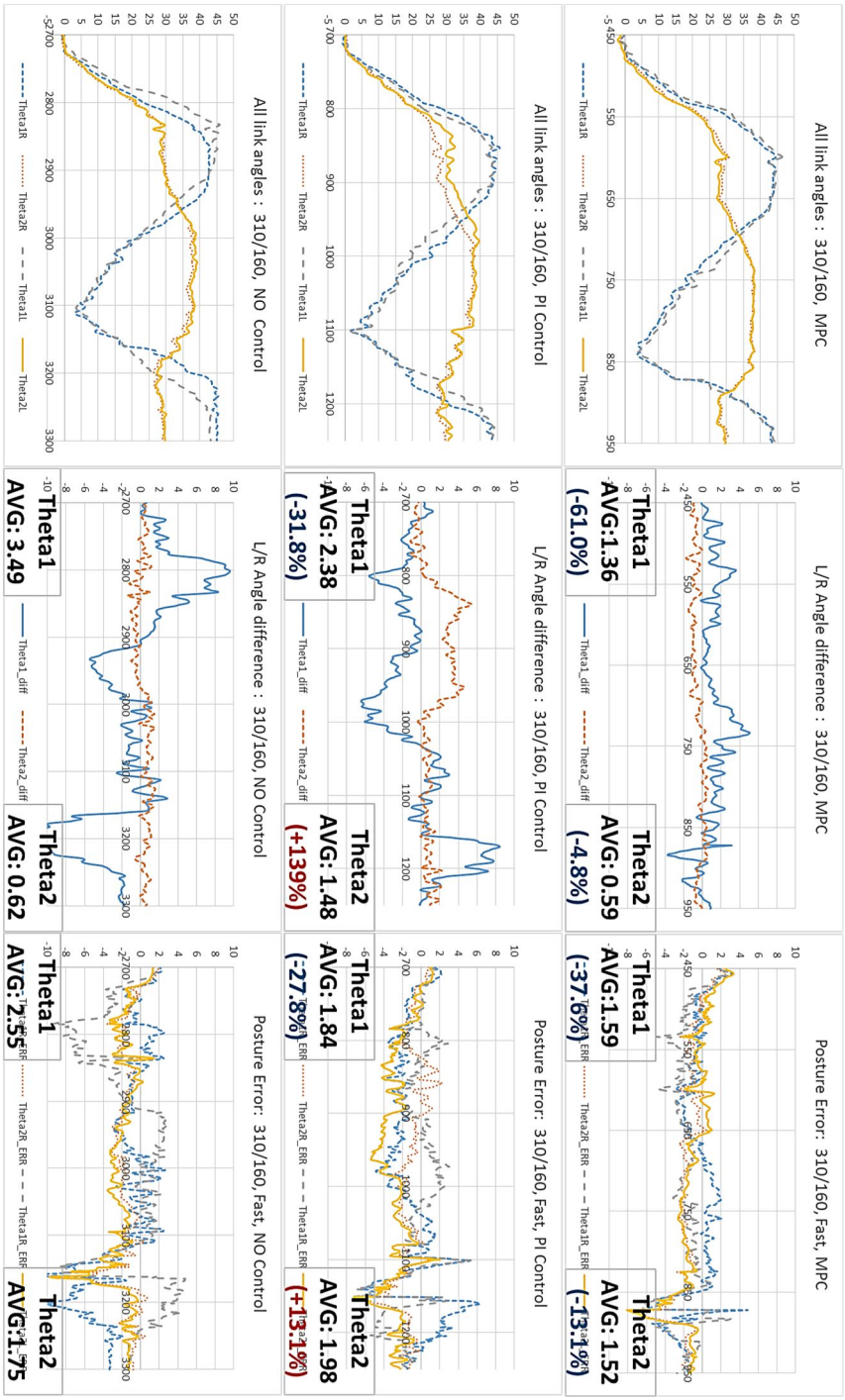

Figure 7.12: Control performance comparison summary – 310X160

As the last phase of the experiment, stair climbing in a real circumstance is performed. As shown in Fig. 7.13. This real stair structure in building has 4 steps, dimensions of these steps are around 300 X 150. Although this stair structure is made of concrete material which causes inaccuracy of stair dimensions and more slippery stair surface, the hybrid link mobile platform proved its stair climbing ability.

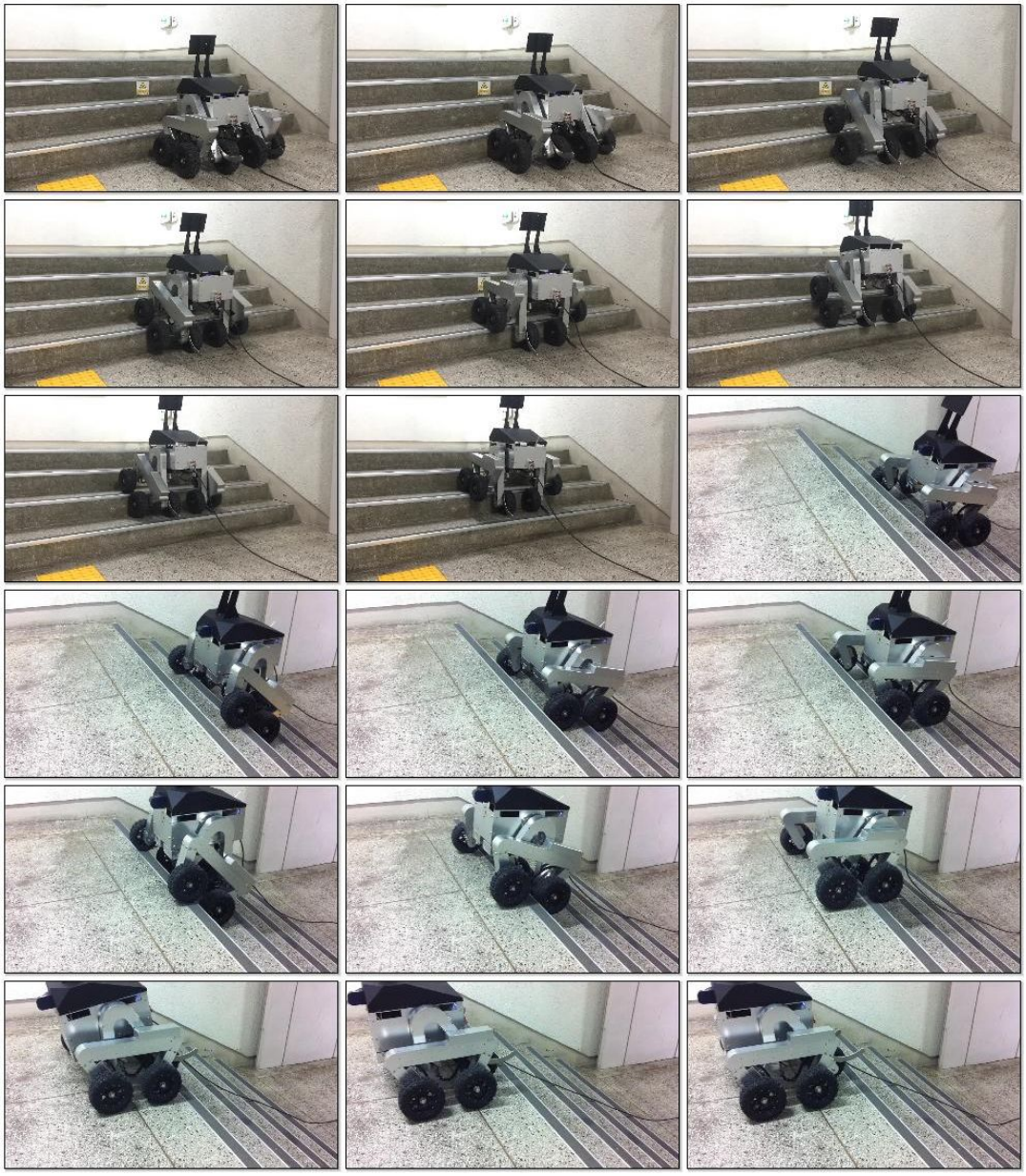

Figure 7.13: Climbing ability verification test in a real circumstance.

Chapter 8

Conclusion

The hybrid mechanism applied in this research is based on the combination of passive joint and active joint. The passive link mechanisms have advantages in mechanism, based on the relatively simple mechanism, so that easier controls are required. But its lack of ability to adapt critical posture or position while ascending or descending stairs, which can cause failure situations. On the other hand, The active link mechanisms can change its structure by using its actuators so that can achieve the better field adaptability, but its complicate mechanism requires the heavier structure, which leads to more complex control system to maximize the performance of the mechanism. Based on these reasons, the new hybrid link mechanism is introduced as an alternative solution. The process of the hybrid mechanism development including candidate production and selection, review and selection is introduced.

To maximize the performance potential of the hybrid linkage mechanism, the design parameter optimization of the mobile platform is performed. The optimization is focused on both stability and energy performance of the mobile platform. By optimization process of MATLAB considering maximizing the mobile platform's CM trajectory close to straight

line and minimizing its backward movement during stair climbing sequence as an objective function, optimized kinematic design variables for wheel radius and link dimensions are obtained.

Also, the kinematic analysis is conducted to obtain the most suitable movement direction strategy to maximize efficiency of the climbing and descending ability of the mobile platform. Wheel Jacobian matrices which derived from this process including wheel contact angles and link angles are applied to direct slip-minimizing wheel speed.

Based on this optimized result, the mobile platform is design and constructed. When designing the mobile platform from a kinematic concept to a detailed one, preventing interference between the mobile platform and ground structure or between the mobile platform's parts themselves is important, so all the predicted cases are checked before manufacturing process.

Sensors and actuators are selected based on the detailed requirements, all these instruments are installed at hallow space of the robot body and links to secure the safety for all instruments. These are controlled by main controller-CompactRIO which installed at body and can communicate with the laptop or personal computer with LAN cable or Wi-Fi signal. Power is supplied by AC cable to SMPS which attached to the mobile platform's body.

After that, stair climbing process including unknown stairs is created by using 2-D scanner to obtain stair dimensions. To ensure that the mobile robot can perform its stair climbing ability successfully, appropriate movement direction for wheels and slide actuators are essential. Individual speed direction for each wheel is obtained from calculated wheel Jacobian matrices and contact angle estimation result between each wheel and stair structure. Meanwhile, maintaining slide joint position is also important to keep the mobile platform's stability with the best condition while ascending or descending staircases. Concept idea and detailed process of the basic actuator control architecture and climbing ability test result of the mobile platform while the control architecture is applied.

Although basic performance of the mobile platform is verified, it requires additional control to maintain accuracy (especially left-right angular equality) to obtain the integrity of the mobile platform.

To achieve this, MPC (Model Predictive Control) is applied to the control. MPC is the optimal control technique for deriving optimized input values via the near-future prediction based on the MIMO (Multi- In, Multi-Out) plant model which satisfy the cost function maintaining technique. By implementing MPC to predict the condition of the mobile platform and direct the compensation movements to actuators, better movement ability, such as accuracy and stability can be obtained.

Implementation process is explained and its performance verification and comparison test is performed. By comparing MPC implemented and PI control implemented cases to various stair shapes, high performance and simplicity of the MPC implementation is verified. As the last phase of the experiment, stair climbing in a real circumstance is performed and proved the effectiveness of the mechanism and its control architecture.

Bibliography

[1] S. Fish, “UGV’s in future combat systems,” in Proceedings of the SPIE-unmanned ground vehicle technology VI, Orlando, USA, 2004, pp. 288–291.

[2] F. L. Menn, P. Bidaud, and F. B. Amar, “Generic differential kinematic modeling of articulated multi-monocycle mobile robots,” in Proceedings of the 2006 IEEE international conference on robotics and automation, Orlando, USA, 2006, pp. 1505–1510.

[3] F. Benamar, P. Bidaud, and F. L. Menn, “Generic differential kinematic modeling of articulated mobile robots,” Mechanism and Machine Theory, vol. 45, no. 7, pp. 997–1012, 2010.

[4] A. Halme, I. Leppanen, J. Soumela, S. Ylonen, and I. Kettunen, “Workpartner: interactive human-like service robot for outdoor applications,” International journal of robotics research, no. 7.

[5] C. Distante, G. Indivery, and G. Reina, “An application of mobile robotics for olfactory monitoring of hazardous industrial sites,” Industrial robot: an interna- tional journal, vol. 36, no. 1, pp. 51–59, 2009.

[6] R. Volpe, J. Balaram, T. Ohm, and R. Ivlev, “Rocky7: a next generation mars rover prototype,” Advanced robotics, vol. 11, no. 4, pp. 341–358, 1997.

[7] R. A. Lindemann and C. J. Voorhees, “Mars exploration rover mobility assembly design, test and performance,” in IEEE international conference on systems, man and cybernetics, Waikoloa, USA, 2005, pp. 450–455.

[8] J. Erickson, “Living the dream: an overview of the mars exploration project,” IEEE transactions on robotics and automation, vol. 13, no. 2, pp. 12–18, 2006.

[9] B. Chen, R. Wang, Y. Jia, L. Guo, and L. Yang, “Design of a high performance suspension for lunar rover based on evolution,” Acta Astronautica, no. 9.

[10] A. Mechdari, H. N. Pishkenari, A. L. Gaskarimahalle, S. H. Mahboobi, and R. Karimi, “A novel approach for optimal design of a rover mechanism,” Journal of intelligent and robotic systems, vol. 44, no. 4, pp. 291–312, 2005.

[11] K. Nagatani, A. Yamasaki, K. Yoshida, and T. Adachi, “Development and control method of six-wheel robot with rocker structure,” in Proceedings of the 2007 IEEE international workshop on safety, security and rescue robotics, Rome, Italy, 2007, pp. 1–6.

[12] W. Chung, G. Kim, and M. Kim, “Development of the multi-functional indoor service robot psr systems,” Autonomous Robotics, vol. 22, no. 1, pp. 1–17, 2007.

[13] M. Wada, “Mechanism and control of a 4wd robotic platform for omnidirectional wheelchairs,” in Proceedings of the 2009 IEEE/RSJ international conference on intelligent robots and systems, St. Louis, USA, 2009, pp. 4855–4862.

[14] F. M. et al., “Multi-modal locomotion robotic platform using leg-track-wheel articulations,” Autonomous robots, vol. 18, no. 2, pp. 137–156, 2005.

[15] R. Siegwart, P. Lamon, T. Estier, M. Lauria, and R. Piguet, “Innovative design for wheeled locomotion in rough terrain,” Robotics and autonomous systems, no. 2.

[16] D. Chugo, K. Kawabata, H. Kaetsu, H. Asama, and T. Mishima, “Step climbing omnidirectional mobile robot with passive linkages,” in Proceedings of SPIE-optomechatronic systems control, Sapporo, Japan, 2005, pp. 1–12.

[17] S. Nakajima, “Development of four-wheel-type mobile robot for rough terrain and verification of its fundamental capability of moving on rough terrain,” in Proceedings of IEEE international conference on robotics and biomimetics, Bangkok, Thailand, 2009, pp. 1968 – 1973.

[18] S. Nakajima, “Concept of a novel four-wheel-type mobile robot for rough terrain, rt-mover,” in Proceedings of IEEE international conference on intelligent robots and systems, St. Louis, USA, 2009, pp. 3257 – 3264.

[19] K. Six and A. Kecskem’ethy, “Steering properties of a combined wheeled and legged striding excavator,” in Proceedings of the 10th world congress on the theory of machines and mechanisms, Oulu, Finland, 1999, pp. 135 – 140.

[20] M. Lacagnina, G. Muscato, and R. Sinatra, “Kinematics, dynamics and control of a hybrid robot wheeleg,” Robotics and autonomous systems, no. 3.

[21] D. Kim, H. Hong, H. S. Kim and J. Kim, “Optimal design and kinetic analysis of a stair climbing mobile robot with rocker-bogie mechanism”, Mechanism and Machine

Theory, Vol.50, pp. 90–108, 2012

[22] S. Li, H. Gao, and Z. Deng, “Mobility performance evaluation of lunar rover and optimization of rocker-bogie suspension parameters,” in The 2nd international symposium on systems and control in aerospace and astronautics, Shenzhen, China, pp. 1 – 6, 2008.

[23] B. D. Harrington and C. Voorhees, “The challenges of designing the rocker-bogie suspension for the mars exploration rover,” in Proceedings of the 37th aerospace mechanisms symposium, Houston, USA, pp. 1 – 12, 2004.

[24] D. S. Iagnemma, K., “Mobile robot rough-terrain control (RTC) for planetary exploration,” in Proceeding of 2000 ASME IDETC/CIE: 26th Biennial Mechanisms and Robotics Conference, Maryland, USA, pp. 1 – 6, 2000.

[25] G. Klančar, I Škrjanc, “Tracking-error model-based predictive control for mobile robots in real time”, Robotics and Autonomous Systems, vol.55, no.6, pp. 460-469, 2007.

[26] F. Künhe, J. Gomes, W Fetter, “Mobile robot trajectory tracking using model predictive control”, IEEE Latin- American Robotics Symposium, São Luís, Brazil, 2005.

[27] I. Maurovic, M. Baotic, I. Petrovic, “Explicit Model Predictive Control for trajectory tracking with mobile robots”, IEEE/ASME International Conference on Advanced Intelligent Mechatronics (AIM2011), Budapest, Hungary, July 3-7, 2011, pp. 712-717.

[28] Francis D, K. Ching, R Steven. Winkel Building Codes Illustrated: A Guide to Understanding the 2012 International Building Code, John Wiley & Sons, 2012

[29] Safety of machinery -- Permanent means of access to machinery -- Part 3: Stairs, stepladders and guard-rails, ISO 14122-3:2001, Geneva, Switzerland: ISO, 2011

[30]http://likms.assembly.go.kr/law/jsp/Law.jsp?WORK_TYPE=LAW_BON&LAW_ID=B2766&PROM_NO=22626&PROM_DT=20110117&HanChk=Y, The National Assembly of the Republic of Korea (retrieved at Jan. 24, 2011, in Korean).

[31] J. Kim, *The Engineering Design*, Munundang, Seoul, 2008.

[32] T. Thueer and R. Siegwart, “Mobility evaluation of wheeled all-terrain robots,” Robotics and autonomous systems, vol. 58, no. 5, pp. 508–519, 2010.

[33] M. Sato, A. Kanda, and K. Ishii, “Simultaneous optimization of a wheeled mobile robot structure and a control parameter,” in 5th international workshop on computational intelligence and applications, Hiroshima, Japan, pp. 230 –235, 2009.

[34] C. Woo, H. Chli, S. Yoon, S. Kim, and Y. Kwak, “Optimal design of a new wheeled mobile robot based on a kinetic analysis of the stair climbing states,” Journal of

intelligent robotic systems, vol. 49, no. 4, pp. 325–354, 2007.

[35] A. Meghdari, H. N. Pishkenari, A. L. Gaskarimahalle, S. H. Mahboobi and R. Karimi, “Optimal design and fabrication of ‘CEDRA’ rescue robot using genetic algorithm”, Proc. of ASME-DETC2004, Salt Lake City, 2004.

[36] B. K. Rout and R. K. Mittal, “Parametric design optimization of 2-dof r-r planar manipulator-a design of experiment approach,” Robotics and computer-integrated manufacturing, vol. 24, no. 2, pp. 239–248, 2008.

[37] H. Kim, D. Kim, H. Yang, K. Lee, K. Seo, D. Chang, and J. Kim, “Development of a wall-climbing robot using a tracked wheel mechanism,” Journal of mechanical science and technology, vol. 22, no. 8, pp. 1490–1498, 2008.

[38] K. Lee and J. Kim, “Controller gain tuning of a simultaneous multi-axis pid control system using the taguchi method,” Control engineering practice, vol. 8, no. 8, pp. 949–958, 2000.

[39] G. S. Peace, *Taguchi methods: hands-on approach*, Addison - Wesley, USA: New York, 1993.

[40] P. F. Muir, “Modeling and control of wheeled mobile robots,” Ph.D. dissertation, Carnegie Mellon University, USA, Aug. 1988.

[41] V. Nguyen, S. Gächter, A. Martinelli, N. Tomatis, R. Siegwart, "A comparison of line extraction algorithms using 2D range data for indoor mobile robotics". Autonomous Robots 23 (2): 97, 2007.

[42] R. M. Murray, *A mathematical Introduction to Robotic Manipulation*, CRC press, USA, 1994.

[43] H. P. Halvorsen, Model Predictive In LabVIEW, Faculty of Technilogy, Norway, 2011.

[44] Control Design User Manual, National Instruments Corporation, 2014.

Abstract in Korean

논 문 초 록

본 연구에서는 새로운 하이브리드 링크 구조를 이용한 실내용 이동 플랫폼이 제작되었으며, 계단 등반 성능을 최대화하기 위한 제어 기법이 제시되었으며, 이를 검증하는 실험이 수행되었다.

이동 플랫폼의 계단 등반 성능을 얻기 위한 첫 단계로, 새로운 하이브리드 링크 메커니즘을 고안하였다. 공학적 설계방법론에 기반하여 제시된 설계대안들 중에서 선정한 새로운 하이브리드 링크 메커니즘은 수동 회전조인트와 능동 직선 조인트의 조합된 특성을 가지며, 무게중심 이동을 통해 바퀴를 이용하면서도 계단면의 등/하강을 안정적으로 수행할 수 있다.

계단등반 과정 중의 높은 안정성, 효율성 그리고 적응성을 이동 플랫폼에 부여하기 위하여, 기구학적 설계변수의 최적화가 수행되었다. 후진현상을 최소화하고 동시에 본체 무게중심 이동궤적의 직선성을 최대화 하는 것을 목적함수로 선정하였다. 또한 다양한 조건과 제약조건들이 지정되어 Genetic Algorithm을 통해 링크 길이들과 바퀴 반경들을 포함하는 최적설계변수들이 결정되었다.

최적화 결과와 간섭 문제를 고려하여 이동 플랫폼 시제품이 설계, 제작되었다. 제작된 이동 플랫폼 시제품의 크기는 650 mm (W) X 600 mm (L) X 460 mm (H)로, 본체 중량은 35 kg, 평지 주행속도는 2 m/s이다. ‘CompactRIO’가 전체를 제어하는 주 제어기로 이동 플랫폼의 본체에 설치되었으며, ‘Labview’가 설치된 단말 랩탑을 통해 무선 통신을 수행한다.

미지의 다양한 계단 형상에 대응하기 위해, 계단 등반을 위한 전략 생성 과정이 제시되었다. 또한 자세 확인을 통해 계단 등/하강 과정 동안 효과적인 바퀴 및 슬라이드 조인트 구동 지시를 수행한다. 계단 등반을 시작하기 전에 2-D 레이저 스캐너와 이를 위한 알고리즘을 통해 등반 목표 계단의 치수를 획득한다. 이를 기반으로 계단을 위한 룩 업 테이블이 생성된다. 이동 플랫폼이 계단을 등반하는 과정 중에는 실제 링크 기울기와 테이블의 비교를 통해 현재 위치와 자세를 파악하여 여기에 해당하는 슬라이드 조인트 위치 목표와 자코비안 행렬을 통해 미끄러짐을 최소화하는 바퀴 별 속도를 계산하기 위한 바퀴 접촉

각을 확인한다. 이 기법을 통해 계단등반과정중의 이동 플랫폼의 안정성을 유지 가능하다.

마지막으로 MPC(Model Predictive Control, 모델 예측 제어)의 적용을 통해 이동 플랫폼과 계단면과의 상태를 포함한 외부 조건에 의한 자세 불균형을 최소화하여 이동 플랫폼의 계단등반과정중의 안정성과 자세 정확성을 향상시킬 수 있음을 보인다. MPC를 통한 바퀴 속도 조절을 수행하고, 계단 형상 별 실험을 통해 일반적인 PI 제어 기법보다 우월한 성능을 확인하였다. 또한 실제 건물내의 계단에서의 등/하강 실험을 통해 본 이동 플랫폼의 메커니즘과 제어 기법의 효용성을 증명하였다.

주요어: 하이브리드 링크 메커니즘, 이동 플랫폼, 계단 등반,
기구학 해석, 기구학적 최적화, 모델 예측 제어

학 번: 2010 – 30970